DECEMBER 2022 Ph.D. in Aircraft and Aerospace Engineering EDİP ÖZTÜRK

REPUBLIC OF TURKEY

GAZİANTEP UNIVERSITY

GRADUATE SCHOOL OF NATURAL & APPLIED SCIENCES

DESIGN AND INTEGRATION OF FULL FLIGHT STABILIZED SPHERICAL SIMULATOR

Ph.D. THESIS

IN

AIRCRAFT AND AEROSPACE ENGINEERING

BY

EDİP ÖZTÜRK

DECEMBER 2022

DESIGN AND INTEGRATION OF FULL FLIGHT STABILIZED SPHERICAL SIMULATOR

Ph.D. Thesis

in

Aircraft and Aerospace Engineering

Gaziantep University

Supervisor

Assoc. Prof. Dr. Kürşad GÖV

by

Edip ÖZTÜRK

December 2022

DESIGN AND INTEGRATION OF FULL FLIGHT STABILIZED SPHERICAL SIMULATOR

submitted by **Edip ÖZTÜRK** in partial fulfilment of the requirements for the degree of Doctor of Philosophy in **Aircraft and Aerospace Engineering, Gaziantep University** is approved by,

Prof. Dr. Mehmet İshak YÜCE
Director of the Graduate School of Natural and Applied Sciences …….....

Assoc. Prof. Dr. İbrahim GÖV
Head of the Department of Aircraft and Aerospace Engineering …….....

Assoc. Prof. Dr. Kürşad GÖV
Supervisor, Aircraft and Aerospace Engineering
Gaziantep University …….....

Exam Date: 5 December 2022

Examining Committee Members:

Assoc. Prof. Dr. Kürşad GÖV
Supervisor, Aircraft and Aerospace Engineering
Gaziantep University …….....

Prof. Dr. Metin KÖK
Machinery and Metal Technology
Kahramanmaraş Sütçü İmam University …….....

Assoc. Prof. Dr. Mehmet Hanifi DOĞRU
Pilotage
Gaziantep University …….....

Assoc. Prof. Dr. Eyüp YETER
Aircraft and Aerospace Engineering
Gaziantep University …….....

Asst. Prof. Dr. Hakan ÜLKER
Mechanical Engineering Department
Bursa Technical University …….....

I hereby declare that all information in this document has been obtained and presented in accordance with academic rules and ethical conduct. I also declare that, as required by these rules and conduct, I have fully cited and referenced all material and results that are not original to this work.

Edip ÖZTÜRK

ABSTRACT

DESIGN AND INTEGRATION OF FULL FLIGHT STABILIZED SPHERICAL SIMULATOR

ÖZTÜRK, Edip
Ph.D. in Aircraft and Aerospace Engineering
Supervisor: Assoc. Prof. Dr. Kürşad GÖV
December 2022
76 pages

Nowadays, with the development of technology, the usage areas of simulators are increasing and diversifying. As simulators can find a place in every sector, they also play a major role in aviation and space studies. Flight simulators are devices that artificially recreate the flight of the aircraft and the environment in which it flies. External effects such as flight systems and turbulence are among the elements that can be simulated by flight simulators, taking into account the dynamics of the aircraft during the modelling of the aircraft. Although aircraft design and research and development studies are among the purposes of flight simulators, the widespread use of flight simulators is pilot training. Since flight training is risky and costly in terms of safety, flight simulators are frequently used in pilot training. In addition, the use of flight simulators is a safe and cost-effective solution for the study of certain scenarios such as engine failure and difficult weather conditions, which are difficult or impossible to implement in real life. The main purpose of simulators is to make the user feel the flight scenarios created in the computer environment in a realistic way. In this study, a new spherical flight simulator was designed and manufactured, and the nonlinear dynamics of the spherical flight simulator was modelled mathematically using the Newton-Euler method. The obtained mathematical model is used in the controller design for the spherical flight simulator. In the controller design, pole placement method and linear quadratic regulator method (LQR) are selected and these methods are compared. The mathematical simulation of the system was performed in SIMULINK environment.

Key Words: Flight Simulator, Newton-Euler Method, Pole Placement, LQR

ÖZET

DENGELENMİŞ KÜRESEL TAM UÇUŞ SİMÜLATÖRÜNÜN TASARIMI VE ENTEGRASYONU

ÖZTÜRK, Edip
Doktora Tezi, Uçak ve Uzay Mühendisliği
Danışman: Doç. Dr. Kürşad GÖV
Aralık 2022
76 sayfa

Günümüzde teknolojinin gelişmesiyle birlikte simülatörlerin kullanım alanları da artmakta ve çeşitlenmektedir. Simülatörler her sektörde kendine yer bulabildiği gibi havacılık ve uzay çalışmalarında da büyük rol oynamaktadır. Uçuş simülatörleri, hava aracının uçuşunu ve uçtuğu ortamı yapay olarak yeniden yaratan cihazlardır. Uçağın modellenmesi sırasında uçağın dinamikleri göz önünde bulundurularak uçuş sistemleri ve türbülans gibi dış etkiler uçuş simülatörleri tarafından simüle edilebilen unsurlar arasındadır. Uçak tasarımı ve araştırma geliştirme çalışmaları uçuş simülatörlerinin kullanım amaçları arasında yer alsa da uçuş simülatörlerinin yaygın kullanım alanı pilot eğitimidir. Ayrıca gerçek hayatta uygulanması zor ya da imkânsız olan motor arızası, zorlu hava koşulları gibi belirli senaryoların çalışılması için de uçuş simülatörlerinin kullanımı güvenli ve maliyet etkin bir çözümdür. Simülatörlerin temel amacı, bilgisayar ortamında oluşturulan uçuş senaryolarının kullanıcıya gerçekçi bir şekilde hissettirilmesidir. Bu çalışmada, yeni bir küresel uçuş simülatörü tasarlanmış, imal edilmiş ve küresel uçuş simülatörünün doğrusal olmayan dinamiği Newton-Euler yöntemi kullanılarak matematiksel olarak modellenmiştir. Elde edilen matematiksel model, küresel uçuş simülatörü için kontrolör tasarımında kullanılmıştır. Kontrolör tasarımında kutup yerleştirme yöntemi ve doğrusal kuadratik regülatör yöntemi (LQR) seçilmiş ve bu yöntemler karşılaştırılmıştır. Sistemin matematiksel simülasyonu SIMULINK ortamında gerçekleştirilmiştir.

Anahtar Kelimeler: Uçuş Simülatörü, Newton-Euler Yöntemi, Kutup Yerleştirme, LQR

"Dedicated to Zühre and Newton"

ACKNOWLEDGEMENTS

I would like to acknowledge and give my warmest thanks to my supervisor Assoc. Prof. Dr. Kürşad GÖV who made this work possible. His guidance and advice carried me through all the stages of writing my thesis.

I would like to thank Assoc. Prof. Dr. İbrahim GÖV, for his support and answers my endless questions.

I would like to thank Assoc. Prof. Dr. M. Hanifi Doğru and Assist. Prof. Dr. Nadide ÖZKUL DOĞRU for always being there for me.

Also, I would like to thank Assist. Prof. Dr. Hakan ÜLKER for his valuable comments and for serving my thesis monitoring committee.

Thanks to Assoc. Prof. Dr. Eyüp YETER for his support and motivation.

Special thanks to my colleague and brother Burak ÇİFTCİOĞLU and my sister Umay Gülfem ÇİFTCİOĞLU, I have always experienced their help during my thesis period.

I would like to express my love and gratitude to my mother Sabiha ÖZTÜRK, my sister Gülçin ÖZTÜRK and my brother Yunus Emre ÖZTÜRK for their support, always best wishes. Their prayer for me was what sustained me this far.

This work is supported by Scientific and Technological Research Council of Turkey (TUBITAK), through project National PhD Scholarship Program in the Priority Fields in Science and Technology (2211-C)

TABLE OF CONTENTS

Page

LIST OF TABLES

Page

LIST OF FIGURES

Page

LIST OF SYMBOLS

$\boldsymbol{\theta}$	Outer sphere angular position, pitch angle
$\boldsymbol{\psi}$	Middle sphere angular position, yaw angle
$\boldsymbol{\phi}$	Inner sphere angular position, roll angle
$\boldsymbol{J_O}$	Outer sphere mass moment of inertia
$\boldsymbol{J_M}$	Middle sphere mass moment of inertia
$\boldsymbol{J_I}$	Inner sphere mass moment of inertia
$\boldsymbol{H_I}$	Inner sphere angular momentum
$\boldsymbol{H_M}$	Middle sphere angular momentum
$\boldsymbol{H_O}$	Outer sphere angular momentum
$\boldsymbol{T_{I-D1}}$	The first term of inner sphere disturbance torque
$\boldsymbol{T_{I-D2}}$	The second term of inner sphere disturbance torque
$\boldsymbol{T_{M-D1}}$	The first term of middle sphere disturbance torque
$\boldsymbol{T_{M-D2}}$	The second term of middle sphere disturbance torque
$\boldsymbol{T_{M-D3}}$	The third term of middle sphere disturbance torque
$\boldsymbol{T_{O-D1}}$	The first term of outer sphere disturbance torque
$\boldsymbol{T_{O-D2}}$	The second term of outer sphere disturbance torque
$\boldsymbol{T_{O-D3}}$	The third term of outer sphere disturbance torque
$\boldsymbol{K_t}$	Torque constant
$\boldsymbol{i}$	Current
$\boldsymbol{K_e}$	Motor constant
$\boldsymbol{b}$	Damping constant
$\boldsymbol{L}$	Inductance

$\boldsymbol{V}$	Voltage
$\boldsymbol{R}$	Resistance
$\boldsymbol{t_s}$	Settling time
$\boldsymbol{M_p}$	Percent overshoot
$\boldsymbol{\zeta}$	Damping ration
$\boldsymbol{\omega_n}$	Natural frequency

CHAPTER I

INTRODUCTION

Flight simulators are devices that artificially recreate the flight of the aircraft and the environment in which it flies. External effects such as flight systems and turbulence are among the elements that can be simulated by flight simulators, taking into account the dynamics of the aircraft during the modelling of the aircraft. Although aircraft design and research and development studies are among the purposes of flight simulators, the widespread use of flight simulators is pilot training. Since flight training is risky and costly in terms of safety, flight simulators are frequently used in pilot training. In addition, the use of flight simulators is a safe and cost-effective solution for the study of certain scenarios such as engine failure and difficult weather conditions, which are difficult or impossible to implement in real life. In the early 20th century, flight training with real aircraft became costly and risky as time passed. The fact that flight trainings depend on external factors such as weather conditions, aircraft maintenance status, adequate number of personnel has also made it difficult to provide these trainings. In addition, without simulator training, it was not possible to perform special missions such as landing on the Moon, which had not been realised before, and the use of flight simulators became inevitable. Initially designed flight simulators consist of a simple model of a real aircraft with no mobility. The main purpose of these simulators was not to provide flight training, but to improve the reflexes of pilot candidates. In the simulators produced later, an exact copy of the cockpit of the aircraft was placed on a moving mechanism and started to be used in flight training. Stewart platform is used in many wide areas in academic and industrial fields. When past simulator studies are analysed, it is seen that the Stewart platform, which is a parallel manipulator, is frequently used as a motion provider in flight simulators due to its simple mechanical structure, high carrying capacity and low maintenance cost. However, these simulators, which have limited motion capability in pitch, roll and yaw axes, have been insufficient in simulation and training studies of military combat and aerobatic aircraft with high manoeuvrability. In order to overcome this disadvantage, a new flight simulator with high manoeuvrability has been designed in this study. The new simulator designed consists of 3 nested sphere-like structures. Since each of the spheres of the spherical flight simulator has the ability to rotate 360 degrees, it can be easily used in the simulation of aerobatic and combat aircraft manoeuvres.

The spherical flight simulator has three rotational degrees of freedom. A review of the literature shows that flight simulators with three degrees of freedom can also be used to simulate aircraft with more than three degrees of freedom. Motion perception

control, which enables this use, is one of the frequently encountered studies in the literature on flight simulators. Before designing a controller for a global flight simulator, a detailed mathematical model must be created. Here, the mathematical model refers to the dynamic equations known as the simulator's equations of motion. The mathematical model represents the dynamic characteristics of the spherical flight simulator. In the literature, there are different methods used to construct the mathematical model. The most well-known of these methods are Newton-Euler and Lagrange-Hamilton methods. In this study, the Newton-Euler method is used to construct the equations of motion of the spherical flight simulator. In control applications, a single controller can be designed or hybrid controllers consisting of more than one controller can be designed. Two different methods were chosen for the controller design for the global flight simulator. The first controller designed for the simulator is based on the pole placement method, which is based on placing the poles of the closed loop system at desired locations on the complex plane. This method allows the system to behave as desired. When the literature is examined, it is seen that the pole placement method is widely used in many fields such as mobile robots, simple mechanical systems such as inverted pendulum and aircraft control.

The second method chosen for the controller designed for the global flight simulator is the linear quadratic regulator (LQR) method. This method is based on minimising the control cost of a dynamic system. LQR calculates the state feedback gain required to minimise the cost function. As with the pole placement method, the linear quadratic regulator is also widely used in the control literature.

Thesis outline

This thesis is composed of 7 chapter. A brief introduction, method and purpose of thesis are given in Chapter 1. Chapter 2 involves literature review. In this chapter addresses past studies and history about simulation, flight simulation, simulators and flight simulators. Chapter 3 contains design and manufacturing of spherical flight simulator. This chapter deals with three-dimensional design and some design issues. Beside three-dimensional design, manufactured flight simulator parts and assembly are accessible in this chapter. Chapter 4 covers all necessary mathematical modelling topics. In this chapter kinematic analysis is given first and dynamic analysis follows the kinematic analysis. Kinematic and dynamic analysis end up with governing equations of spherical flight simulator. In this chapter enables short brief of method of solving governing equations. At the end of the chapter, Simulation method of dynamic behaviour of spherical flight simulator is presented. Chapter 5 deals with controller design for spherical flight simulator. In this chapter mathematics of controller design process and two different controllers are presented. Chapter 6 presents obtained results and compares controller performance. Chapter 7 involves final conclusion and last comments on study.

CHAPTER II

LITERATURE SURVAY

2.1 History of Flight Simulator

In the beginning of first powered flight age, flying machines was pretty dangerous. Flight operations and aircrafts were not subjected to standardized safety protocols. Therefore, crashes and injuries were common in aviation environments. After first powered flight was practised people needed to find more safer way for flight training. First device that can be answer the description of flight simulator called “Model B” was built by wright brothers [1]. Model B was used for simulating Wright brothers’ aircraft “Flyer B” But it was not a flight simulator as used in present. Model B was designed without tail and engine part. Main objective of this device was pilot training. Since Model B was very simple in detail, expected pilot behaviour can be achieved in a few hours. An aircraft called Antoinette was built by French company in 1908 (Fig.2.1).

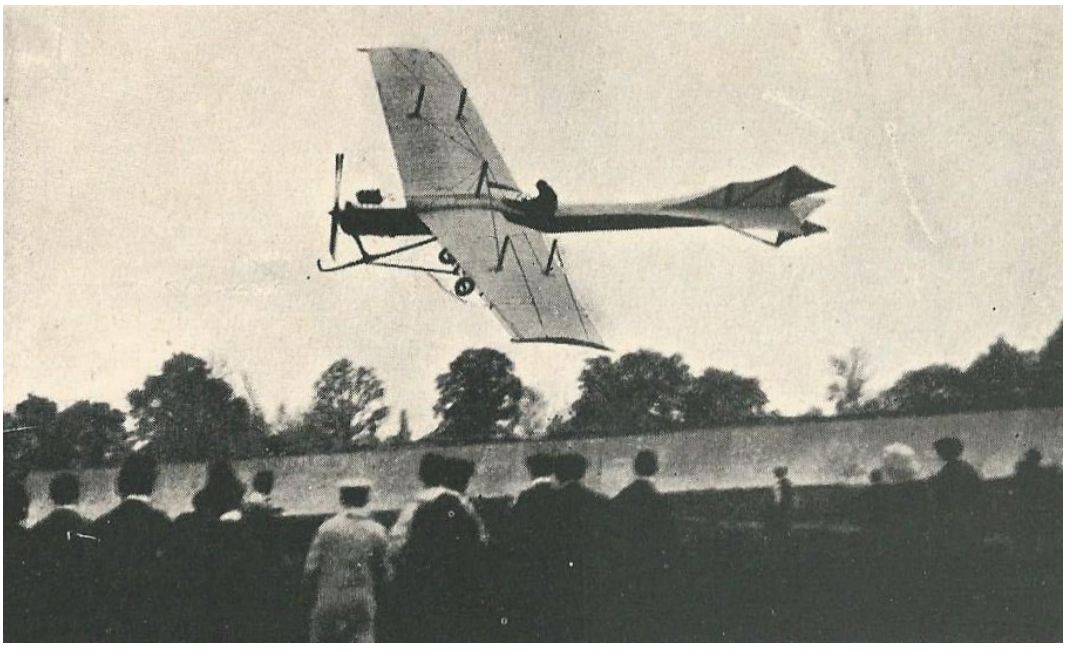

Figure 2.1 Antoinette aircraft.

Flight simulator for the aircraft Antoinette was developed by French aviation manufacturer in 1910 (Fig.2.2).

Figure 2.2 Antoinette flight simulator**.**

Antoinette flight simulator was consisted of two semi barrel one barrel was located to top of the other barrel. Simulator was able to simulate only roll and pitch motion of the aircraft manually [2]. A more sophisticated flight simulator called “Link trainer “or “Blue box” was built by Link Aviation Devices in the beginning of 1930’s (Fig.2.3).

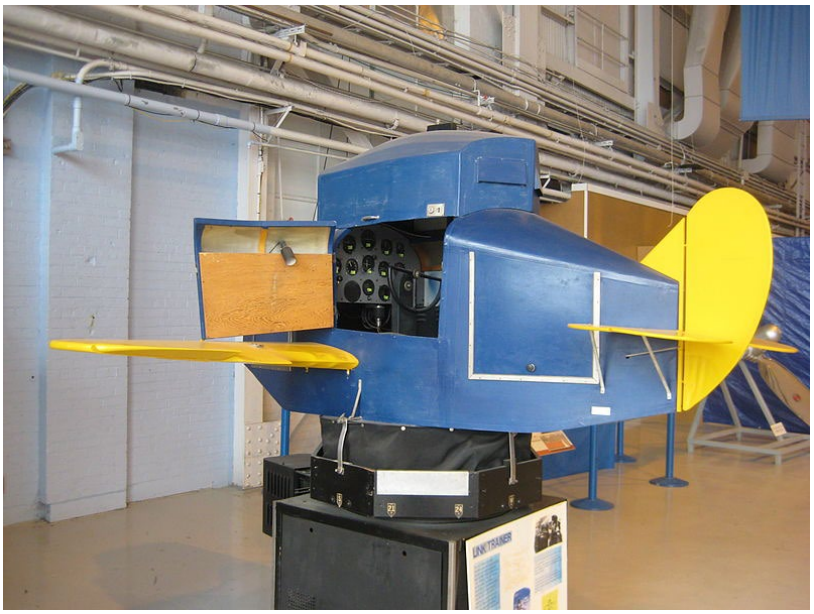

Figure 2. 3 Link trainer.

Full flight instruments were available in the Link trainer and it had single pilot seat stick, rudder controls. Link trainer was also first mass produced flight simulator in the history [3]. Also link trainer was accepted as the beginning of virtual reality.

However, first simulator studies focused on aviation, driving simulator studies takes huge volume in literature. First pc-based driving simulator was developed by German car manufacturer Volkswagen company in the beginning of 1970's. This simulator was equipped with a flat screen and limited motion capability in roll, yaw and pitch direction without vehicle cabin [4]. This simulator was enhanced by Hamburg Institute of Automotive Engineering and Piston Engines in 1984. A Volkswagen car cabin was used as cockpit and lateral linear rails were added in order to enablement of platform motion. After one decade these simulators was redesigned. A 6 DOF motion platform was mounted on lateral rails. After this arrangement the simulator was called modular automotive road simulator (MARS) [5]. Many automobile companies increased simulator studies in 1990's. French automobile manufacturer Renault developed a 6 DOF simulator. Electro-mechanical actuators were used to drive motion platform of the simulator and simulator validation was done by real driving parameters [6]. A different simulator was designed by General Motors. Real vehicle mockup was used as simulator cabin and main purpose of the simulator was vehicle research and development [7]. A fixed-base simulator was designed by Ford automobile industry. This simulator was used to enhance man-machine interface [8]. A 4 DOF simulator was designed by Mazda Yokohama Research Center. Simulator was designed to enhance user reflexes in case of emergency situations [9]. A hybrid simulator was developed by Iowa university in 1994. Simulator motion platform was allowing to be used both as driving simulator and flight simulator. Flight simulator was designed to simulate Boeing 737 and car simulator was used for Ford Taurus model automobile [10]. In the beginning of the 21th century, new simulator technologies were appeared with the development of electrical actuating systems. Hydraulic actuators were used before electro-mechanical actuation systems and these hydraulic actuators were heavy and laborious in terms of maintenance.

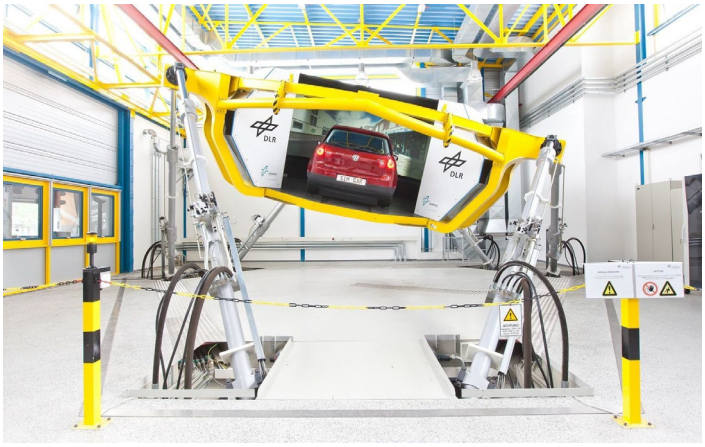

Figure 2.4 DLR flight simulator.

The simulator designed at Hannover German Aerospace Center Transport Research Institute was actuated by hydraulic actuators. Unlike other simulators, vehicle cockpit was hanged below actuators instead locating the top of the actuators (Fig.2.4) [11].

2.2 Motion Cueing Studies

Flight simulator consists of a motion platform which is source of simulator movement and a cockpit or a cabin which simulate simulated vehicle environment [12]. Motion platform of a flight simulator has limited workspace. Human body in the flight simulator feels force and motion when the flight simulator moves. These motion stimuli are called motion cues and algorithm that provides realistic stimuli is called motion cueing algorithm [13]. The general name of the motion cueing algorithm is called washout filter [14-17]. Motion platform of a flight simulator has limited workspace. The reason calling algorithm as washout filter is that algorithm should provide realistic motion cues and makes motion platform to its starting position[18-23]. This motion sequences called washout. Basic high-pass, low-pass filters are used for washout algorithm, as well as control algorithms like adaptive, optimal and model prediction control. Classical washout filter includes only basic filters.

Classical motion cueing algorithm was developed by NASA in 1969 [24]. The algorithm includes first order, second order low-pass and high-pass filters. Algorithm uses gravitational acceleration while calculating acceleration in vertical direction. Algorithm scales translational acceleration and angular velocity in the beginning of the washout sequence and ,in returning sequence it uses second order and third order filters [25] Tilt coordination filter was developed shortly after development of classical motion cueing algorithm [26]. Tilt coordination is used to create translational motion perception on human body by using tilt motion [27].

Motion platforms for using flight simulators can have different number of degrees of freedom. Number of degrees of freedom is directly affects the motion perception. Classical motion cueing algorithm was studied for flight simulators which have different numbers of degrees of freedom and results were compared. A 3 DOF, 6 DOF and 8 DOF platforms were tested [28]. 3 DOF platform was successful in terms of translational motion feedbacks, 6 DOF platform was successful for handling large amplitude cues and 8 DOF platform operated similar to 6 DOF platform. Motion platforms need degrees of freedom to operate successfully. But it does not mean that platforms which have more degrees of freedom can produce more realistic cues at any time. Mentioned study showed that five degrees of freedom flight can be simulated with only three degrees of freedom motion platform [29].

Motion cueing algorithm was tried to be optimized by Cleij et al. An algorithm added to motion cueing algorithm and new algorithm was experienced by participants. No big difference can be achieved at the end of the study [30]. Comparison of four different motion cueing algorithm is presented in the study by Garrett et al. In the study, linear optimal control filtering, adaptive filtering, classical washout filtering and model predictive control-based filtering are implemented. All algorithms tend to give false cues except model predictive control-based algorithm. But perceptions produced by model predictive control-based algorithm was found unnatural by users [31]. Three motion cueing algorithms were implemented into a two degrees of freedom small

simulator by Neheoua et al. No significant difference between algorithms was observed according to experimental results [32]. Implementing a motion cueing algorithm, into a simulator is a difficult task. Since motion cueing algorithms consist of linear and non-linear filters, some filter parameters such ass cut off frequency value and damping value are needed to be tuned. Filter parameter of motion cueing algorithm were tuned by using genetic algorithm by Asadi et al. and noticeable reduction was observed in terms of false cue production of filters [33]. Same tuning method was studied by Asadi et al. but in mentioned study linear quadratic regulator based motion cueing algorithm was used and more realistic perception was obtained [34]. Particle swarm optimization is a well-known optimization method in literature. Motion cueing filter parameters were optimized and reasonable positive difference was obtained by Asadi et al. [35]. Tuning of motion cueing algorithm parameters is a manual operation. Therefore, it is time consuming and its success is limited by tuning operator. Tuning operation was automized and speeded up by Casas et al. and performance improvement was achieved [17]. Motion cueing is not only important for flight simulator also it is important for other type of simulators. Importance of motion cueing algorithm in driving simulation is presented by Pais et al. [36]. Motion cueing is not only parameter for simulation perception reality. Effect of simulator working space on simulator realism was studied Feenstra et al. [37]. Preparing a simulator cockpit is not a cheap operation. Therefore, producing a new cockpit for every vehicle is time-consuming and expensive. A universal cockpit was presented by Heesbeen et al. for overcoming these disadvantages [38]. Simulator usage is not only limited by pilot training. Some simulator studies were based on aircraft flight characteristic development. A six degree of flight simulator was used to improve a light aircraft flight characteristic by Coiro et al. [39].

2.3 Control studies

Flight simulators are dynamic devices which move in order to create real flight perception. Dynamics of vehicle which is going to be simulated is should be known as the first step of flight simulation. Beside dynamics of simulated vehicle also, environmental effects are should be taken into account. These environmental effects such as atmosphere conditions which the aircraft fly in, air density, air temperature, weather conditions wind speed etc. directly affect the air vehicle. Many flight simulator software packages are available in the market in order to complete this dynamic calculation task. These softwares are also capable to simulate more complex case like failures in the air vehicle and more tough whether conditions. Main purpose of flight simulation software packages is to create visual and auditory cues for user. Linear acceleration and angular velocity values are extracted via auxiliary software package and these numerical values are sent into motion cueing algorithm [40]. Translational acceleration and angular velocity values are input of the motion cueing algorithm [41].Motion cueing algorithm filters these values and at the end of the filtering operation integrates angular acceleration values and creates angular position values, and in the same manner double integrate the filtered translational acceleration

values in order to create translational position values [18]. Translational and angular position values are ready to send to motion platform of the flight simulator. Therefore, motion platform of flight simulator should be position controlled. Many modern control and classical control methods are available in literature. The most well-known classical control method is PID control undoubtedly. PID controller is easy to apply and it has very wide application fields in industry. Since PID controller designed for linear applications, it is not successful enough for more complex applications. Therefore, in this study two types state feedback controller is studied. Pole placement method is used as the first control method and linear quadratic regulator controller is used as the second control method [42].

Parallel manipulators are used for motion platform for flight simulators. Flight simulator payloads are usually heavy since it carries simulator cockpit equipment and pilot. Therefore, hydraulic actuated parallel manipulators are usually used for flight simulator motion platforms. Stewart platform is the most widely used for simulator applications due to its six degrees of freedom and payload capacity [43]. Stewart platform is also known as hexapod mechanism in simulator literature. The control of parallel manipulators should be well known and for this reason, when the literature for flight simulators is examined, it is seen that control studies are mainly centred around the Stewart platform. Force computations and four different control methods for hydraulic actuated Stewart platform were studied by Chin et al. [44]. In paper published. Path tracking with a possible minimum tracking error was aimed and achieved. Stewart platforms are driven with electro-hydraulic actuators as well as hydraulic actuators. Electro-hydraulic actuated Stewart platform control study was carried out by Davliakos and Papadopoulos [45]. A novel impedance control method was applied to motion platform and results were compared with PD control. Impedance control method was more successful than PD control. Controller design both includes linear and non-linear controllers. Non-linear robust controller was designed for six degrees of freedom parallel manipulator by Kim et al. [46]. Beside robust controller a friction estimator was added to control algorithm. Robust control with friction estimator was superior to proportional plus integral plus derivative controller with friction estimator. Forward kinematics based controller algorithm was designed for six degrees of freedom by Chen and Fu [47]. Non-linear observer was used for designing controller. Since inverse kinematics needs to big computational cost, researcher aimed to reduce computational cost for real-time applications. Model-based controllers are very common for electro-mechanical systems. But when it comes to hydraulic actuated systems, applying model-based controller is not straight forward due to non-linear dynamics of system. Application method for model-based controller was presented by Honegger and Corke [48].

2.4 Problem Statement

In this chapter brief summary of literature review about flight simulator and related studies is presented. Flight simulator studies It has been observed that most of the flight simulator studies are related to the motion perception algorithm and the Stewart

platform is generally preferred as the motion platform. The limited number of studies on flight simulator motion platforms in the literature and the limited motion capabilities of the existing motion platforms such as the Stewart platform require the design of a simulator with better motion capability.

CHAPTER III

DESIGN AND MANUFACTURING OF SPHERICAL FLIGHT SIMULATOR

3.1 Computer aided design

Flight simulator physical hardware is a mechanical machine that works under external and inertial loads. This machine usually has movable parts and joints. A set of analysis are essential when it comes to a mechanical machine. Ozturk and Gov, performed kinematic analysis of spherical flight simulator, they used rotation matrix method to obtain kinematic parameters of simulator analytically, and they validated analytical results with numerical analysis [49]. Since spherical flight simulator has similar structure with gimbal like mechanical systems, they can be treated as gimbal in dynamical perspective. Usubamatov, derived mathematical model of a similar structure and examined motion characteristics of the system. At the end of the study, he collated mathematical results with experimental results [50]. Static structural analysis is also should be considered for mechanisms and machines as well. Because, in kinematic and dynamic analysis case, all parts of machine are assumed as they do not deform under applied loads. But, in real life applications, machine links and parts deform under loads. Therefore, deformations of parts and stresses on parts have great importance and they are not negligible. Computer aided design is the starting point of design process. In this study models with two different geometries designed by using computer aided design software SOLIDWORKS. Flight simulator consists of three nested spherical like structures Figure 3.1. Each structure can rotate relative to each other by means of revolute joints which are formed by ball bearings [51].

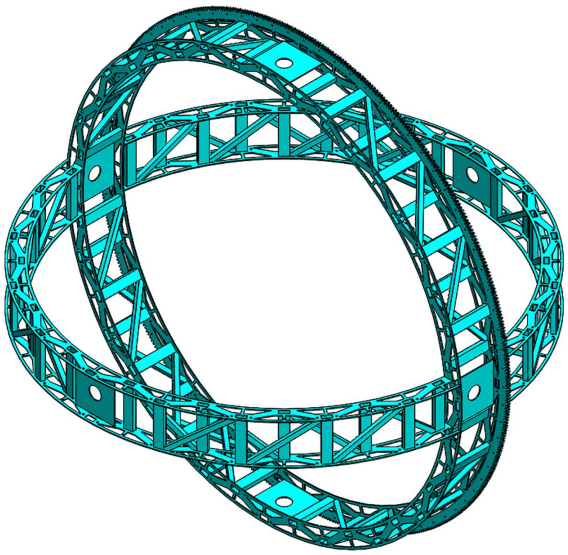

Figure 3.1 Inner part of the first model of flight simulator.

All three rotating parts of the flight simulator have external gear and they are designed to be driven with dc motors.

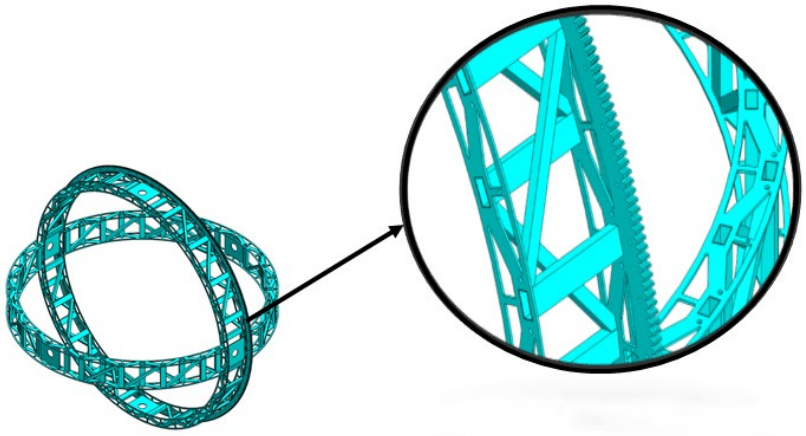

Figure3.2 Detail view of external gear.

All three rotating parts have same geometry and the only difference between parts is dimensions. Each part consists of two vertical circular structure. 20x40x1.2 mm steel hollow sections are used for vertical supports and 20x20x1 mm steel hollow sections are used for cross supports. Assembly of whole system is can be seen figure below. Three nested structures rotate about their rotation axis and three rotation axes are perpendicular to each other. These three-rotation motion enables inner part of the flight simulator to has three rotational degrees of freedom. A base carries all three parts and St-52 steel is selected for spherical flight simulator material.

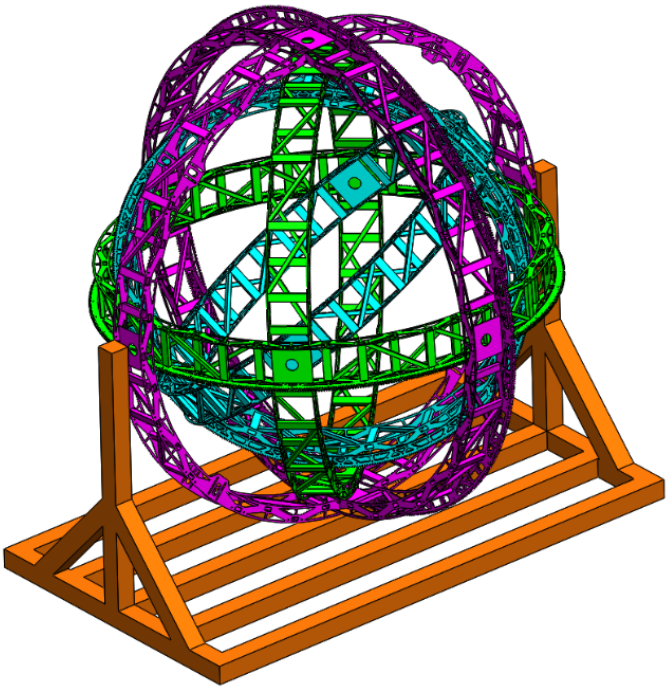

Figure 3.3 Assembly of the first model of flight simulator.

Second model of the spherical flight simulator has same dimensions as the first model. But every rotating part of the simulator is covered with 1 mm thick sheet steel metal.

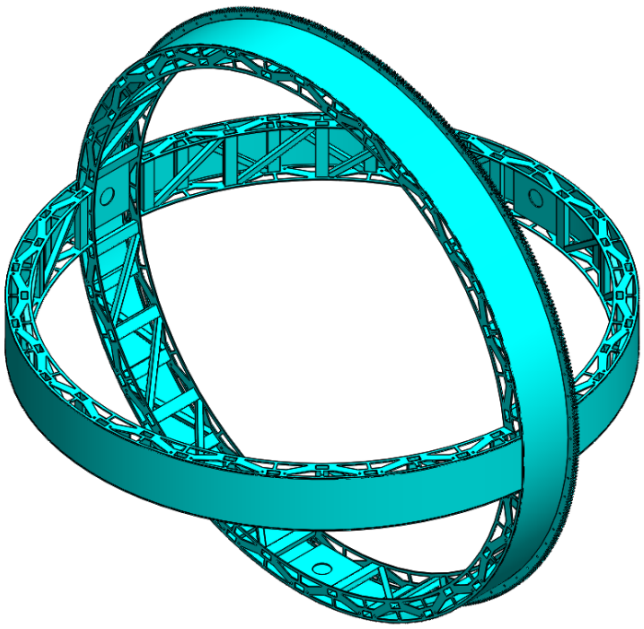

Figure 3.4 Inner part of the second model of flight simulator.

Since other parts of the simulator are same in terms of geometry, and only differences are dimensions and weight, middle part and outer part of the second model are not given as separately in figures.

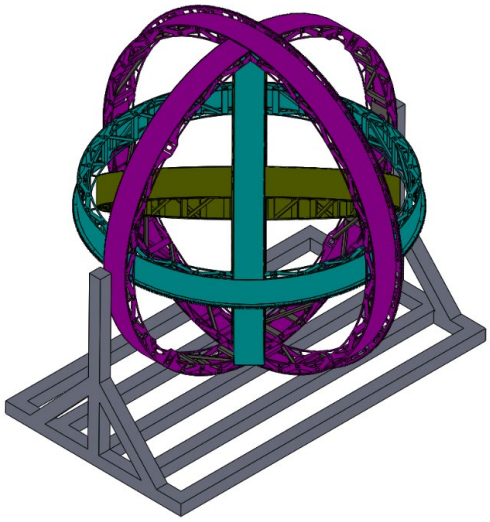

Figure 3.5 Assembly of the second model of flight simulator.

Diameters of the spherical flight simulator and their masses are given in Table 1. below.

Table 3.1 Physical properties of the simulator parts.

	First Model		Second Model	
	Diameter (mm)	**Mass (kg)**	**Diameter (mm)**	**Mass (kg)**
Inner Part	1960	90.97	1960	106.88
Middle Part	2220	100.23	2220	116.9
Outer Part	2480	115.81	2480	133.92

3.1.2 Static Structural Analysis of Spherical Flight Simulator

Flight simulator structure is subjected to payload in addition to its own weight.

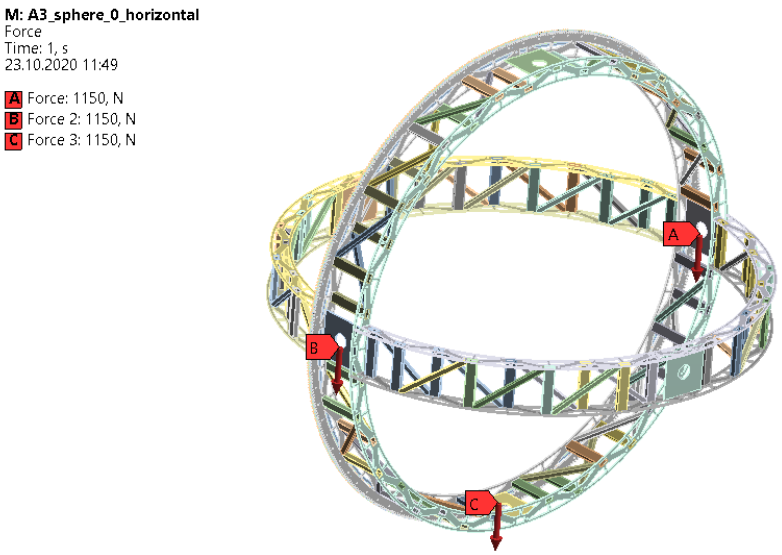

Figure 3.6 Applied forces on inner part of the first model flight simulator.

This payload includes electrical and mechanical hardware and pilot weight. In this study payload is determined as 250 kg. 250 kg payload and 90.97 kg inner part load are divided three equal forces and applied as in Figure 3.7.

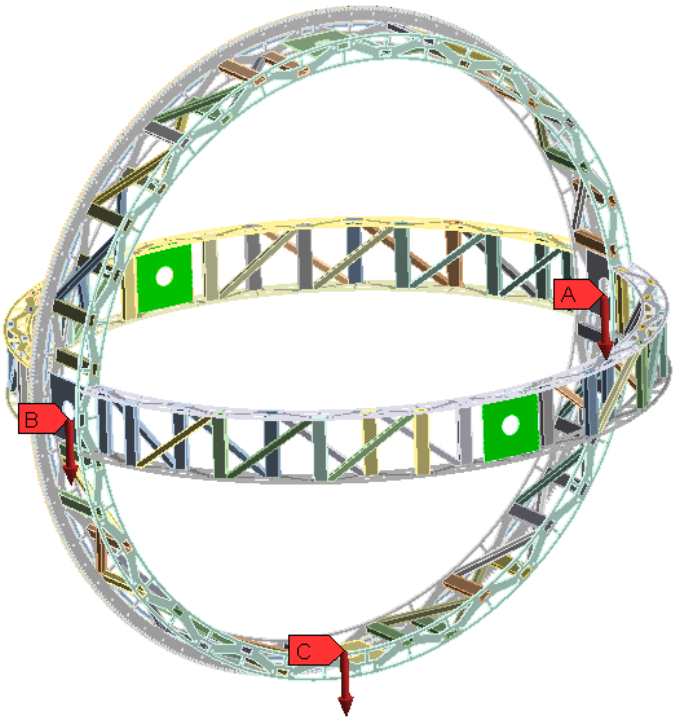

Figure 3.7 Fixed support locations on inner part of the first model flight simulator.

Fixed supports are utilized as boundary condition to green coloured mounts. Those mounts hold bearings for real life application.

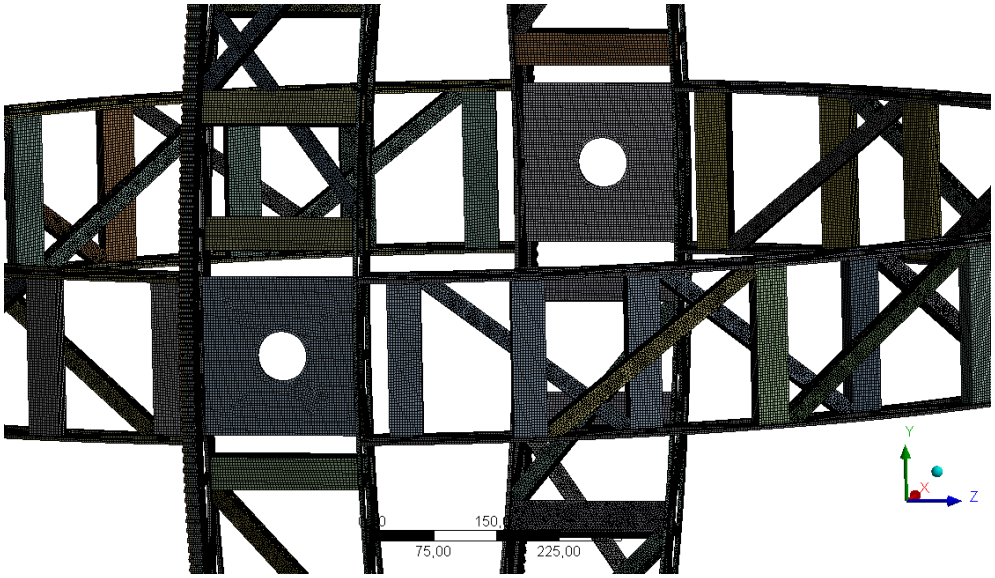

Figure 3.8 Mesh view of inner part of the first model flight simulator.

After meshing operation in ANSYS, element number is obtained as 494571.

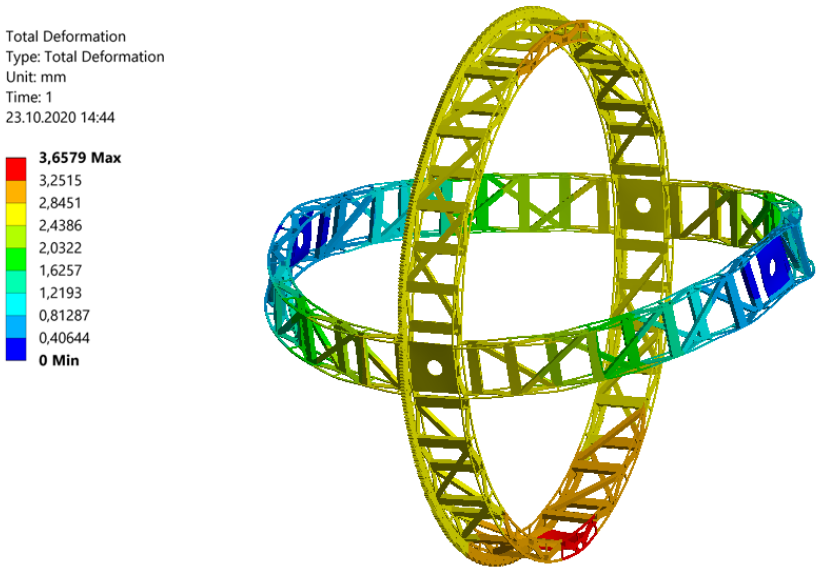

Figure 3.9 Deformed view of inner part of the first model flight simulator.

Deformation value is obtained as 3.65 mm for the inner part of the flight simulator.

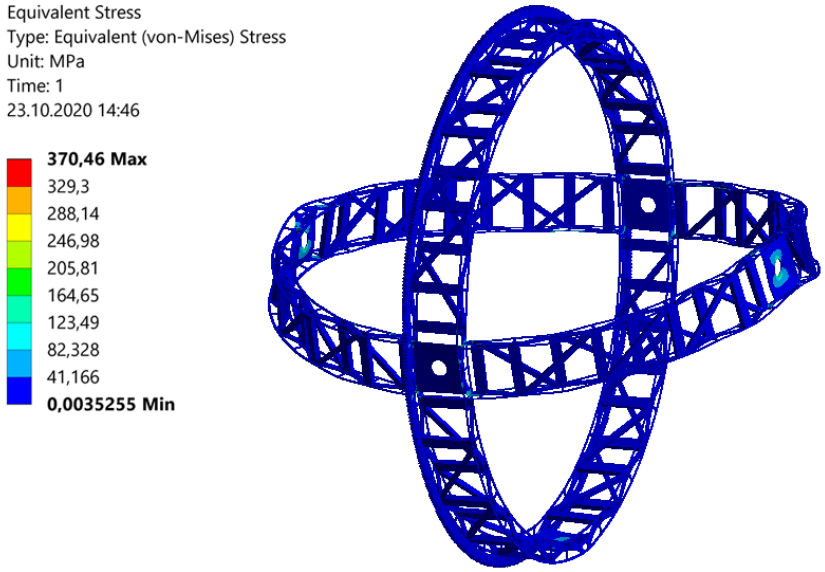

Figure 3.10 Von-Mises stress for inner part of the first model flight simulator.

Stress value for the inner part of the flight simulator is obtained as 370 MPa.

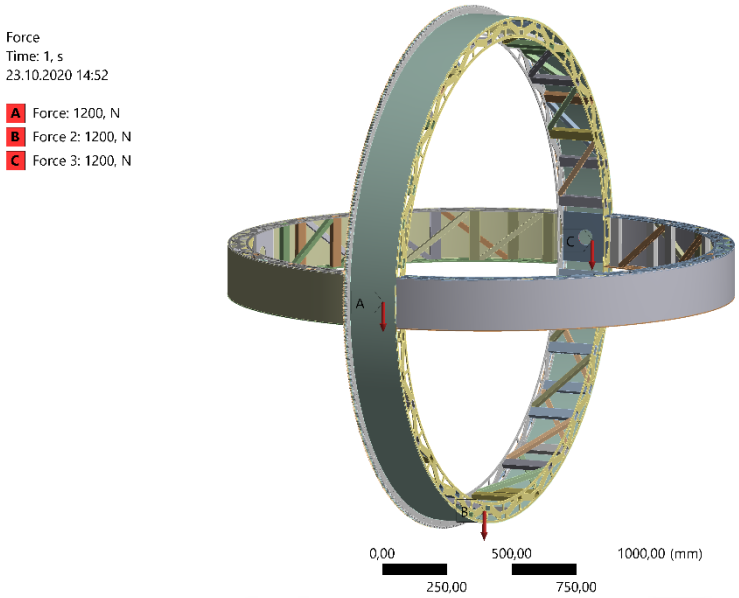

Figure 3.11 Applied forces on inner part of the second model flight simulator.

250 kg payload and 106.80 kg inner part load are divided three equal forces and applied as in Figure 3.11.

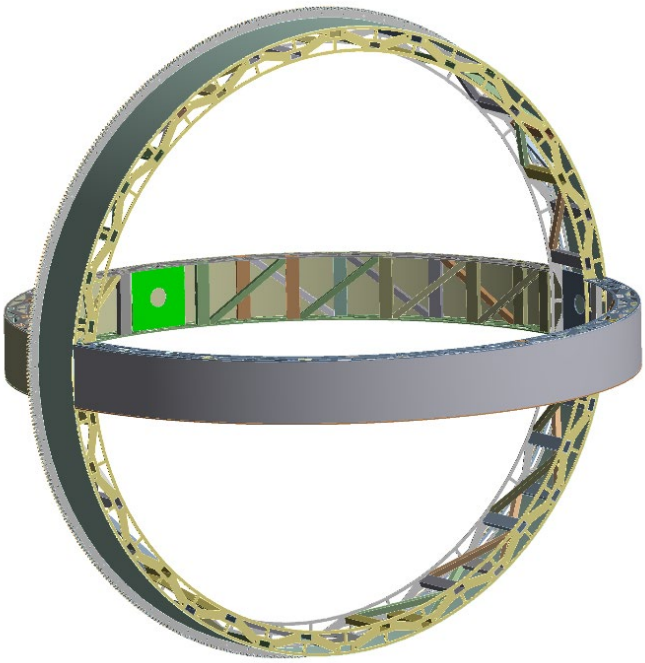

Figure 3.12 Fixed support locations on inner part of the second model flight simulator.

Fixed supports are utilized as boundary condition to green-coloured mounts. Those mounts hold bearings for real life application. Two fixed supports are assigned but second fixed support is cannot be seen in Figure 3.12 due to geometry.

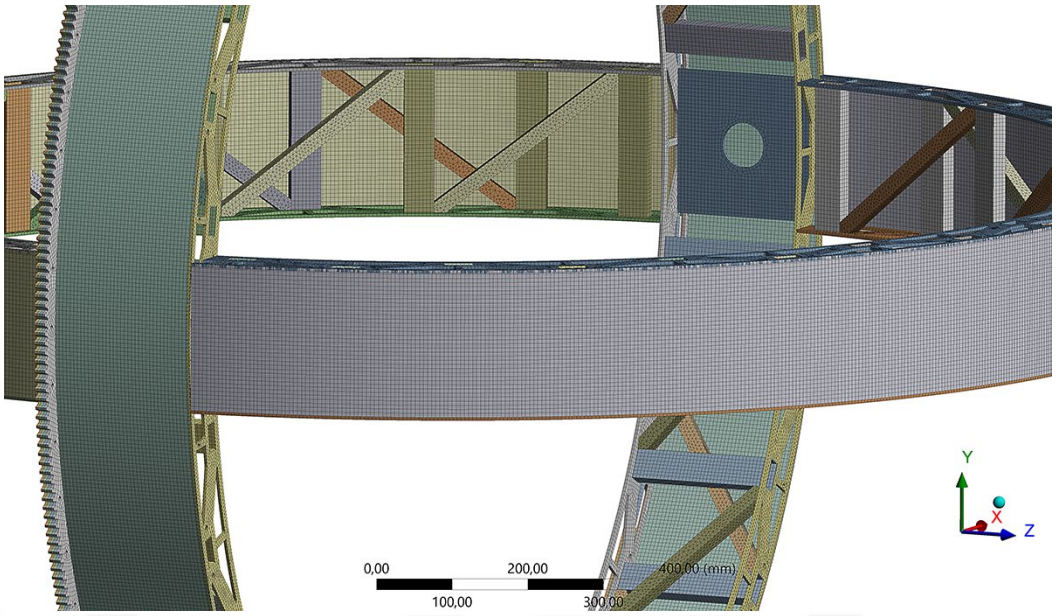

Figure 3.13 Mesh view of inner part of the second model flight simulator.

After meshing operation in ANSYS, element number is obtained as 587555 Figure 3.13.

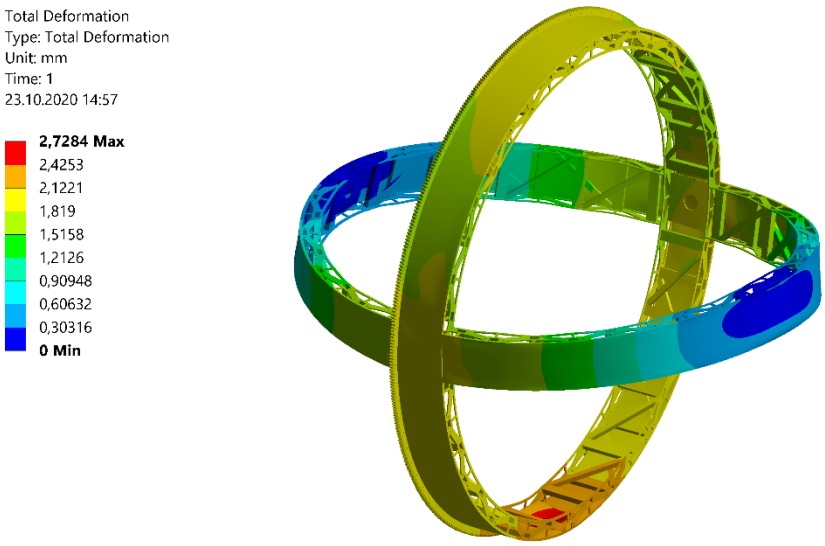

Figure 3.14 Deformed view of inner part of the second model flight simulator.

Deformation value is obtained as 2.72 mm for the inner part of the flight simulator in Figure 3.14.

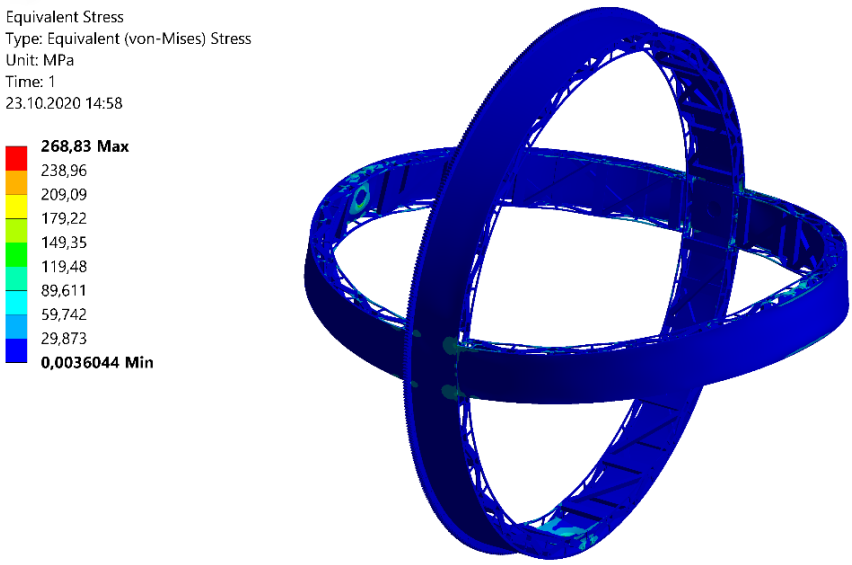

Figure 3.15 Von-Mises stress for inner part of the second model flight simulator.

Stress value for the inner part of the flight simulator is obtained as 268 MPa in Figure 3.15. Since other parts of all of two flight simulators are same as geometrically, it is not necessary to add their solid models. In addition, applied load and fixed support locations, and their deformed shapes are same as given figures. Therefore, analysis result and physical data of remain parts is given as tabulated in Table 3.2 and Table 3.3.

Table 3.2 Results for the first model flight simulator.

First Model				
	number of elements	**mass (kg)**	**deformation (mm)**	**stress (MPa)**
Inner Part	494571	90.97	3.7	370
Middle Part	582914	100.23	4	434
Outer Part	994835	115.81	5.5	547

Since outer part carries middle part and inner part in addition to its own weight, the biggest stress and deformation occurs on it.

Table 3.3 Results for the second model flight simulator.

Second Model				
	number of elements	**mass (kg)**	**deformation (mm)**	**stress (MPa)**
Inner Part	587555	106.88	2.7	268
Middle Part	708750	116.9	3	321
Outer Part	1101013	133.92	4.1	394

Analysis results can be observed in Table 3.3 Main difference between first model and second model is, parts form second model flight simulator are covered 1 mm thick steel sheet metal. Due to this covering operation, weight of every part is increased approximately by 17%. On the other hand, while weight increases, stress and deformation values decrease by 27%. Since, static analysis in ANSYS is based on numerical method, these methods can contain some solutions error. Even so, it is a good starting point for real life applications. Since deformation and stress values are not so sufficient, a third belt is decided to add for each sphere. This third belt also balances mass moment of inertia. Spheres of spherical flight simulator are decided to be redesigned due to mass moment of inertia distribution and strength issues.

Based on the problem definition mentioned in chapter 2, a design with three rotational degrees of freedom is considered appropriate to overcome the lack of flight simulator studies [52-54]. Computer aided design is the starting point of design process. Flight simulator consists of three nested spherical like structures. Each structure can rotate relative to each other by means of revolute joints which are formed by ball bearings.

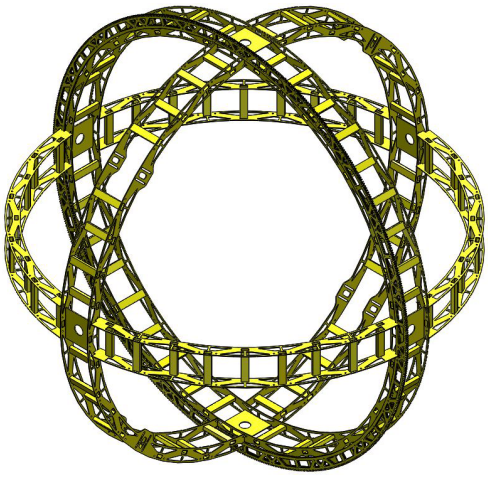

Figure 3.16 Sphere of flight simulator.

Figure 3.16 shows one of three identical spheres. Each sphere is identical by geometry but their dimensions are different

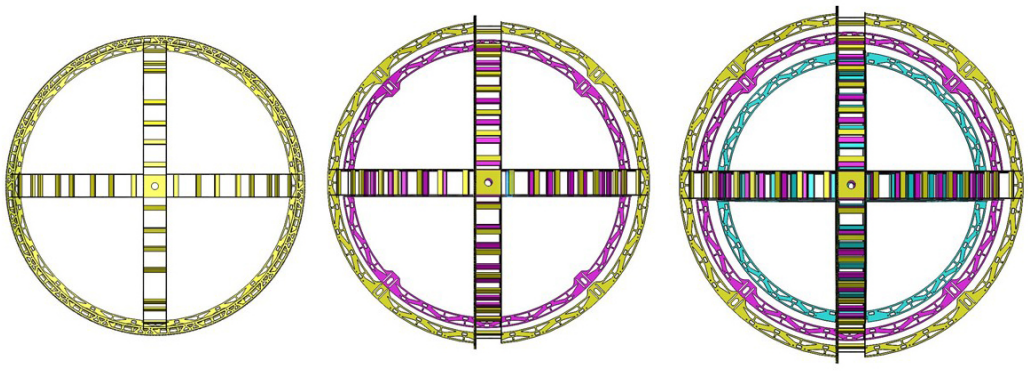

Figure 3.17 Spheres assembly front view.

Figure 3.17 shows three spheres and their assembly view. From outside to in, yellow part is the outer sphere, pink part is the middle sphere and cyan part is the inner sphere.

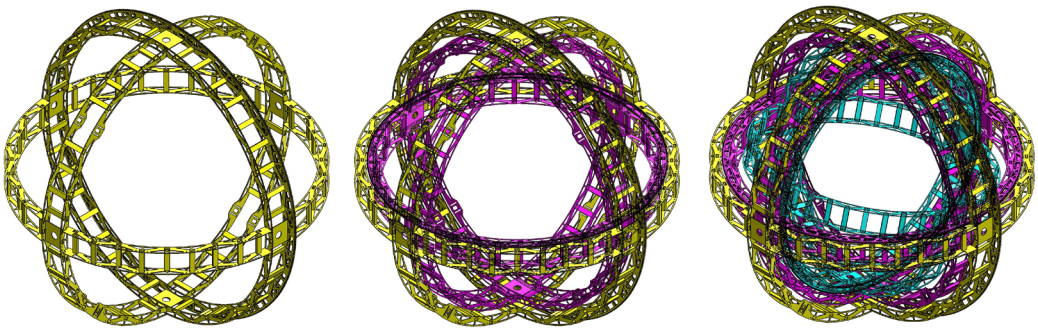

Figure 3.18 Spheres assembly isometric view.

Isometric assembly view of spheres can be seen in Figure 3.18.

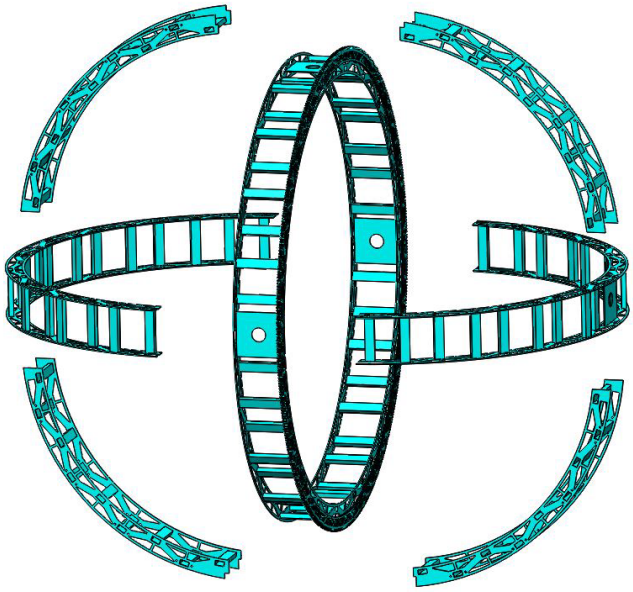

Figure 3.19 Sphere sub-assembly exploded view.

Figure 3.19 shows sub-assembly sections of one sphere. One sphere consists of one full circle, two half circles and four quarter circles.

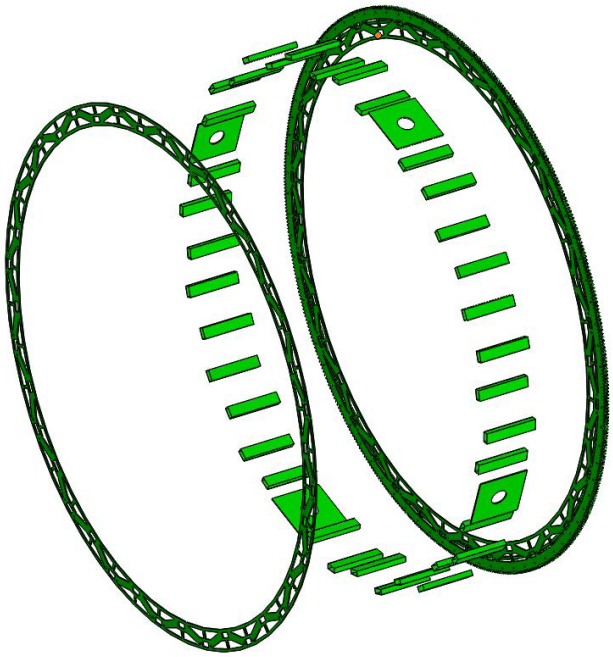

Figure 3.20 Full circle exploded view.

All parts of spheres are designed to be cut from sheet metal. For full circle sheet metal parts and hallow sections are available in Figure 3.20. There is one full circle sub assembly for each sphere and three full circle sub-assemblies in total.

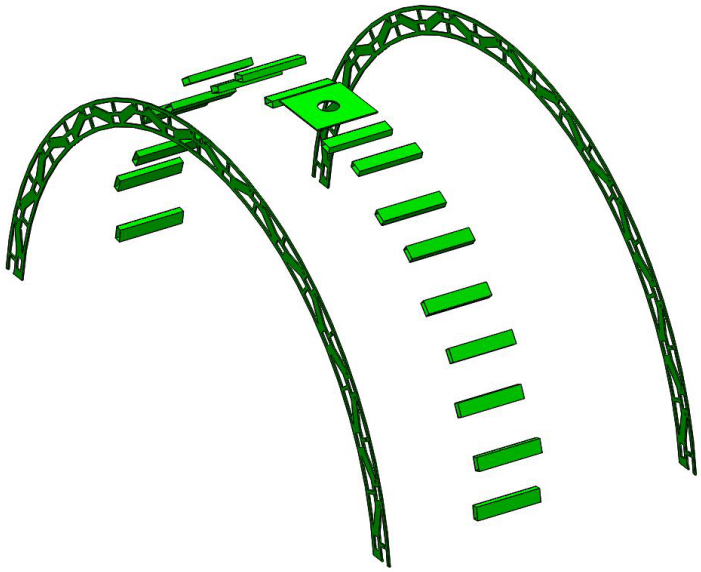

Figure 3.21 Semi circle exploded view.

For half circle sheet metal parts and hallow sections are available in Figure 3.21. There are two half circle sub-assemblies for each sphere and six half circle sub-assemblies in total.

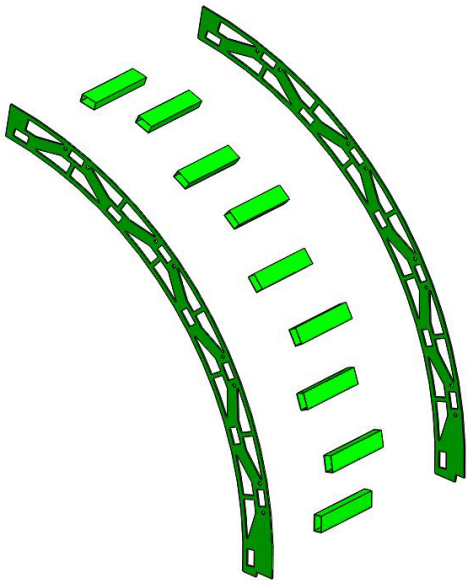

Figure 3.22 Quarter circle assembly view.

For quarter circle sheet metal parts and hallow sections are available in Figure 3.22. There are four half circle sub-assemblies for each sphere and twelve half circle sub-assemblies in total.

Figure 3.23 Full circle laser cut parts.

Full circle laser cut parts are joined by welding operation and in some place, they are fastened with bolted joints. One side of full circle and parts before assembly can be seen in Figure 3.23.

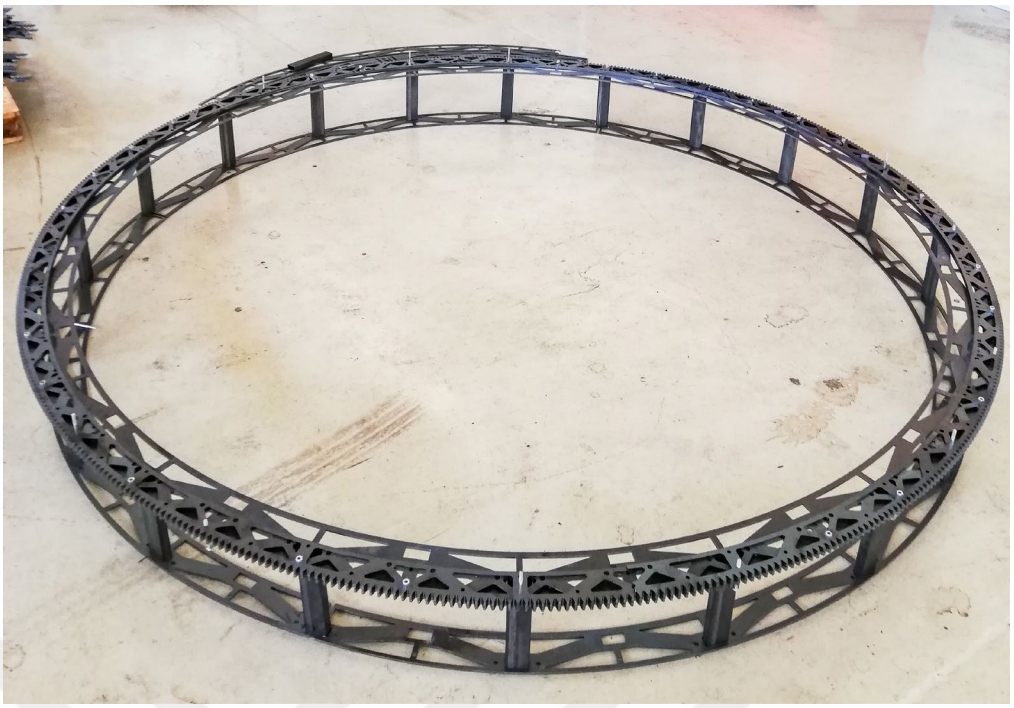

Figure 3.24 Full circle.

Final shape of assembled full circle is available in Figure 3.24. Full circle is ready to be used as base part for half circle and quarter circle assemblies.

Figure 3.25 Half circles.

Half circle assemblies are produced and ready for further assembly in Figure 3.25. Since quarter circle assemblies are produced in a same way there is no needed to give an extra image.

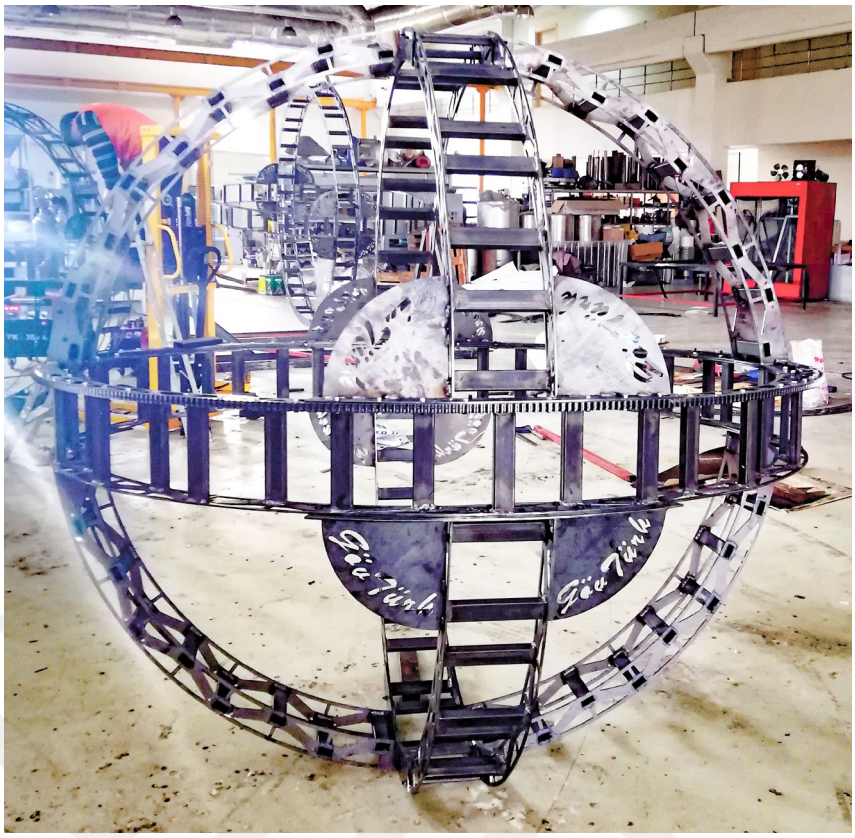

Figure 3.26 Manufactured sphere.

Figure 3.27 Spherical flight simulator assembly view.

The last form of a sphere after all assembly and production process is given in Figure 3.27. These mentioned production steps are same for all three spheres. After three spheres are ready, three sphere located to be formed a nested spheres structure. At the end three nested sphere assembly is mounted to a main chassis to form final spherical flight simulator.

Figure 3.28 Spherical flight simulator side view.

Proposed spherical flight simulator structure assembly is given in Fig. 3.27. and in Fig. 3.28 side view of assembly is available.

CHAPTER IV

MATHEMATICAL MODELLING OF FLIGHT SIMULATOR

4.1. Kinematic Analysis of Flight Simulator

Kinematics is a branch of science that deals with motion of particles, bodies and group of particles or bodies. Kinematics is referred to “shape of the motion” or “geometry of motion” which means kinematics is only considers position, velocity, acceleration and time relationship of motion without considering forces cause the motion. Spherical flight simulator is a multibody system which consists of three spheres physically linked each other. Therefore, absolute position, absolute velocity and absolute acceleration relationship between spheres should be derived by using kinematic principles.

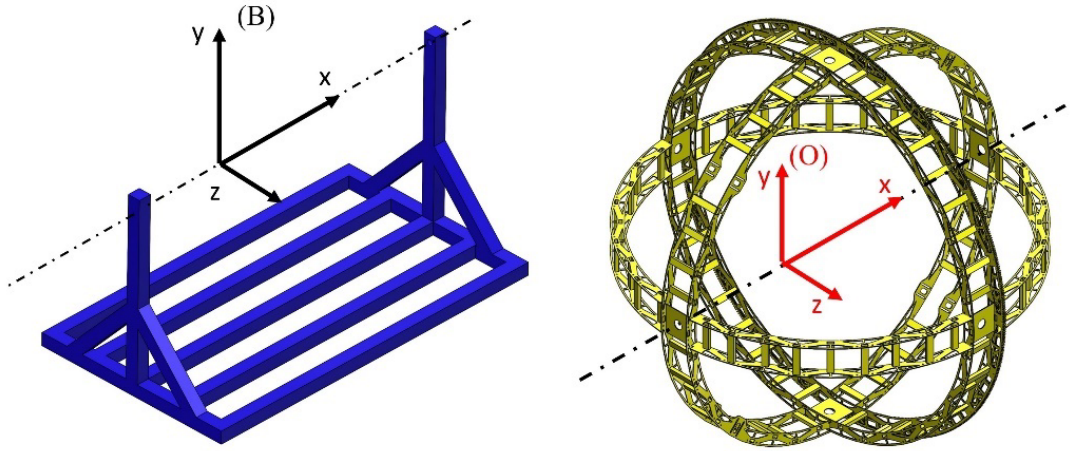

Figure 4.1 Base and outer sphere and their reference coordinate frames.

Each sphere that makes up the spherical flight simulator has rotational degrees of freedom. The inner sphere is mounted on the middle sphere, the middle sphere on the outer sphere and the outer sphere on the main chassis of the simulator. Kinematic problem starts with determination of fixed (earth) coordinate frame and moving coordinate frames. Figure 4.1 shows the main chassis (base part) and main chassis coordinate frame (B) and outer sphere and outer sphere coordinate frame (O).

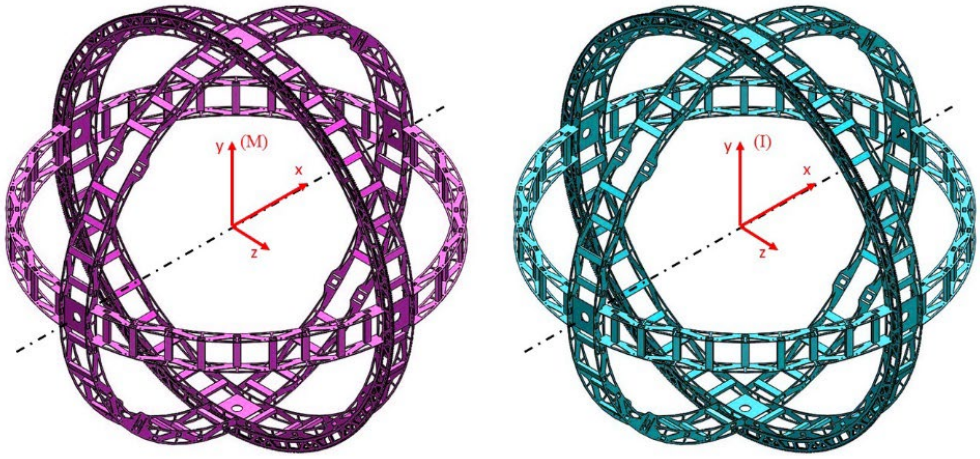

Figure 4.2 Middle and outer sphere and their reference coordinate frames.

Figure 4.2 shows the middle sphere and middle sphere coordinate frame (M) and inner sphere and inner sphere coordinate frame (I).

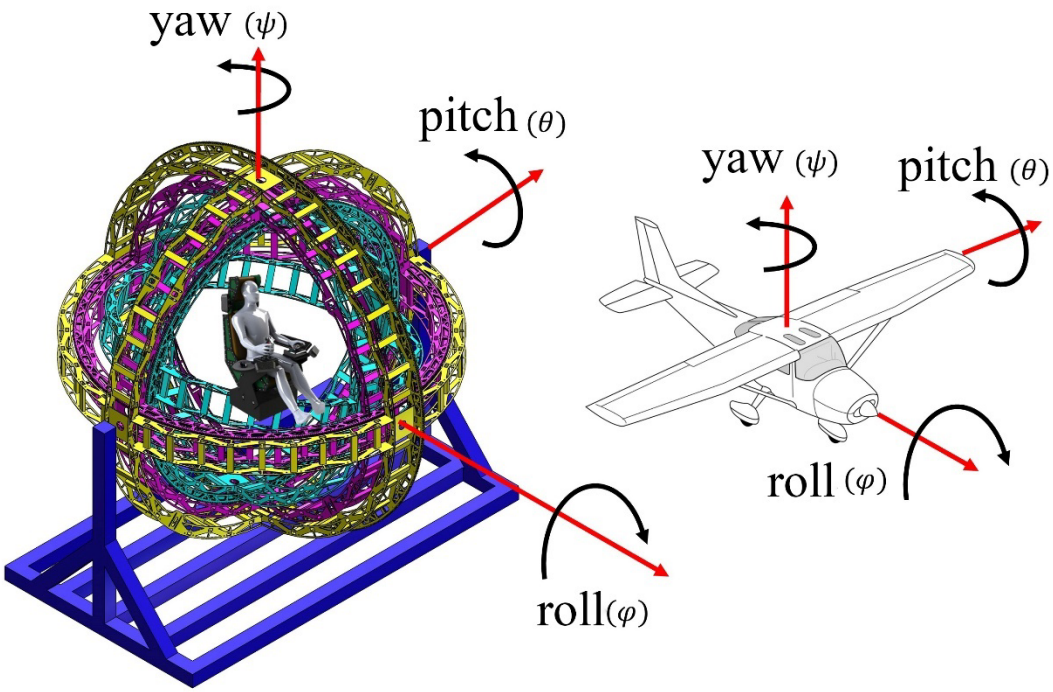

Figure 4.3 Roll, pitch and yaw angles.

Spherical flight simulator is designed to rotate and simulate aircraft manoeuvres Figure 4.3 shows aircraft manoeuvre angles and corresponding flight simulator angles.

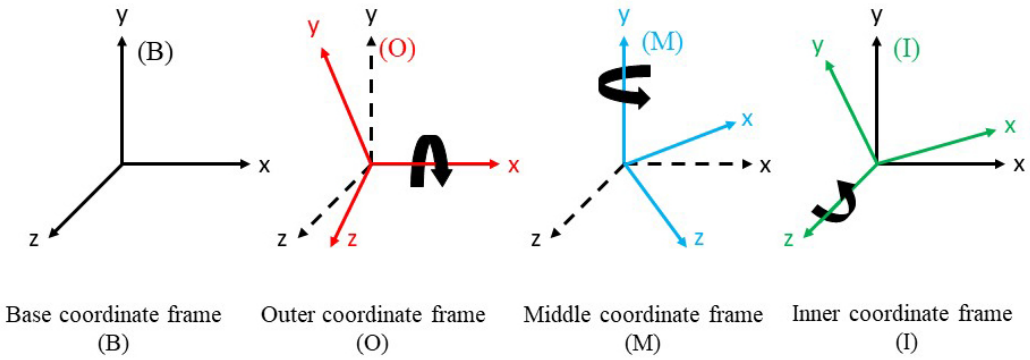

Figure 4.4 Flight simulator coordinate frames.

The coordinate frames and orientations to be used for the kinematic and dynamic analyses of the spherical flight simulator are given in Figure 4.4. The origins of the four coordinate frames in total are coincident, and the ground coordinate frame (B) are fixed. The outer sphere coordinate frame (O) is positioned so that it can rotate about the 'x' axis of the base coordinate frame (B). The angle of rotation here is called “θ”. Likewise, the middle sphere coordinate frame (M) is placed in such a way that it can rotate around the 'y' axis of the outer sphere coordinate frame (O) and this rotation angle is called "Ψ". The rotation movement of the inner sphere coordinate frame (I), which is the last coordinate frame, is around the 'z' axis of the middle sphere coordinate frame (M), and the rotation angle is named as "Φ".

Coordinate frames are mathematically connected to each other by transformation matrices. Transformation matrices are used to project a vector displayed in one coordinate frame to another coordinate frame. The relationships between coordinate frames are shown in Figure 4.5.

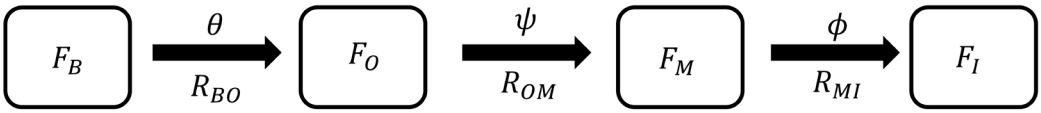

Figure 4.5 Coordinate frame relations.

Point P is arbitrarily located in Figure 4.6 Frame 0 is attached to fix point so it is inertial coordinate frame and frame 1 is relative coordinate frame. When frame 1 is rotated about Z axis of frame 0, relation between location of point P according to frame 0 and location of point P according to frame 1 is called Pure rotation coordinate transformation.

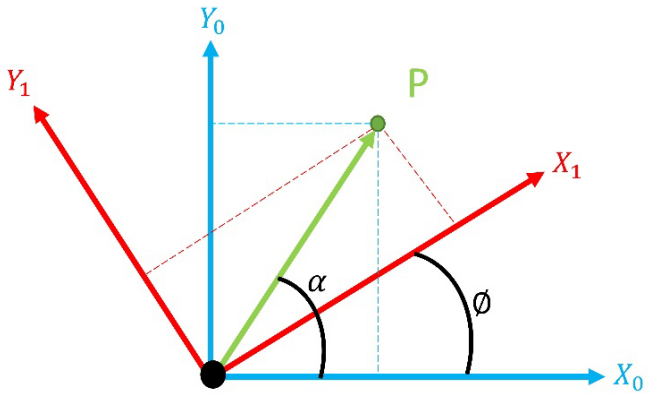

Figure 4.6 Pure rotation of coordinate frame.

Location of point P according to frame 0 are written as follows;

$$x_o = r\,cos\alpha \tag{4.1}$$

$$y_o = r\,sin\alpha \tag{4.2}$$

Location of point P according to frame 1 are written as follows;

$$x_1 = r\,cos(\alpha - \Phi) \tag{4.3}$$

$$y_1 = r\,sin(\alpha - \Phi) \tag{4.4}$$

$$x_1 = r\,cos\alpha\,cos\Phi + r\,sin\alpha\,sin\Phi \tag{4.5}$$

$$y_1 = r\,sin\alpha\,cos\Phi - r\,cos\alpha\,sin\Phi \tag{4.6}$$

If equation 4.1 and 4.2 is substituted to equation 4.5 and 4.6, equations become;

$$x_1 = x_0\ cos\Phi + y_0\,sin\Phi \tag{4.7}$$

$$y_1 = -x_0\ sin\Phi + y_0\,cos\Phi \tag{4.8}$$

Equation 4.7 and 4.8 in matrix form;

$$\begin{bmatrix} x_1 \\ y_1 \end{bmatrix} = \begin{bmatrix} cos\Phi & sin\Phi \\ -sin\Phi & cos\Phi \end{bmatrix} \begin{bmatrix} x_0 \\ y_0 \end{bmatrix} \tag{4.9}$$

The matrix which consists of trigonometric terms is called rotation matrix and it shows rotation about Z axis amount of Φ.

In a same manner, if we write rotation matrices for three-dimensional case one row should be added to rotation matrix.

The rotation matrix between the base (B) and the outer sphere coordinate frames (O) provides a vector shown in the base coordinate frame (B) to be projected onto the outer sphere coordinate frame (O) Eq.10.

$$R_{BO} = \begin{bmatrix} 1 & 0 & 0 \\ 0 & cos\theta & sin\theta \\ 0 & -sin\theta & cos\theta \end{bmatrix} \tag{4.10}$$

The rotation matrix between the outer sphere coordinate frame (O) and the middle sphere coordinate frames (M) provides a vector shown in the outer sphere coordinate frame (O) to be projected onto the middle sphere coordinate frame (M) Eq. 4.11.

$$R_{OM} = \begin{bmatrix} cos\psi & 0 & sin\psi \\ 0 & 1 & 0 \\ -sin\psi & 0 & cos\psi \end{bmatrix} \tag{4.11}$$

The rotation matrix between the middle sphere coordinate frame (M) and the inner sphere coordinate frames (I) provides a vector shown in the middle sphere coordinate frame (M) to be projected onto the inner sphere coordinate frame (I) Eq. 4.12.

$$R_{MI} = \begin{bmatrix} cos\phi & -sin\phi & 0 \\ sin\phi & cos\phi & 0 \\ 0 & 0 & 1 \end{bmatrix} \tag{4.12}$$

In case of reversing the projection direction of an arbitrary vector from one coordinate frame to another coordinate frame, transposes of rotation matrices are used Eq. 4.13-4.15

$$R_{OB} = \begin{bmatrix} 1 & 0 & 0 \\ 0 & cos\theta & -sin\theta \\ 0 & sin\theta & cos\theta \end{bmatrix} = R_{BO}^{T} \tag{4.13}$$

$$R_{MO} = \begin{bmatrix} cos\psi & 0 & -sin\psi \\ 0 & 1 & 0 \\ sin\psi & 0 & cos\psi \end{bmatrix} = R_{OM}^{T} \tag{4.14}$$

$$R_{IM} = \begin{bmatrix} cos\phi & sin\phi & 0 \\ -sin\phi & cos\phi & 0 \\ 0 & 0 & 1 \end{bmatrix} = R_{MI}^{T} \tag{4.15}$$

Before writing the kinematic equations, the unit vectors of the coordinate frames should be determined. Unit vectors of coordinate frames are expressed in Eq. 4.16-4.18.

$$\vec{u}_x = \begin{bmatrix} 1 \\ 0 \\ 0 \end{bmatrix} \tag{4.16}$$

$$\vec{u}_y = \begin{bmatrix} 0 \\ 1 \\ 0 \end{bmatrix} \tag{4.17}$$

$$\vec{u}_z = \begin{bmatrix} 0 \\ 0 \\ 1 \end{bmatrix} \tag{4.18}$$

Unit vectors expressed in Eq.16, Eq.17 and Eq.18 represents unit vectors in "x"," y" and "z" axis respectively. Since all of three degrees of freedom of spherical flight simulator is rotational type, spheres of flight simulator are only able to do rotational motion. Inner sphere is chosen for taking all measurements and deriving equations of motion because the cockpit is planned to locate in inner sphere. Angular velocity expressions are should be written according to inner sphere coordinate frame. Accordingly, spheres angular velocities are written in Eq. 4.19, Eq. 4.20 and Eq. 4.21 respectively.

$$\vec{\Omega}_O = R_{BO}\vec{\Omega}_B + \dot{\theta}\vec{u}_x \tag{4.19}$$

$$\vec{\Omega}_M = R_{OM}\vec{\Omega}_O + \dot{\psi}\vec{u}_y \tag{4.20}$$

$$\vec{\Omega}_I = R_{MI}\vec{\Omega}_M + \dot{\phi}\vec{u}_z \tag{4.21}$$

$$\vec{\Omega}_O = \begin{bmatrix}\theta_{Ox}\\ \theta_{Oy}\\ \theta_{Oz}\end{bmatrix} = \begin{bmatrix}\dot{\theta}\\ 0\\ 0\end{bmatrix} \tag{4.22}$$

$$\vec{\Omega}_M = \begin{bmatrix}\theta_{Mx}\\ \theta_{My}\\ \theta_{Mz}\end{bmatrix} = \begin{bmatrix}cos\psi\dot{\theta}\\ \dot{\psi}\\ -sin\psi\dot{\theta}\end{bmatrix} \tag{4.23}$$

$$\vec{\Omega}_I = \begin{bmatrix}\theta_{Ix}\\ \theta_{Iy}\\ \theta_{Iz}\end{bmatrix} = \begin{bmatrix}cos\phi cos\psi\dot{\theta} - sin\phi\dot{\psi}\\ cos\psi sin\phi\dot{\theta} + cos\phi\dot{\psi}\\ \dot{\phi} - sin\psi\dot{\theta}\end{bmatrix} \tag{4.24}$$

The calculation of the angular velocities of the spheres is a necessary step for the mathematical modelling of the spherical flight simulator. While creating the mathematical model of the simulator, the angular velocities must be known precisely both for the calculation of the angular momentum when using the Newton-Euler method, which is one of the classical mechanics methods, and for the calculation of the kinetic energy of the system when using the Lagrange-Hamilton principle, which is one of the analytical dynamics methods.

Angular acceleration vector is time derivative of angular velocity vector. Angular acceleration is important for deriving total external moment angular acceleration relationship equation which is called Euler law. Angular acceleration vectors are given Eq. 4.26-4.28.

$$\vec{\alpha} = \frac{d}{dt}\vec{\Omega} \tag{4.25}$$

$$\vec{\alpha}_O = \begin{bmatrix}\alpha_{Ox}\\ \alpha_{Oy}\\ \alpha_{Oz}\end{bmatrix} = \begin{bmatrix}\ddot{\theta}\\ 0\\ 0\end{bmatrix} \tag{4.26}$$

$$\vec{\alpha}_M = \begin{bmatrix} \alpha_{Mx} \\ \alpha_{My} \\ \alpha_{Mz} \end{bmatrix} = \begin{bmatrix} cos\psi\ddot{\theta} - sin\psi\dot{\psi}\dot{\theta} \\ \ddot{\psi} \\ -sin\psi\ddot{\theta} - cos\psi\dot{\psi}\dot{\theta} \end{bmatrix} \tag{4.27}$$

$$\vec{\alpha}_I = \begin{bmatrix} \alpha_{Ix} \\ \alpha_{Iy} \\ \alpha_{Iz} \end{bmatrix} =$$

$$\begin{bmatrix} cos\phi cos\psi\ddot{\theta} - cos\phi\dot{\phi}\dot{\psi} - sin\phi\ddot{\psi} - cos\psi sin\phi\dot{\phi}\dot{\theta} - cos\phi sin\psi\dot{\psi}\dot{\theta} \\ cos\phi\ddot{\psi} - sin\phi\dot{\phi}\dot{\psi} + sin\phi cos\psi\ddot{\theta} + cos\psi cos\phi\dot{\phi}\dot{\theta} - sin\phi sin\psi\dot{\psi}\dot{\theta} \\ \ddot{\psi} - cos\psi\dot{\psi}\dot{\theta} - sin\psi\ddot{\theta} \end{bmatrix} \tag{4.28}$$

The equation which refers to total external moment angular acceleration relationship is called dynamic equation or equation motion of system. According to equation if external moment is known, angular acceleration can be obtained easily. This problem refers to forward dynamic analysis. If angular acceleration is known, net external moment can be calculated. This problem refers to inverse dynamic analysis.

4.2 Dynamic Analysis of Flight Simulator

When designing a controller that can provide the desired performance criteria for complex systems with multiple degrees of freedom, a mathematical model of the system is needed. The closer this mathematical model, in which the system dynamics is modelled, is to reality, the more successful the controller will be. While modelling the system dynamics mathematically, Newton-Euler method and Hamilton-Lagrange method are common methods in the literature. In this study, the Euler equation is used to derive the dynamic equations of the spherical flight simulator. Euler's equation states that the change of angular momentum of a rigid body with respect to time is equal to the total moment acting on it. The angular momentum of a rigid body is equal to the product of the inertia tensor and the angular velocity vector. Since the structure of the spherical flight simulator does not consist of regular geometric shapes, its analytical calculation is laborious and error-prone. Therefore, the inertia tensors of the spheres in the simulator were obtained from the SOLIDWORKS model.

$$J_O = \begin{bmatrix} O_{11} & 0 & 0 \\ 0 & O_{22} & 0 \\ 0 & 0 & O_{33} \end{bmatrix} \tag{4.29}$$

$$J_M = \begin{bmatrix} M_{11} & 0 & 0 \\ 0 & M_{22} & 0 \\ 0 & 0 & M_{33} \end{bmatrix} \tag{4.30}$$

$$J_I = \begin{bmatrix} I_{11} & 0 & 0 \\ 0 & I_{22} & 0 \\ 0 & 0 & I_{33} \end{bmatrix} \tag{4.31}$$

Eq. 4.29-4.31 give the inertia tensors of the outer, middle and inner sphere, respectively. Since the geometry of the spheres is symmetric and the mass distribution

is homogeneous, the mass moment of inertia matrices are in diagonal matrix form. While calculating the inertia tensors of the spheres, their own coordinate frames are used. Angular momentum of the spheres is obtained by using their inertia tensors and angular velocities.

$$\vec{H}_I = J_I \vec{\Omega}_I \tag{4.32}$$

$$\vec{H}_M = J_M \vec{\Omega} + R_{IM} \vec{H}_I \tag{4.33}$$

$$\vec{H}_O = J_O \vec{\Omega}_O + R_{MO} \vec{H}_M \tag{4.34}$$

$$\vec{\mathrm{H}}_I = \begin{bmatrix} H_{Ix} \\ H_{Iy} \\ H_{Iz} \end{bmatrix} = \begin{bmatrix} I_{11}\left(cos\psi cos\phi\dot{\theta} - sin\phi\dot{\psi}\right) \\ I_{22}\left(cos\psi sin\phi\dot{\theta} + cos\phi\dot{\psi}\right) \\ I_{33}\left(\dot{\phi} - sin\psi\dot{\theta}\right) \end{bmatrix} \tag{4.35}$$

$$\vec{\mathrm{H}}_M = \begin{bmatrix} H_{Mx} \\ H_{My} \\ H_{Mz} \end{bmatrix} = \begin{bmatrix} I_{22} sin\phi \#\mathbf{2} - I_{11} cos\phi \#\mathbf{1} + M_{11} cos\psi\dot{\theta} \\ M_{22}\dot{\psi} + I_{22} cos\phi \#\mathbf{2} + I_{11} sin\phi \#\mathbf{1} \\ -I_{33}\left(sin\psi\dot{\theta} - \dot{\phi}\right) - M_{33} sin\psi\dot{\theta} \end{bmatrix} \tag{4.36}$$

Where;

$$\#1 = sin\phi cos\psi - cos\phi cos\psi\dot{\theta}$$

$$\#2 = cos\phi\dot{\psi} + sin\phi cos\psi\dot{\theta}$$

$$\vec{\mathrm{H}}_O = \begin{bmatrix} H_{Ox} \\ H_{Oy} \\ H_{Oz} \end{bmatrix} = \begin{bmatrix} O_{11}\dot{\theta} + sin\psi \#\mathbf{1} + cos\psi \#\mathbf{2} \\ M_{22}\dot{\psi} + I_{22} cos\phi \#\mathbf{4} + I_{11} sin\phi \#\mathbf{3} \\ sin\psi \#\mathbf{2} - cos\psi \#\mathbf{1} \end{bmatrix} \tag{4.37}$$

Where;

$$\#1 = I_{33}\left(sin\psi\dot{\theta} - \dot{\phi}\right) + M_{33} sin\psi\dot{\theta}$$

$$\#2 = I_{22} sin\phi\left(cos\phi\dot{\psi} + sin\phi cos\psi\dot{\theta}\right) - I_{11} cos\phi\left(sin\phi\dot{\psi} - cos\phi cos\psi\dot{\theta}\right)$$

$$+ M_{11} cos\psi\dot{\theta}$$

$$\#3 = sin\phi\dot{\psi} - cos\phi cos\psi\dot{\theta}$$

$$\#4 = cos\phi\dot{\psi} + sin\phi cos\psi\dot{\theta}$$

The variations of the obtained angular momentum expressions with respect to time give the moments applied to the spheres.

$$\vec{T} = \frac{d}{dt}\vec{H} + \vec{\Omega} x \vec{H} \tag{4.38}$$

The torque relations for the inner, middle and outer sphere are as in Eq. 4.39, Eq. 4.40 and Eq. 4.41 respectively.

$$T_I = (I_{11} - I_{22})\left(cos\phi\dot{\psi} + cos\psi sin\phi\dot{\theta}\right)\left(sin\phi\dot{\psi} - cos\phi cos\psi\dot{\theta}\right)$$
$$-I_{33}\left(sin\psi\ddot{\theta} + cos\psi\dot{\theta}\dot{\psi} - \ddot{\phi}\right) \quad (4.39)$$

$$T_M = M_{22}\ddot{\psi} + \left(\frac{I_{33} - M_{11} + M_{33}}{2}\right) sin2\psi\dot{\theta}^2 + I_{22}cos^2\phi\ddot{\psi} + I_{11}sin^2\phi\ddot{\psi}$$
$$-I_{33}cos\psi\dot{\phi}\dot{\theta}$$
$$+(I_{11} - I_{22})sin2\phi\dot{\phi}\dot{\psi} - I_{11}cos^2\phi cos\psi sin\psi\dot{\theta}^2 + (I_{22} - I_{11})cos^2\phi cos\psi\dot{\phi}\dot{\theta}$$
$$-I_{22}cos\psi sin^2\phi sin\psi\dot{\theta}^2$$
$$+(I_{11} - I_{22})cos\psi sin^2\phi\dot{\phi}\dot{\theta} + (I_{22} - I_{11})cos\phi cos\psi sin\phi\ddot{\theta}$$
$$+2(I_{11} - I_{22})cos\phi sin\phi sin\psi\dot{\psi}\dot{\theta} \quad (4.40)$$

$$T_O = O_{11}\ddot{\theta} - I_{33}sin\psi\ddot{\phi} + (I_{33} + M_{33})sin^2\psi\ddot{\theta}$$
$$+cos^2\psi\ddot{\theta}(M_{11} + I_{11}cos^2\phi + I_{22}sin^2\phi)$$
$$-I_{33}cos\psi\dot{\phi}\dot{\psi} + (I_{33} - M_{11} + M_{33})sin2\psi\dot{\psi}\dot{\theta} + (I_{22} - I_{11})cos^2\phi cos\psi\dot{\phi}\dot{\psi}$$
$$+(I_{11} - I_{22})cos\psi sin^2\phi\dot{\phi}\dot{\psi} + (I_{11} - I_{22})cos\phi sin\phi sin\psi\dot{\psi}^2$$
$$+(I_{22} - I_{11})cos\phi cos\psi sin\phi\ddot{\psi}$$
$$+2(I_{22} - I_{11})cos\phi cos^2\psi sin\phi\dot{\phi}\dot{\theta} - 2I_{11}cos^2\phi cos\psi sin\psi\dot{\psi}\dot{\theta}$$
$$-2I_{22}cos\psi sin^2\phi sin\psi\dot{\psi}\dot{\theta} \quad (4.41)$$

4.2.1 Solution method for dynamic equations

Solution of nonlinear coupled differential equation is required numerical integration techniques like Euler method, Runge-Kutta method, etc. [55]. Simple two degrees of freedom dynamic model is used for presenting solution method. Elastic pendulum or mass spring pendulum is a good example for solving coupled differential equations [56].

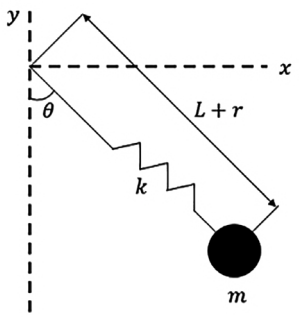

Figure 4.7 Elastic Pendulum.

Elastic pendulum consists of a spring and a point mass which is attached to end of the spring Figure 4.7. Main difference between flexible pendulum and simple pendulum is, flexible pendulum has spring instead of rigid rod.

Dynamic equation of the flexible pendulum system is obtained by Lagrange method. The system has two generalized coordinates which are r and θ respectively. Position of pendulum end is simply [56]:

$$x = (L + r)\sin\theta \tag{4.42}$$

$$y = -(L + r)\cos\theta \tag{4.42}$$

Velocities in x and y direction are obtained differentiating equation 4.41 and 4.42 with respect to time.

$$\frac{dx}{dt} = \dot{x} = \dot{r}\sin\theta + (L + r)\dot{\theta}\cos\theta \tag{4.43}$$

$$\frac{dy}{dt} = \dot{y} = -\dot{r}\cos\theta + (L + r)\dot{\theta}\sin\theta \tag{4.44}$$

Kinetic energy of the flexible pendulum system is:

$$T = \frac{1}{2}mV^2 \tag{4.45}$$

$$V^2 = \dot{x}^2 + \dot{y}^2 \tag{4.46}$$

$$\dot{x}^2 = \dot{r}^2 sin^2\theta + (L + r)^2\dot{\theta}^2 cos^2\theta + 2\dot{r}\dot{\theta}(L + r)\sin\theta\cos\theta \tag{4.47}$$

$$\dot{y}^2 = \dot{r}^2 cos^2\theta + (L + r)^2\dot{\theta}^2 sin^2\theta - 2\dot{r}\dot{\theta}(L + r)\sin\theta\cos\theta \tag{4.48}$$

$$T = \frac{1}{2}mV^2 = \frac{1}{2}m(\dot{r}^2 + (L + r)^2\dot{\theta}^2) \tag{4.49}$$

Potential energy of the system depends on spring elastic potential energy and mass potential energy due to gravity.

$$P = -mgy + \frac{1}{2}kr^2 = -mg(L + r)\cos\theta + \frac{1}{2}kr^2 \tag{4.50}$$

Lagrange function is stated as difference between system total kinetic energy and total potential energy.

$$L = T - P = \frac{1}{2}m\left(\dot{r}^2 + (L + r)^2\dot{\theta}^2\right) + mg(L + r)\cos\theta - \frac{1}{2}kr^2 \tag{4.51}$$

Since system has two degree of freedom, two generalized coordinates are declared below in equation 12 and 13.

$$q_1 = r \tag{4.52}$$

$$q_2 = \theta \tag{4.53}$$

General form of the equation of Motion of the system is given in equation 4.54.

$$\frac{d}{dt}\left(\frac{\partial L}{\partial \dot{q}_1}\right) - \frac{\partial L}{\partial q_1} = 0 \tag{4.54}$$

When calculations are proceeded from equation 4.54 to 4.59, final form of the equation of motion is achieved for one generalized coordinate.

$$\frac{\partial L}{\partial \dot{q}_1} = m\dot{r} \tag{4.55}$$

$$\frac{d}{dt}\left(\frac{\partial L}{\partial \dot{q}_1}\right) = m\ddot{r} \tag{4.56}$$

$$\frac{\partial L}{\partial q_1} = m(L+r)\dot{\theta}^2 + mg\cos\theta - kr \tag{4.57}$$

$$m\ddot{r} - m(L+r)\dot{\theta}^2 - mg\cos\theta + kr = 0 \tag{4.58}$$

$$\ddot{r} = (L+r)\dot{\theta}^2 + gcos\theta - \frac{k}{m}r \tag{4.59}$$

If same procedure is applied for other generalized coordinate θ, other equation of motion is obtained as follows.

$$\frac{d}{dt}\left(\frac{\partial L}{\partial \dot{q}_2}\right) - \frac{\partial L}{\partial q_2} = 0 \tag{4.60}$$

$$\frac{\partial L}{\partial \dot{q}_2} = m(L+r)^2\dot{\theta} \tag{4.61}$$

$$\frac{d}{dt}\left(\frac{\partial L}{\partial \dot{q}_2}\right) = 2m(L+r)\dot{r}\dot{\theta} + m(L+r)^2\ddot{\theta} \tag{4.62}$$

$$\frac{\partial L}{\partial q_2} = -mg(L+r)\sin\theta \tag{4.63}$$

$$m(L+r)^2\ddot{\theta} + 2m(L+r)\dot{r}\dot{\theta} + mg(L+r)\sin\theta = 0 \tag{4.64}$$

$$\ddot{\theta} = -\frac{2}{L+r}\dot{r}\dot{\theta} - \frac{g}{L+r}\sin\theta \tag{4.65}$$

Equations 4.59 and 4.65 are called governing equations of the dynamic system. These equations nonlinear second order differential equations and they need to initial conditions in order to identify system behaviour [56].

Solution of nonlinear coupled differential equation is required numerical integration techniques like Euler method, Runge-Kutta method, etc. Since it is accurate and easy to apply method, Runge-Kutta method is chosen in this study. Second order differential equations of the system should be reduced to first order to apply Runge-Kutta method [56].

$$\dot{Y} = \begin{bmatrix} \dot{r} \\ (L+r)\dot{\theta}^2 + gcos\theta - \frac{k}{m}r \\ \dot{\theta} \\ -\frac{2}{L+r}\dot{r}\dot{\theta} - \frac{g}{L+r}\sin\theta \end{bmatrix} \tag{4.66}$$

Equation 26 is the reduced form of the governing equations of the system and MATLAB ode45 command is used to solve these equations. Initial conditions r $\dot{r}$ θ and $\dot{\theta}$ should be defined for numerical integration. Two m-file are required for applying ode45 command. First m-file defines initial conditions and includes inputs of the functions. Second m-file contains ode45 command and equations to solve. Initial conditions are defined as below [56].

$$IC = \left[r\ \dot{r}\ \theta\ \dot{\theta}\ \right]^T \tag{4.67}$$

$$r = 0\ m \tag{4.68}$$
$$\dot{r} = 0\ \ m/sec \tag{4.69}$$
$$\theta = 0.646\ rad \tag{4.70}$$
$$\dot{\theta} = 0\ rad/sec \tag{4.71}$$

Other physical parameters are as follows:

$$m = 1\ kg \tag{4.72}$$
$$L = 0.5\ m \tag{4.73}$$
$$g = 9.81\ m/sec^2 \tag{4.74}$$
$$k = 10\ N/m \tag{4.75}$$

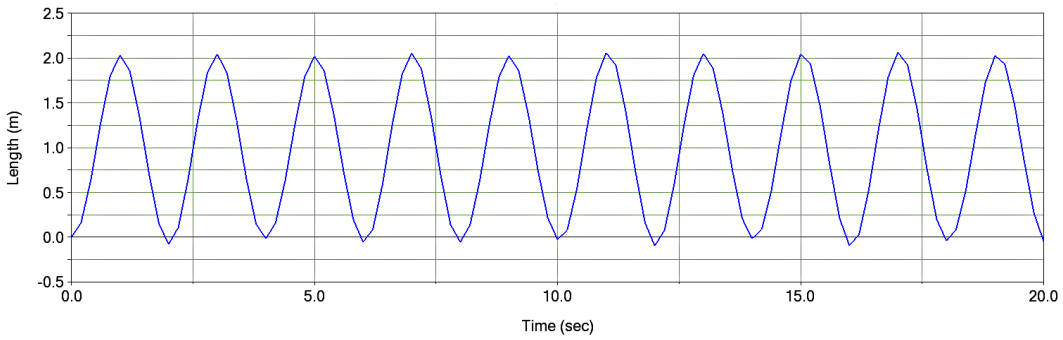

Figure 4.8 Spring deflection during simulation in MATLAB**.**

Maximum spring deflection is observed as 2.05 m and minimum spring deflection is observed as -0.08 m during 20 seconds in MATLAB in Figure 4.8.

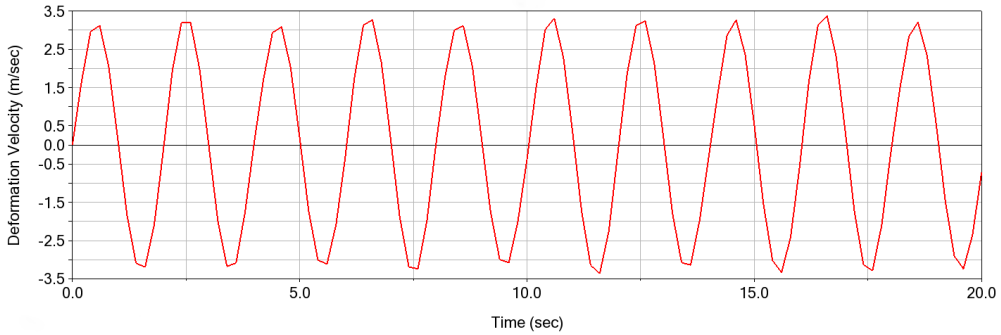

Figure 4.9 Spring deflection velocity during simulation in MATLAB.

Maximum spring deflection velocity is observed as 3.38 m/sec and minimum spring deflection velocity is observed as -3.38 m/sec during 20 seconds in MATLAB in Figure 4.9.

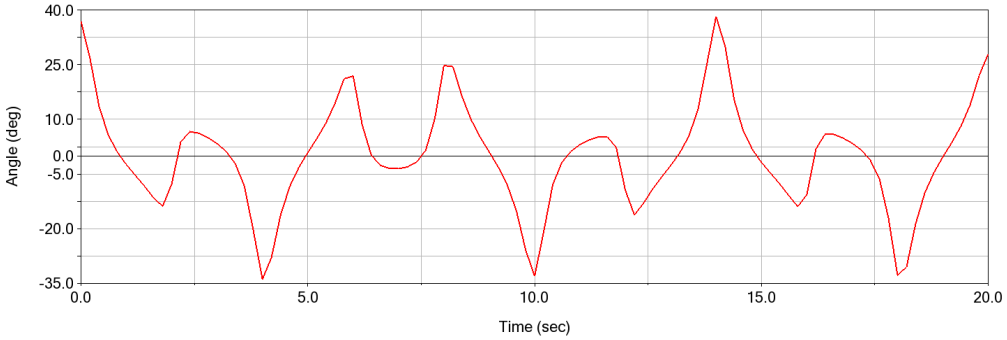

Figure 4.10 Pendulum angular position during simulation in MATLAB.

Maximum pendulum angular position is observed as 37 degrees and minimum pendulum angular position is observed as -37 degrees during 20 seconds in MATLAB in Figure 4.10.

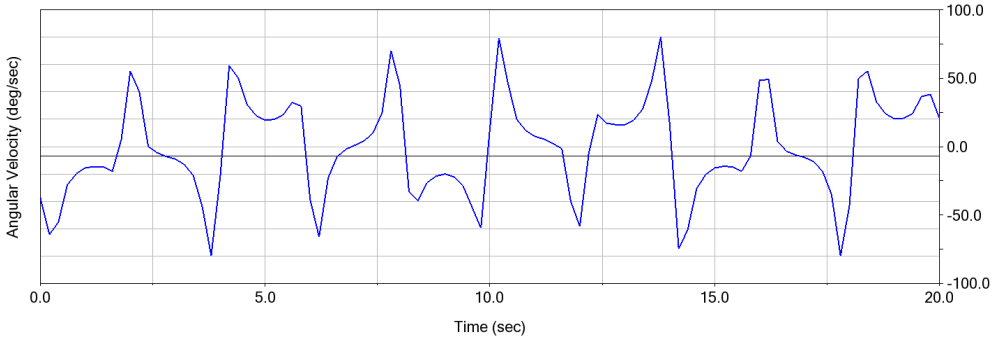

Figure 4.11 Pendulum angular velocity during simulation in MATLAB.

Maximum pendulum angular velocity is observed as 83 deg/sec and minimum pendulum angular velocity is observed as -83 deg/sec during 20 seconds in MATLAB in Figure 4.11.

4.2.1 Simulation of Spherical Flight Simulator Dynamic Model

The dynamic equations of the system are non-linear differential equations with no analytical solution. In order to observe the system dynamics, these equations must be solved numerically. Therefore, in order to investigate the behaviour of the spherical flight simulator, the dynamic equation of each sphere is modelled in SIMULINK environment. The more realistic this model is, the better the controller designed will be able to meet the desired performance criteria.

4.2.1.1 Inner Sphere Model

When the dynamic equation of the inner sphere is analysed, it is seen that there are non-linear terms besides the externally applied torque T_I. These terms are torque

components arising from the motion of the other spheres and these terms can be considered as disturbance torques acting on the system when modelling the system.

$$T_I - (I_{11} - I_{22})\left(cos\phi\dot{\psi} + cos\psi sin\phi\dot{\theta}\right)\left(sin\phi\dot{\psi} - cos\phi cos\psi\dot{\theta}\right)$$

$$+I_{33}\left(sin\psi\ddot{\theta} + cos\psi\dot{\theta}\dot{\psi}\right) = I_{33}\ddot{\phi} \quad (4.76)$$

$$T_I + T_{I-D1} + T_{I-D2} = I_{33}\ddot{\phi} \quad (4.77)$$

For ease of modelling, the disturbance torque terms will be expressed in two terms. The first term of the disturbance torque acting on the inner sphere due to the motion of the other spheres is given in Eq. 4.78.

$$T_{I-D1} = -(I_{11} - I_{22})\left(cos\phi\dot{\psi} + cos\psi sin\phi\dot{\theta}\right)\left(sin\phi\dot{\psi} - cos\phi cos\psi\dot{\theta}\right) \quad (4.78)$$

$$T_{I-D2} = I_{33}\left(sin\psi\ddot{\theta} + cos\psi\dot{\theta}\dot{\psi}\right) \quad (4.79)$$

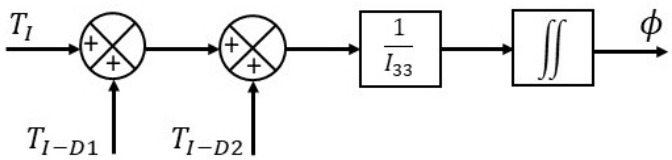

Figure 4.12 Inner sphere dynamic equation representation.

The SIMULINK model created for the inner sphere is given in detail in Figure 4.12. In this model, in addition to the torque $\boldsymbol{T_I}$ applied to the inner sphere as input to the system, the disturbance torque is added and the angular acceleration of the inner sphere is obtained as output. When the double integral of the angular acceleration of the inner sphere with respect to time is taken, the angular position of the inner sphere is obtained.

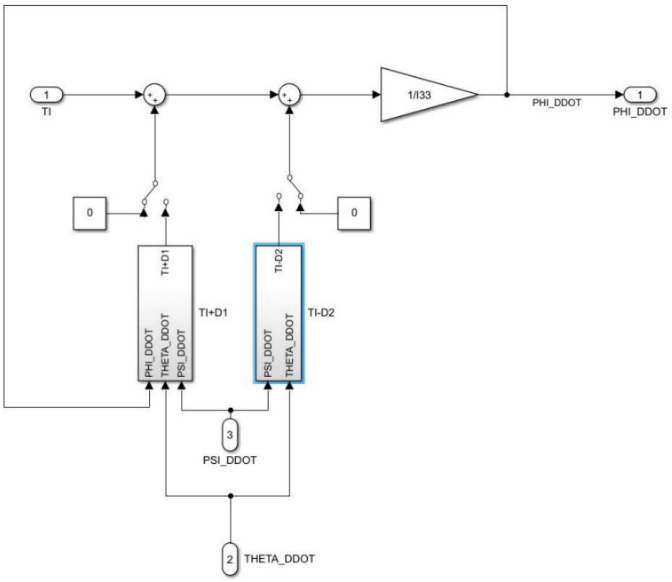

Figure 4.13 Inner Sphere block diagram

The model of the nonlinear disturbance torque mentioned prepared in SIMULINK environment is given in Figure 4.13. As can be seen in this model, the disturbance torque is obtained as output against the angular acceleration of each sphere as input.

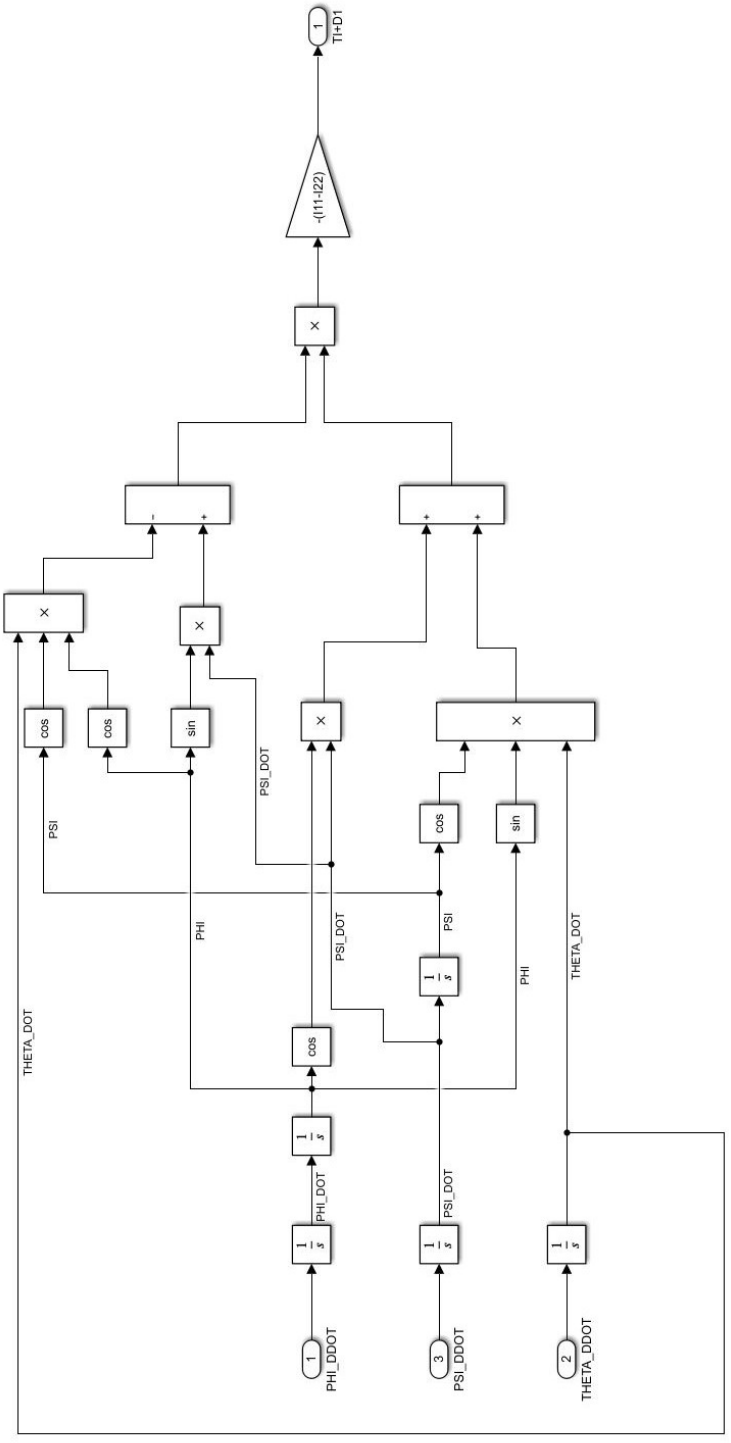

Figure 4.14 First part of disturbance torque for inner sphere.

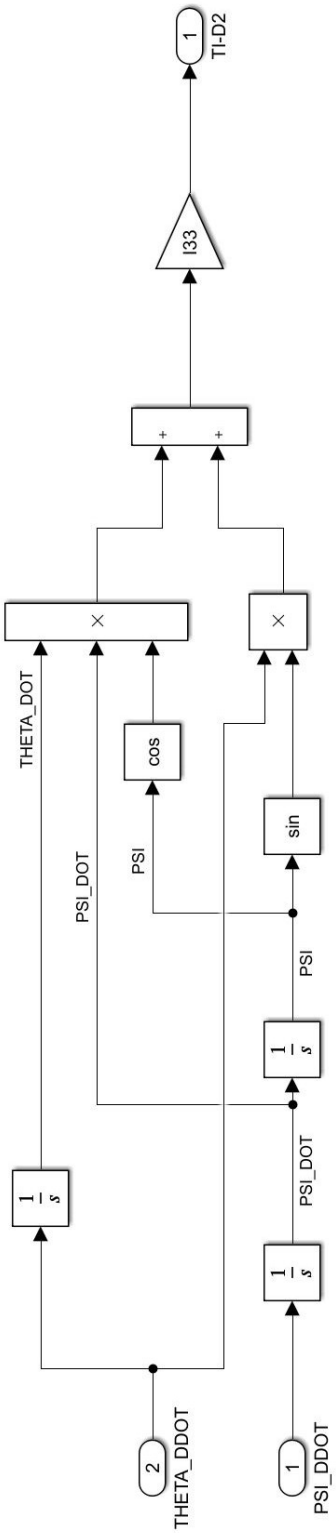

Figure 4.15 Second part of disturbance torque for inner sphere.

Detailed Simulink model of the first and the second part of disturbance torque can be seen in Fig. 4.14 and Fig. 4.15.

4.2.1.1 Middle Sphere Model

When the dynamic equation of the middle sphere is analysed, besides the TM torque acting on the middle sphere, non-linear torque terms arising from the motion of the inner and outer sphere can be clearly seen. These nonlinear torque terms can be considered as nonlinear disturbance torque as in the dynamic model of the inner sphere. For ease of modelling, the nonlinear disturbance torque term is written in three parts as well.

$$T_M - \left(\frac{I_{33} - M_{11} + M_{33}}{2}\right) sin2\psi\dot{\theta}^2 + I_{33}cos\psi\dot{\phi}\dot{\theta} - (I_{11} - I_{22})sin2\phi\dot{\phi}\dot{\psi}$$

$$+I_{11}cos^2\phi cos\psi sin\psi\dot{\theta}^2$$

$$-(I_{22} - I_{11})cos^2\phi cos\psi\dot{\phi}\dot{\theta} + I_{22}cos\psi sin^2\phi sin\psi\dot{\theta}^2 - (I_{11} - I_{22})cos\psi sin^2\phi\dot{\phi}\dot{\theta}$$

$$-(I_{22} - I_{11})cos\phi cos\psi sin\phi\ddot{\theta} - 2(I_{11} - I_{22})cos\phi sin\phi sin\psi\dot{\psi}\dot{\theta}$$

$$= (M_{22} + I_{22}cos^2\phi + I_{11}sin^2\phi)\ddot{\psi} \quad (4.80)$$

$$T_M + T_{M-D1} + T_{M-D2} + T_{M-D3} = I_{M-EQ}\ddot{\psi} \quad (4.81)$$

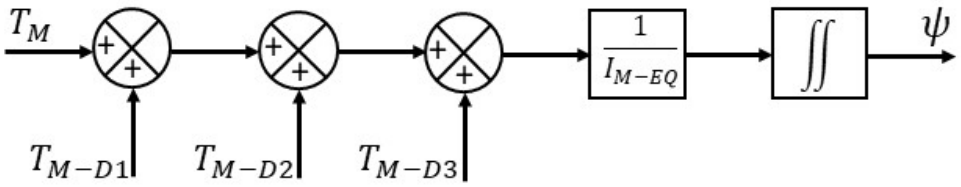

Figure 4.16 Middle sphere dynamic equation representation

The nonlinear SIMULINK model for the middle sphere can be seen in Figure 4.16. In the model, besides the torque $\boldsymbol{T_M}$ acting on the centre sphere, disturbance torques are added, the equivalent mass moment of inertia including the mass moment of inertia terms of the inner sphere is calculated and the angular acceleration of the centre sphere is obtained as an output. After obtaining the angular acceleration, it is possible to access the angular velocity and angular position data of the middle sphere by taking the integral of the obtained acceleration.

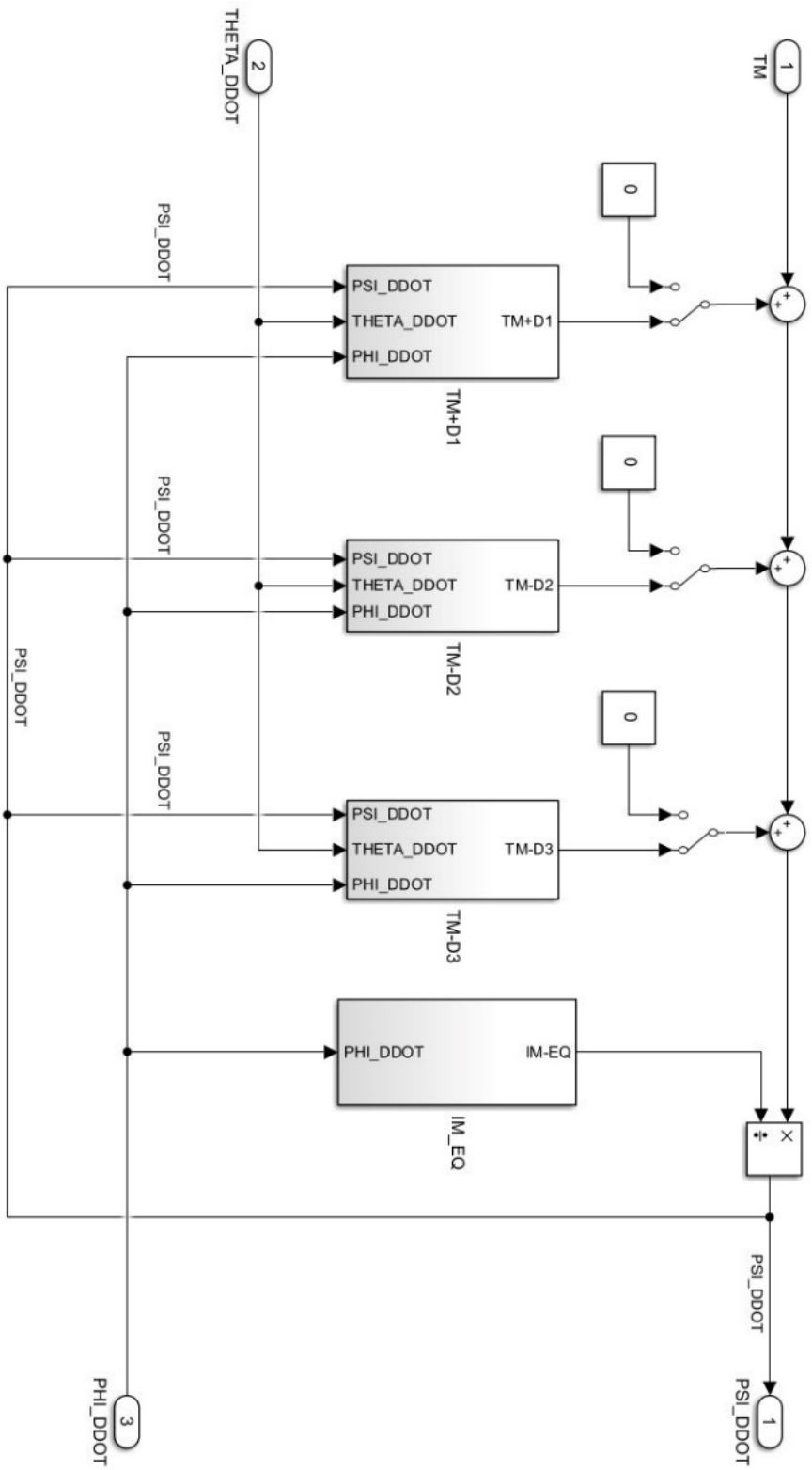

Figure 4.17 Middle sphere block diagram

The model of the nonlinear disturbance torque mentioned prepared in SIMULINK environment is given in Figure 4.17. As can be seen in this model, the disturbance torque is obtained as output against the angular acceleration of each sphere as input.

$$T_{M-D1} = -\left(\frac{I_{33} - M_{11} + M_{33}}{2}\right) sin2\psi\dot{\theta}^2 + I_{33}cos\psi\dot{\phi}\dot{\theta} - (I_{11} - I_{22})sin2\phi\dot{\phi}\dot{\psi}$$
$$+I_{11}cos^2\phi cos\psi sin\psi\dot{\theta}^2 \quad (4.82)$$

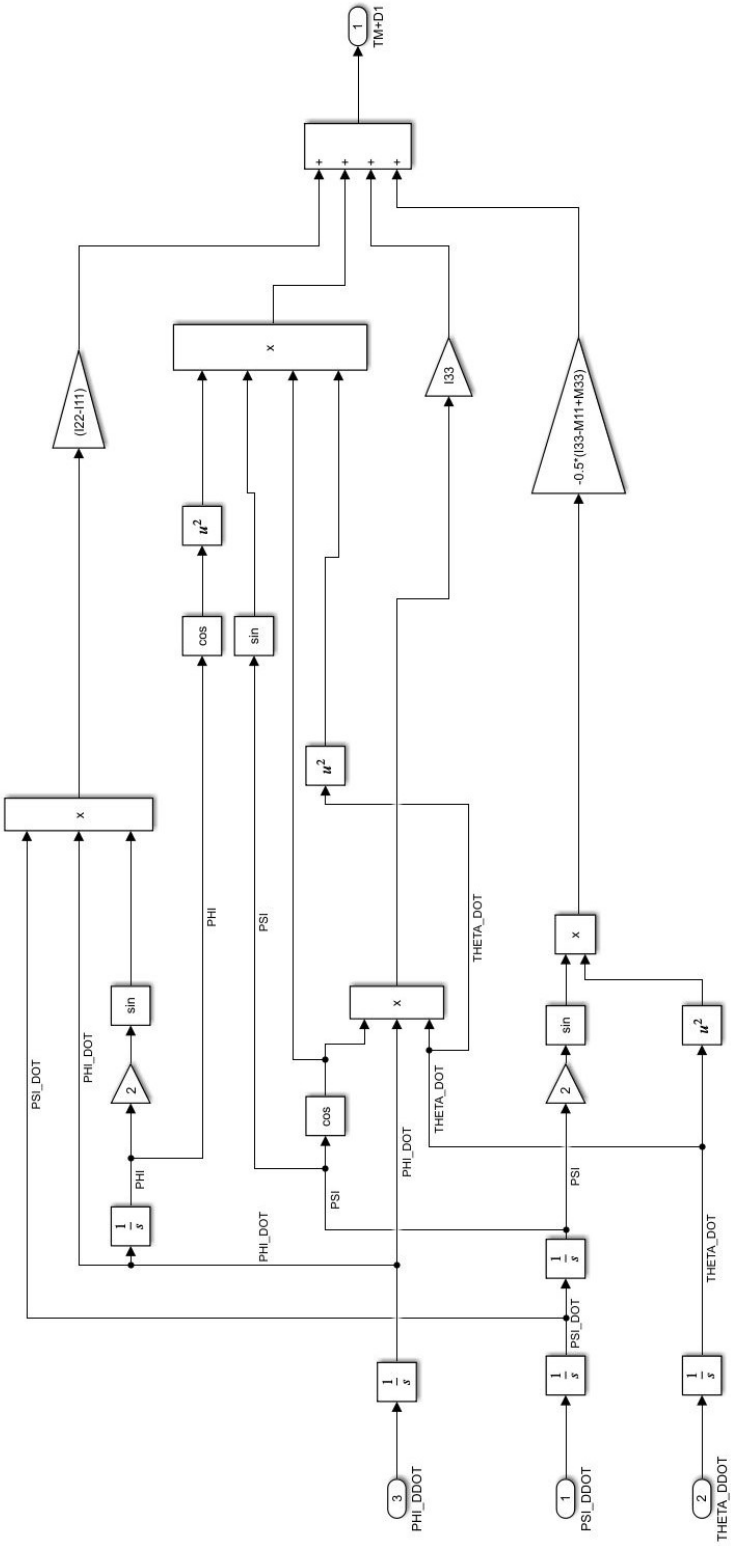

Figure 4.18 First part of disturbance torque for middle sphere

Detailed Simulink model of the first, the second and the third part of disturbance torque can be seen in Fig. 4.18, Fig. 4.19 and Fig.19.

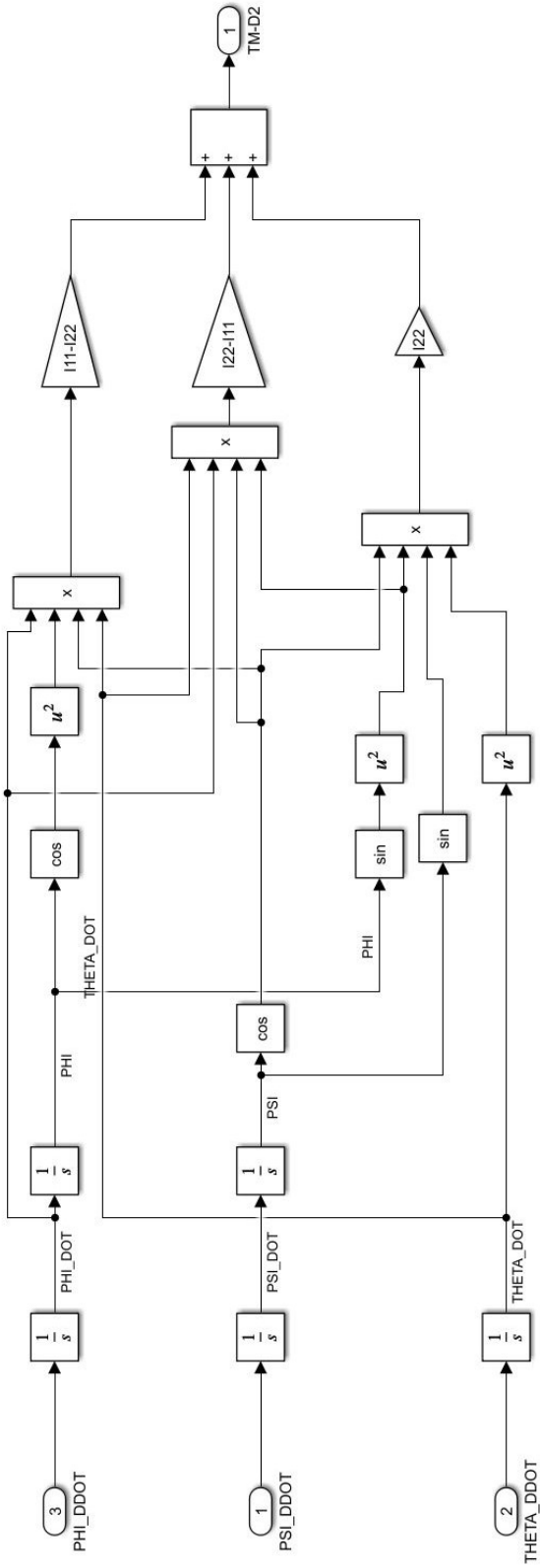

Figure 4.19 Second part of disturbance torque for middle sphere

$$T_{M-D3} = -(I_{22} - I_{11})cos\phi cos\psi sin\phi\ddot{\theta} - 2(I_{11} - I_{22})cos\phi sin\phi sin\psi\dot{\psi}\dot{\theta} \quad (4.84)$$

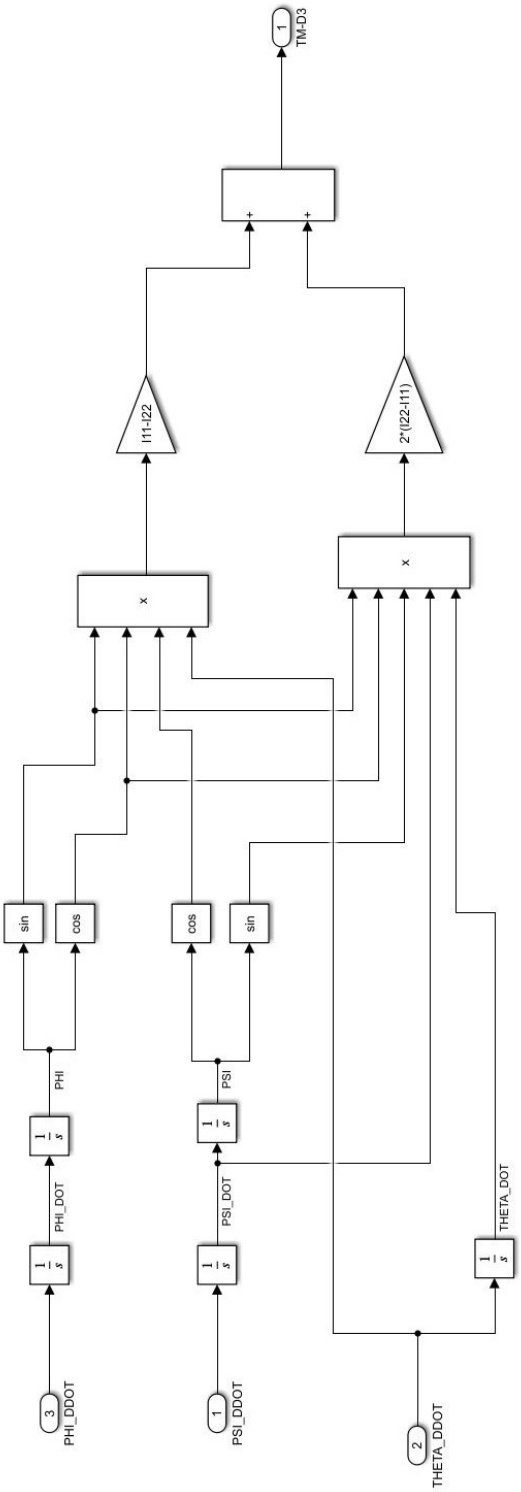

Figure 4.20 Third part of disturbance torque for middle sphere.

While the mass moment of inertia of the inner sphere consists of a single term, since the middle sphere contains the inner sphere, the mass moment of inertia of the middle sphere contains more than one term and varies according to the angular position of the

inner sphere. If we call this complex mass moment of inertia as the equivalent mass moment of inertia, the equivalent mass moment of inertia for the middle sphere is given in Eq. 4.85.

$$I_{M-EQ} = M_{22} + I_{22}cos^2\phi + I_{11}sin^2\phi \tag{4.85}$$

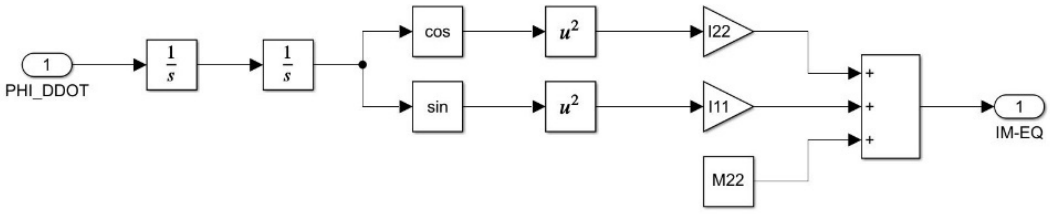

Figure 4.21 Middle sphere equivalent mass moment of inertia block diagram.

The SIMULINK model of the equivalent mass moment of inertia for the middle sphere given in Eq.4.85 is shown in Figure 4.21. When the equivalent mass moment of inertia is analysed, it is seen that in addition to the mass moment of inertia of the middle sphere, there are also mass moment of inertia terms of the inner sphere.

4.2.1.2 Outer Sphere Model

$$T_O + I_{33}cos\psi\dot{\phi}\dot{\psi} - (I_{33} - M_{11} + M_{33})sin2\psi\dot{\psi}\dot{\theta} - (I_{22} - I_{11})cos^2\phi cos\psi\dot{\phi}\dot{\psi}$$

$$+I_{33}sin\psi\ddot{\phi}$$

$$-(I_{11} - I_{22})cos\psi sin^2\phi\dot{\phi}\dot{\psi} - (I_{11} - I_{22})cos\phi sin\phi sin\psi\dot{\psi}^2$$

$$-(I_{22} - I_{11})cos\phi cos\psi sin\phi\ddot{\psi}$$

$$-2(I_{22} - I_{11})cos\phi cos^2\psi sin\phi\dot{\phi}\dot{\theta} + 2I_{11}cos^2\phi cos\psi sin\psi\dot{\psi}\dot{\theta}$$

$$+2I_{22}cos\psi sin^2\phi sin\psi\dot{\psi}\dot{\theta}$$

$$= (O_{11} + (I_{33} + M_{33})sin^2\psi + cos^2\psi(M_{11} + I_{11}cos^2\phi + I_{22}sin^2\phi))\ddot{\theta}$$

$$T_O + T_{O-D1} + T_{O-D2} + T_{O-D3} = I_{O-EQ}\ddot{\theta} \tag{4.86}$$

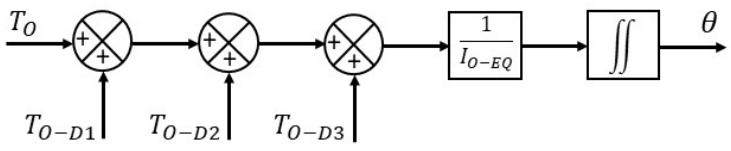

Figure 4.22 Outer sphere dynamic equation representation.

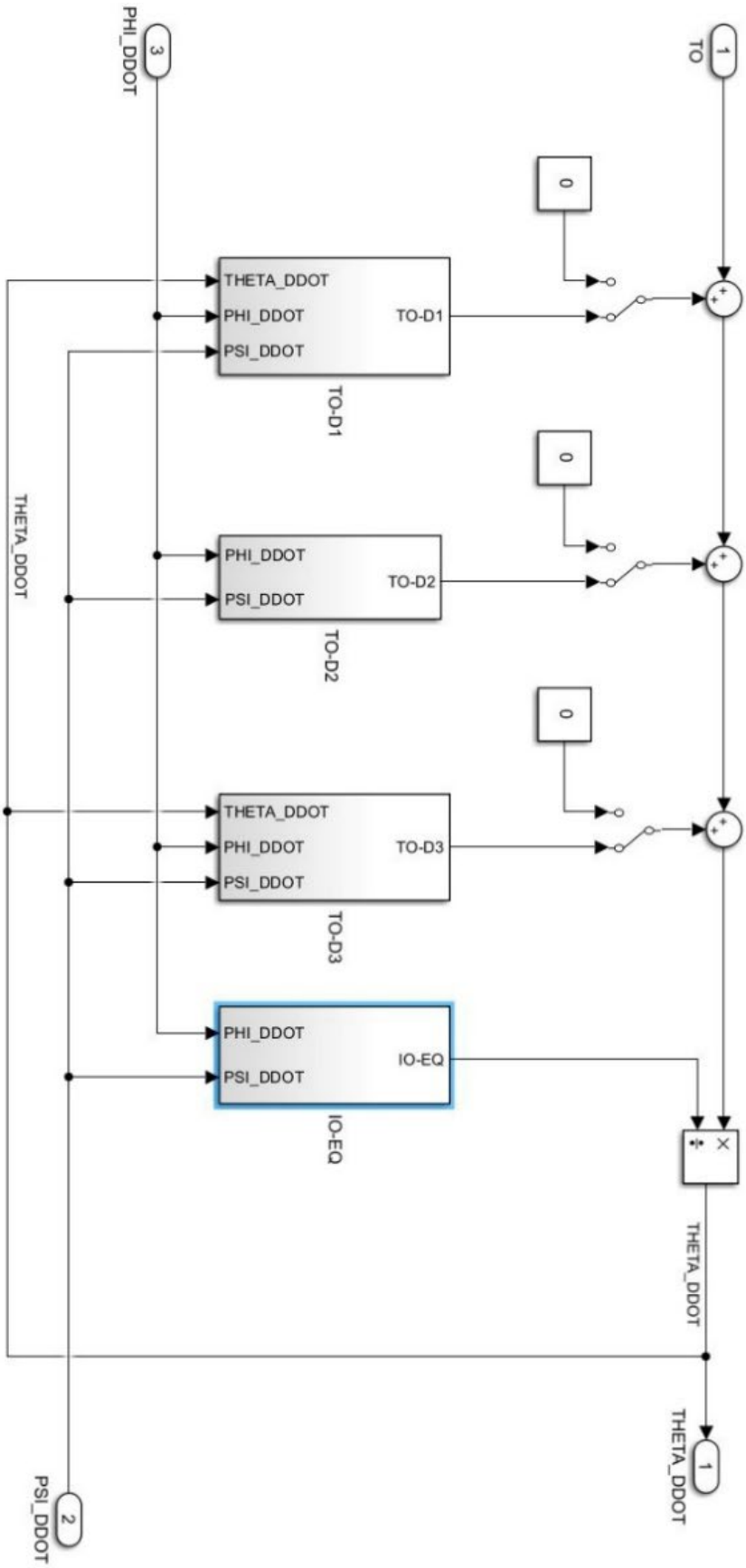

Figure 4.23 Outer sphere block diagram.

The nonlinear SIMULINK model for the middle sphere can be seen in Figure 4.23. In the model, besides the torque $\boldsymbol{T_O}$ acting on the centre sphere, disturbance torques are added, the equivalent mass moment of inertia including the mass moment of inertia terms of the inner sphere is calculated and the angular acceleration of the centre sphere is obtained as an output. After obtaining the angular acceleration, it is possible to access the angular velocity and angular position data of the middle sphere by taking the integral of the obtained acceleration.

Detailed Simulink model of the first, the second and the third part of disturbance torque can be seen in Fig. 4.24, Fig. 4.25 and Fig.26.

The SIMULINK model of the equivalent mass moment of inertia for the outer sphere given in Eq.4.89 is shown in Figure 4.27. When the equivalent mass moment of inertia is analysed, it is seen that in addition to the mass moment of inertia of the outer sphere, there are also mass moment of inertia terms of the inner and middle spheres.

$$T_{O-D1} = I_{33}cos\psi\dot{\phi}\dot{\psi} - (I_{33} - M_{11} + M_{33})sin2\psi\dot{\psi}\dot{\theta} - (I_{22} - I_{11})cos^2\phi cos\psi\dot{\phi}\dot{\psi} + I_{33}sin\psi\ddot{\phi} \quad (4.87)$$

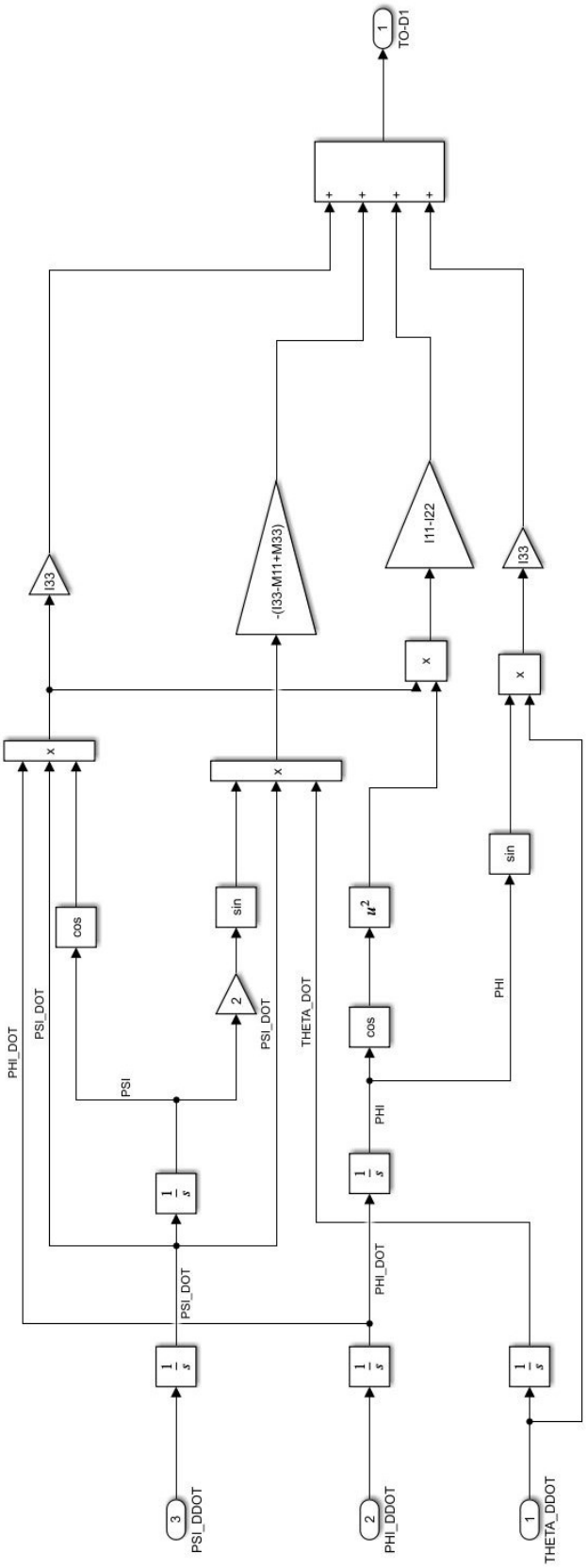

Figure 4.24 First part of disturbance torque for outer sphere.

$$T_{O-D2} = -(I_{11} - I_{22})cos\psi sin^2\phi\dot{\phi}\dot{\psi} - (I_{11} - I_{22})cos\phi sin\phi sin\psi\dot{\psi}^2$$
$$-(I_{22} - I_{11})cos\phi cos\psi sin\phi\ddot{\psi} \quad (4.88)$$

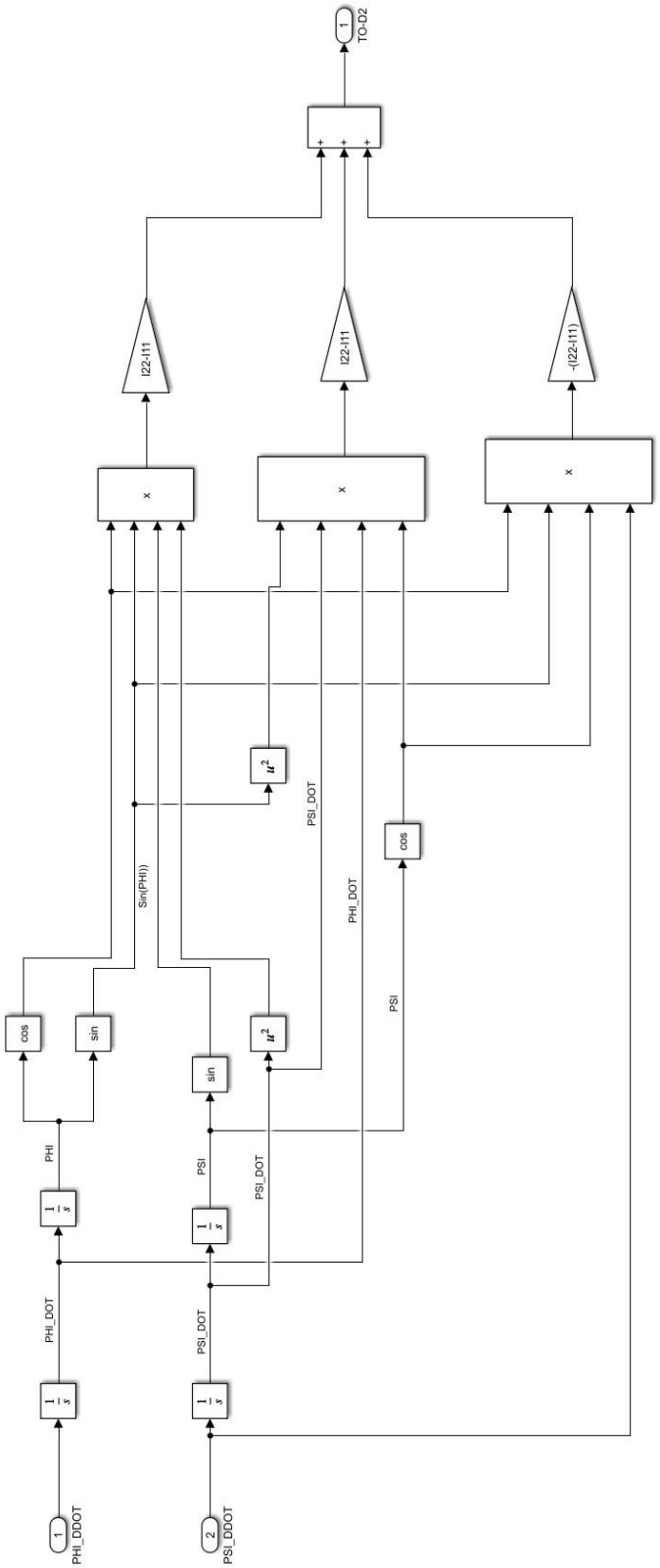

Figure 4.25 Second part of disturbance torque for outer sphere.

$$T_{O-D3} = -2(I_{22} - I_{11})cos\phi cos^2\psi sin\phi\dot{\phi}\dot{\theta} + 2I_{11}cos^2\phi cos\psi sin\psi\dot{\psi}\dot{\theta}$$
$$+2I_{22}cos\psi sin^2\phi sin\psi\dot{\psi}\dot{\theta} \quad (4.89)$$

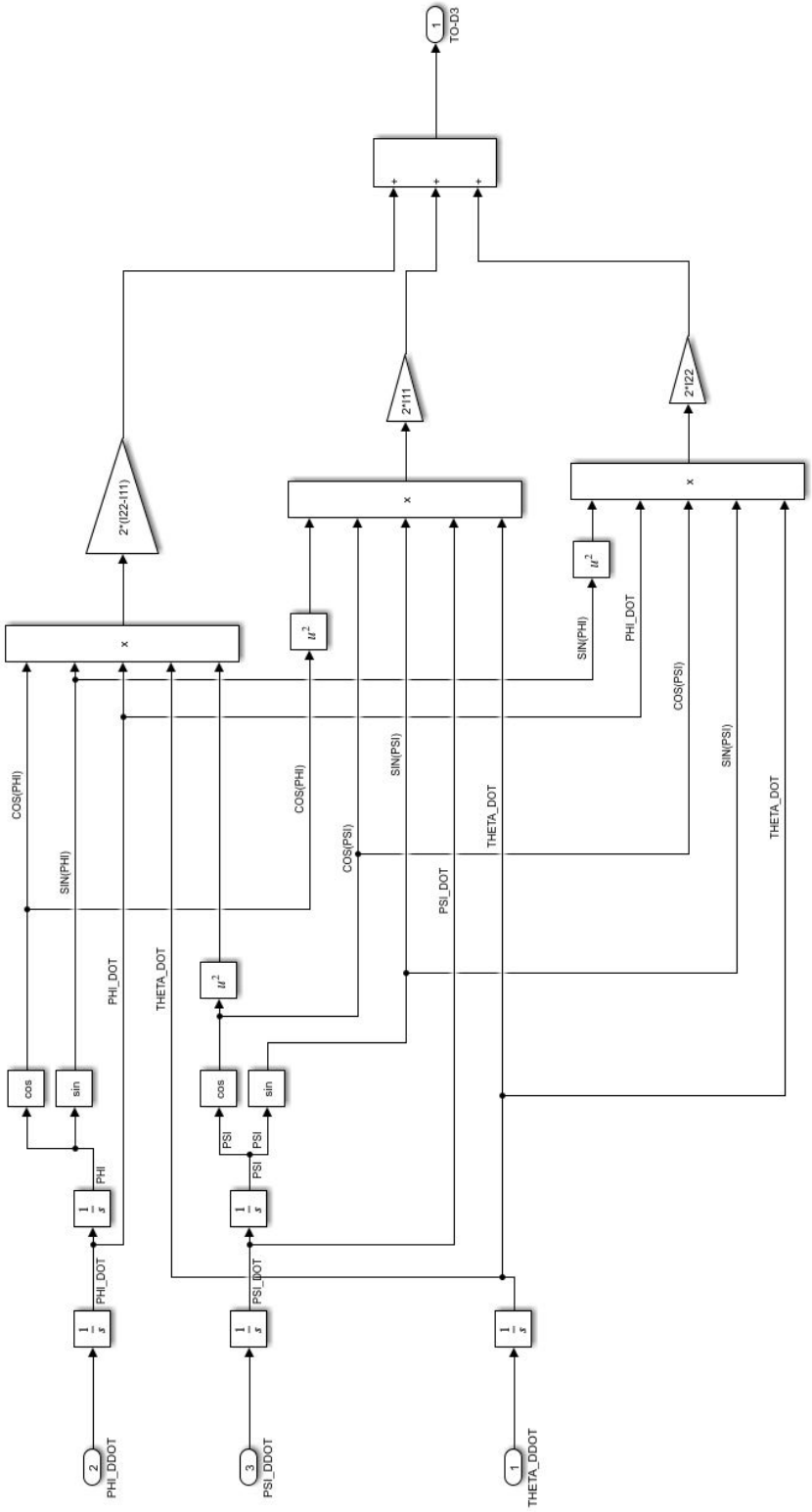

Figure 4.26 Third part of disturbance torque for outer sphere.

$$I_{O-EQ} = O_{11} + (I_{33} + M_{33})sin^2\psi + cos^2\psi(M_{11} + I_{11}cos^2\phi + I_{22}sin^2\phi) \quad (4.89)$$

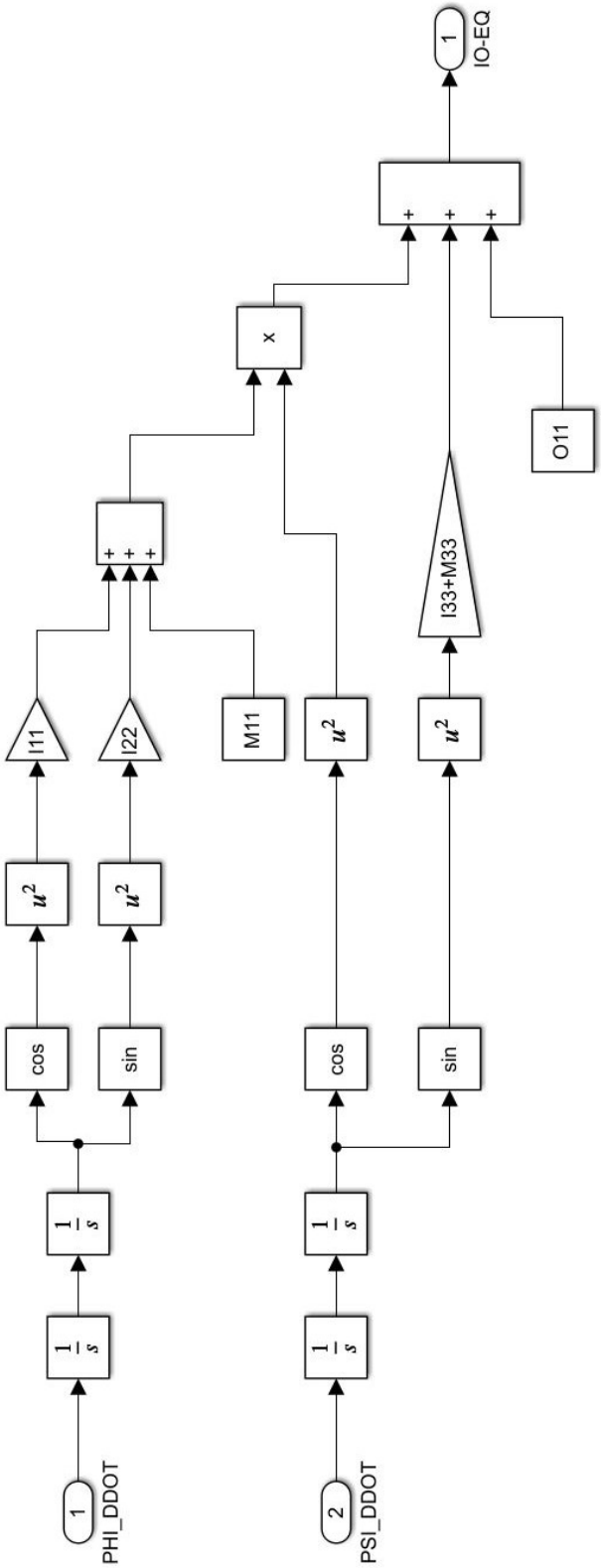

Figure 4.27 Outer sphere equivalent mass moment of inertia block diagram.

CHAPTER V

CONTROLLER DESIGN FOR FLIGHT SIMULATOR

5.1 Linearization of Equations of Motion of Spherical Flight Simulator

Although many physical systems are expressed by linear equations, in most cases these equations expressing physical connections are not linear. In fact, when linear systems are analysed, it is seen that these systems are linear only under limited conditions [57, 58]. The equations of motion of the spherical flight simulator are not linear as in most systems. However, the nonlinear equations of motion of systems operating around a certain equilibrium point can be linearised for this equilibrium point. The linear system and the nonlinear system obtained as a result of this linearisation process are almost equivalent. After determining the equilibrium point around which the linearisation process will be performed for each sphere, the equations of motion of the sphere are linearised. Since both controllers to be applied in this study are controllers that can be applied for linear systems, before proceeding to the controller design, the equations of motion of the spheres are linearised as given in Eq. 5.1–5.15.

$$y - \bar{y} = K_1(x_1 - \bar{x}_1) + K_2(x_2 - \bar{x}_2) + K_3(x_3 - \bar{x}_3) + K_4(x_4 - \bar{x}_4) \tag{5.1}$$

$$\bar{y} = f(\bar{x}_1, \bar{x}_2, \bar{x}_3, \bar{x}_4) \tag{5.2}$$

$$x_1 = \psi \quad , x_2 = \dot{\theta} \quad , x_3 = \dot{\psi} \quad , x_4 = \phi \tag{5.3}$$

$$\bar{x}_1 = 0, \bar{x}_2 = 0, \bar{x}_3 = 0, \bar{x}_4 = 0 \tag{5.4}$$

$$K_1 = \frac{\partial f}{\partial x_1}\Big| \; x_1 = \bar{x}_1, x_2 = \bar{x}_2, x_3 = \bar{x}_3, x_4 = \bar{x}_4 \tag{5.5}$$

$$K_2 = \frac{\partial f}{\partial x_2}\Big| \; x_1 = \bar{x}_1, x_2 = \bar{x}_2, x_3 = \bar{x}_3, x_4 = \bar{x}_4 \tag{5.6}$$

$$K_3 = \frac{\partial f}{\partial x_3}\Big| \; x_1 = \bar{x}_1, x_2 = \bar{x}_2, x_3 = \bar{x}_3, x_4 = \bar{x}_4 \tag{5.7}$$

$$K_4 = \frac{\partial f}{\partial x_4}\Big| \; x_1 = \bar{x}_1, x_2 = \bar{x}_2, x_3 = \bar{x}_3, x_4 = \bar{x}_4 \tag{5.8}$$

$$\bar{y} = I_{33}\ddot{\phi} \tag{5.9}$$

$$K_1 = K_2 = K_3 = K_4 = 0 \tag{5.10}$$

$$y - \bar{y} = 0 \tag{5.11}$$

$$y = \bar{y} \tag{5.12}$$

$$T_I = I_{33}\ddot{\phi} \tag{5.13}$$

$$T_M = (M_{22} + I_{22})\ddot{\psi} \tag{5.14}$$

$$T_O = (O_{11} + M_{11} + I_{11})\ddot{\theta} \tag{5.15}$$

5.2 Mathematical Model of DC Motor

Direct current motors are a drive element that has no or very little maintenance cost due to their structure and has many brands model options commercially. Considering the physical characteristics of the spherical flight simulator, it is deemed appropriate to use the direct current motor produced by KOLLMORGEN, which is frequently used in many defence industry projects. The parameters of the direct current motor to be used are given in Table 2 [59].

Table 5.1 DC motor specifications.

Resistance (ohm)	0.83
Inductance (mH)	0.91
Rotor mass moment of inertia (kg. m^2)	0.149
Torque constant (N.m/A)	5.11
Back emk constant (V/rad/s)	5.11
Peak torque value (N.m)	203

Since each sphere of the spherical flight simulator is driven by a DC motor, a mathematical model of the DC motor must be obtained in addition to the mathematical model of the simulator. Since the DC motors are directly connected to the spheres of the simulator, the simulator sphere can be considered as a mass connected to the shaft of the DC motor. Kirchoff's law is used when modelling the electrical part of the DC motor and Newton-Euler equations are used when modelling the mechanical part [42].

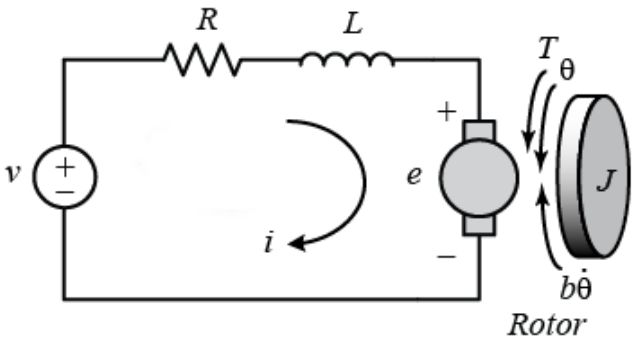

Figure 5.1 DC motor model

$$T = K_t i \tag{5.16}$$

$$e = K_e \dot{\theta} \tag{5.17}$$

$$J_{eq}\ddot{\theta} + b\dot{\theta} = K_e i \tag{5.18}$$

$$L\frac{di}{dt} + Ri = V - K\dot{\theta} \tag{5.19}$$

$$J_{eq} = J + J_{sphere} \tag{5.20}$$

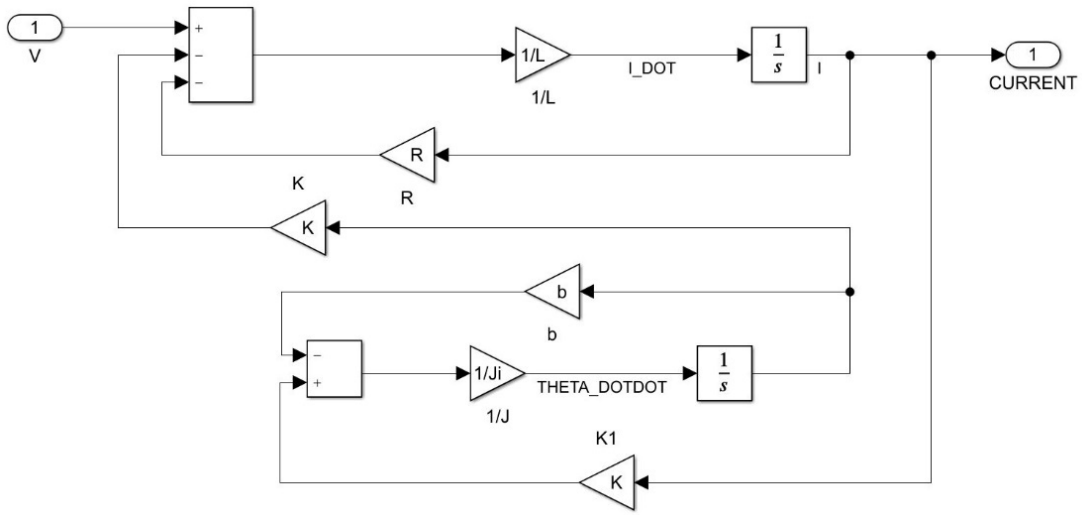

Figure 5.2 DC motor SIMULINK model.

5.3 State Feedback Controller Design via Pole Placement Method

After obtaining the linear equations of motion for the spherical flight simulator and the mathematical model of the DC motor, the combined state space model of the DC motor and the spherical flight simulator for the controller design is obtained in Eq. 5.23.

$$\dot{x} = Ax + Bu \tag{5.21}$$

$$y = Cx + Du \tag{5.22}$$

$$x_1 = \theta, x_2 = \dot{\theta}, x_3 = i$$

$$\dot{x} = \begin{bmatrix} 0 & 1 & 0 \\ 0 & -b/J_{eq} & K/J_{eq} \\ 0 & -K/L & -R/L \end{bmatrix} x + \begin{bmatrix} 0 \\ 0 \\ 1/L \end{bmatrix} V \tag{5.23}$$

$$y = [1 \quad 0 \quad 0]x \tag{5.24}$$

With the pole placement method, all poles of the system can be placed at desired locations on the root-locus graph. For arbitrary pole placement, the controllability of the system must be tested. The controllability matrix M is given in Eq.5.25. In order to say that the system is completely controllable, the rank of the matrix M must be equal to the number of state variables of the system.

$$M = [B \vdots AB \vdots A^2B] \tag{5.25}$$

Matrices A and B for the inner sphere are as follows.

$$A = \begin{bmatrix} 0 & 1 & 0 \\ 0 & -0.0008 & 1.3079 \\ 0 & -4.7450 & -59.00 \end{bmatrix} \tag{5.26}$$

$$B = \begin{bmatrix} 0 \\ 0 \\ 5 \end{bmatrix} \tag{5.27}$$

The controllability matrix for the inner sphere is constructed using matrices A and B.

$$M = \begin{bmatrix} 0 & 0 & 6.539 \\ 0 & 6.539 & -385.8 \\ 5 & -295 & 17370 \end{bmatrix}$$

Since the rank of the M matrix and the number of state variables of the system are three, the system is completely controllable.

The poles of the system are the eigenvalues of the matrix A given in Eq. 5.26, while the control signal is the eigenvalues of the matrix A given in Eq.83, the control signal is defined as in Eq. 5.28 is obtained. In this case, the eigenvalues of the $(A - BK_g)$ matrix are the poles of the system. Since matrix A and B are invariant for the system, the poles of the system can be assigned as desired by changing the state feedback gain matrix K_g.

$$u = -K_g x \tag{5.28}$$

$$\dot{x} = Ax - BK_g x = (A - BK_g)x \tag{5.29}$$

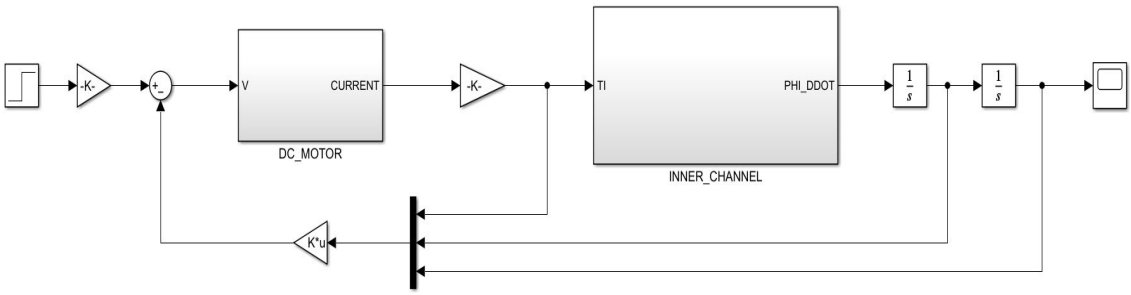

Figure 5.3 State feedback controller block diagram.

For the inner sphere, when the settling time is less than one second and the maximum percentage overshoot is chosen as five percent from the design claims, the first two poles of the system are calculated as in Eq. 5.36 and Eq. 5.37.

$$t_s = \frac{4}{\zeta \omega_n} \tag{5.30}$$

$$M_p = e^{-(\frac{\zeta}{\sqrt{1-\zeta^2}})\pi} \tag{5.31}$$

$$M_p = \%5 \tag{5.32}$$

$$\zeta = 0{,}69 \tag{5.33}$$

$$t_s \leq 1 \tag{5.34}$$

$$\omega_n \geq 5{,}9 \tag{5.35}$$

$$\mu_1 = -4{,}0000 + 4{,}1948i \tag{5.36}$$

$$\mu_2 = -4{,}0000 - 4{,}1948i \tag{5.37}$$

For the inner sphere, the third pole should be at least five times further from the imaginary axis than the dominant poles in the root locus graph [58]. In this case, the third and last pole is chosen as in Eq. 5.38.

$$\mu_3 = -20 \tag{5.38}$$

$$K_g = [k_1 \quad k_2 \quad k_3] \tag{5.39}$$

$$|sI - A + BK_g| = (s - \mu_1)(s - \mu_2)(s - \mu_3) \tag{5.40}$$

Table 5.2. Gain values obtained with pole placement.

	K_g
Inner Sphere	[102,7492 28,6521 -6,2002]
Middle Sphere	[98,9259 27,5505 -6,2002]
Outer Sphere	[414,7069 118,5345 -6,2000]

When the state feedback gains shown in Table 5.2 are placed separately on each of the spheres as in the control diagram given in Figure 5.3, the unit step response of the spheres is obtained as shown in Figure 5.4. In this case, the disturbance torques are neglected. When the disturbance torques are neglected in the state feedback controller application, the unit step response of each sphere of the spherical flight simulator is observed to be the same [42].

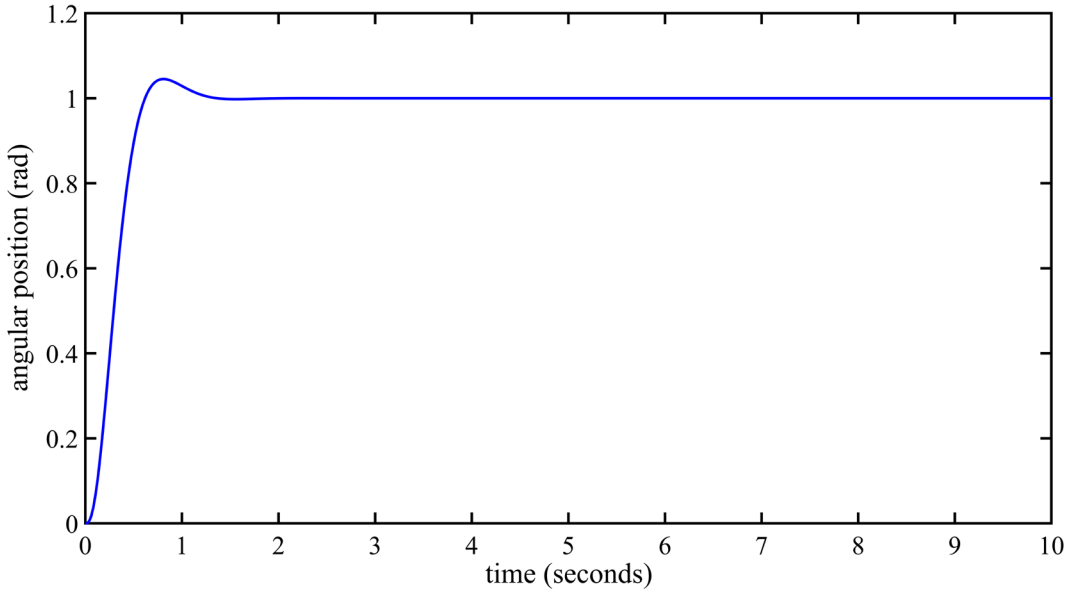

Figure 5.4 Step response of spheres**.**

When a sphere is considered independently of other spheres and a controller is designed for a direct current motor driving the sphere, it is usual to achieve a unit step response as shown in Figure 5.4. However, the spherical flight simulator consists of three nested spheres and these spheres are physically connected to each other. In the case of three rotating masses connected to each other, centrifugal and Coriolis forces arise from the relative motions of these masses [59, 60]. The torques arising from these forces can be considered as disturbance torques. The mathematical expressions and block diagrams of the disturbance torques acting on the spheres are given in detail in Chapter 4

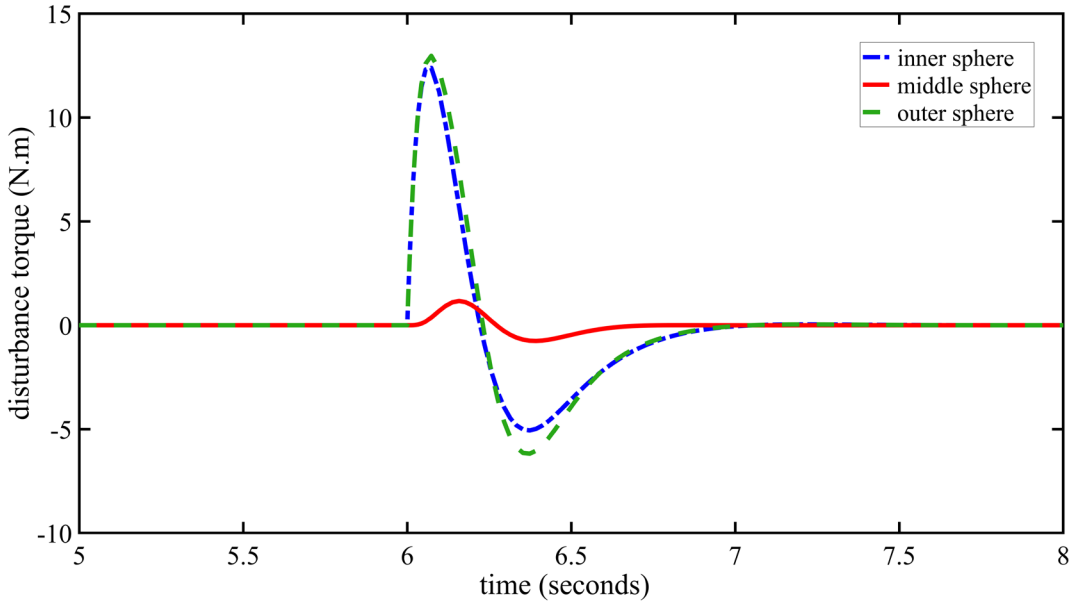

Figure 5.5 Disturbance torque values.

In order to observe the effect of disturbance torques on the system, a ten-second simulation was run in the specified scenario. A unit step input was applied to the inner sphere in the first second of the simulation, to the middle sphere in the third second and to the outer sphere in the fifth second. In this scenario, the disturbance torques acting on the spheres throughout the simulation are shown in Figure 5.5. In order to see the ability of the state feedback controller designed by pole placement method to eliminate the disturbance torques, the unit step response of each sphere was obtained in the presence and absence of disturbance torque. The unit step response of the inner sphere, middle sphere and outer sphere are given in Figure 5.6, Figure 5.7 and Figure 5.8, respectively.

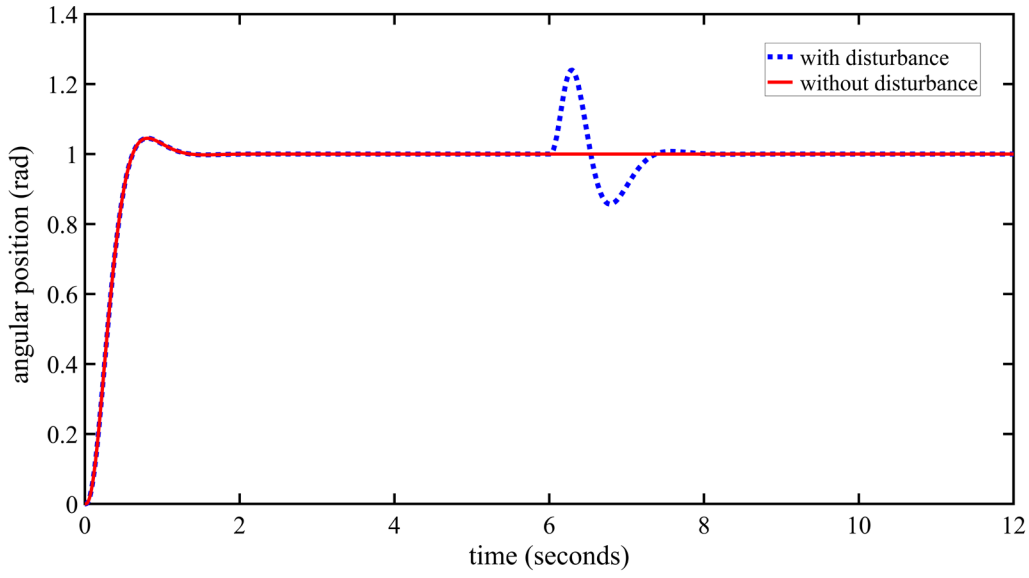

Figure 5.6 Inner sphere step response.

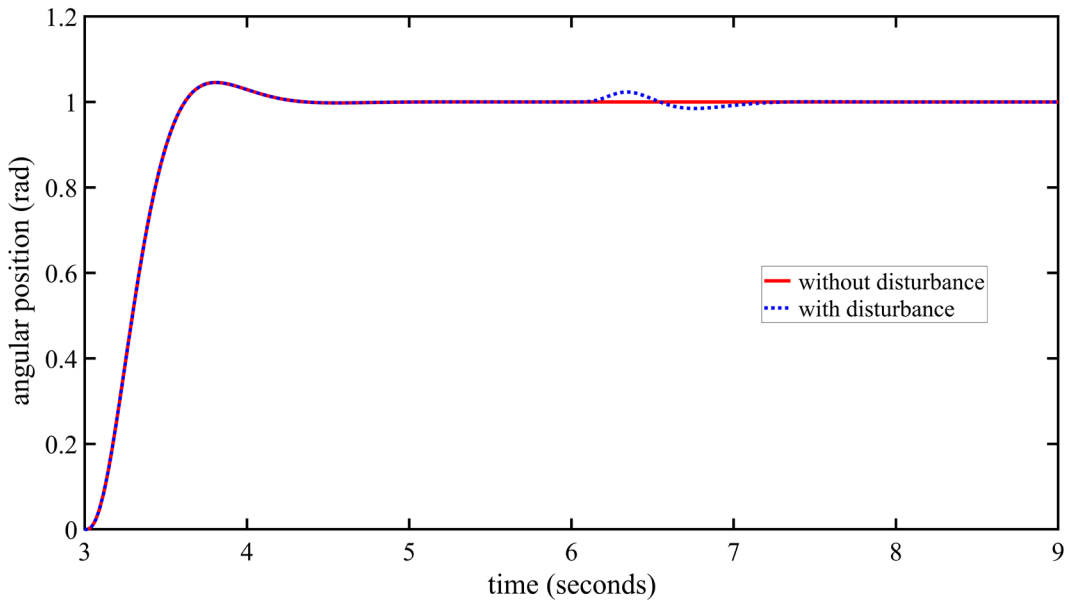

Figure 5.7 Middle sphere step response.

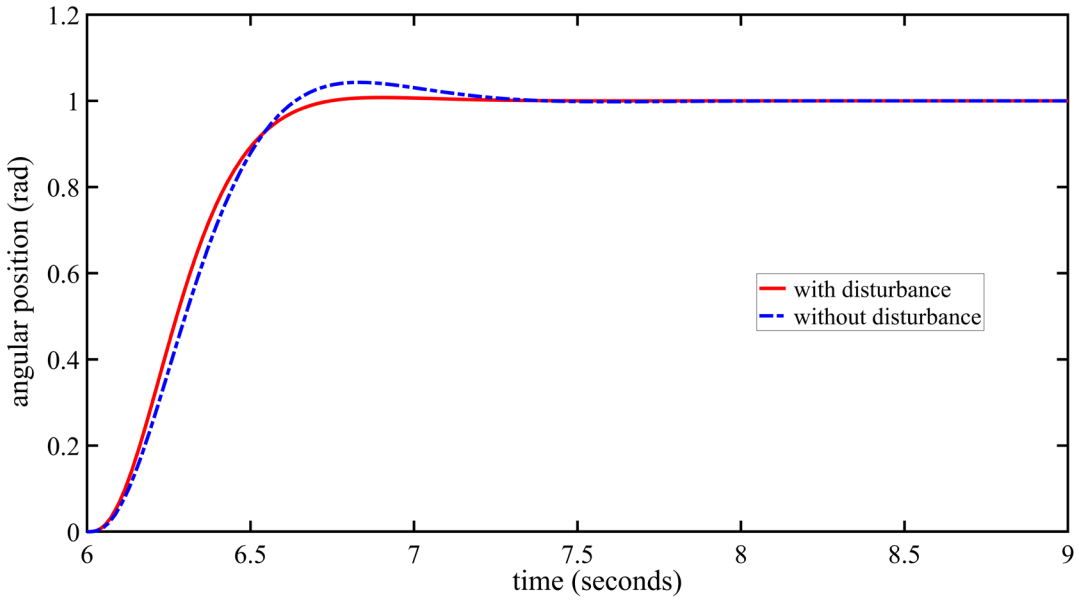

Figure 5.8 Outer sphere step response.

5.4 State Feedback Controller Design via LQR method

While the state feedback gain matrix is chosen arbitrarily in the pole placement method, the state feedback gain matrix is determined systematically in the linear quadratic regulator method. When the cost function J is defined as in Eq. 5.41, minimising this function leads to the optimal regulator problem. The state feedback gain is obtained by minimising the cost function for the selected weight matrices Q and R [42].

$$J = \int_0^\infty (x^T Q x + u^T R u) dt \tag{5.41}$$

$$u = -K_g x = -R^{-1} B P x \tag{5.42}$$

$$K_g = -R^{-1} B P \tag{5.43}$$

$$A^T P + P A - P B R^{-1} B^T P + Q = 0 \tag{5.44}$$

Eq. 5.44 is solved for the P matrix and substituted in Eq. 5.43 the state feedback gain matrix is calculated.

The state feedback gains obtained for $Q = \begin{bmatrix} 1000 & 0 & 0 \\ 0 & 1 & 0 \\ 0 & 0 & 1 \end{bmatrix}$ and R=0.01 are given in Table 5.3

Table 5.3. Gain values obtained by LQR.

	K_g
Inner Sphere	[316,2278 90,0572 5,1220]
Middle Sphere	[316,2278 88,4413 5,1498]
Outer Sphere	[316,2278 177,099 4,3924]

When the state feedback gain values obtained by the linear quadratic regulator method are substituted in the control diagram given in Figure 5.3, the unit step responses for each sphere are given in Figure 5.9, Figure 5.10 and Figure 5.12.

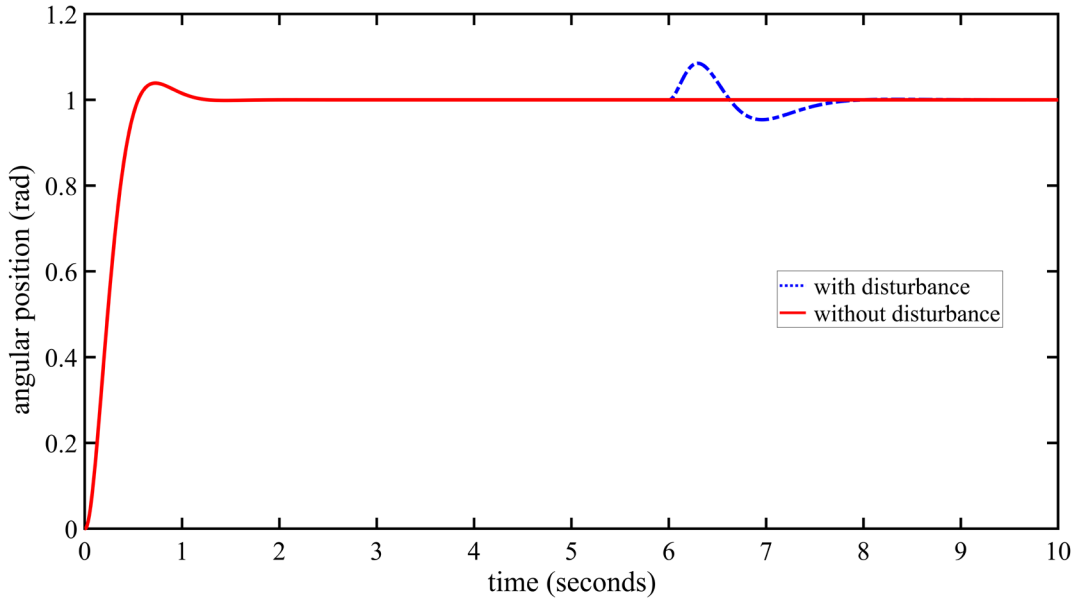

Figure 5.9 Inner sphere step response.

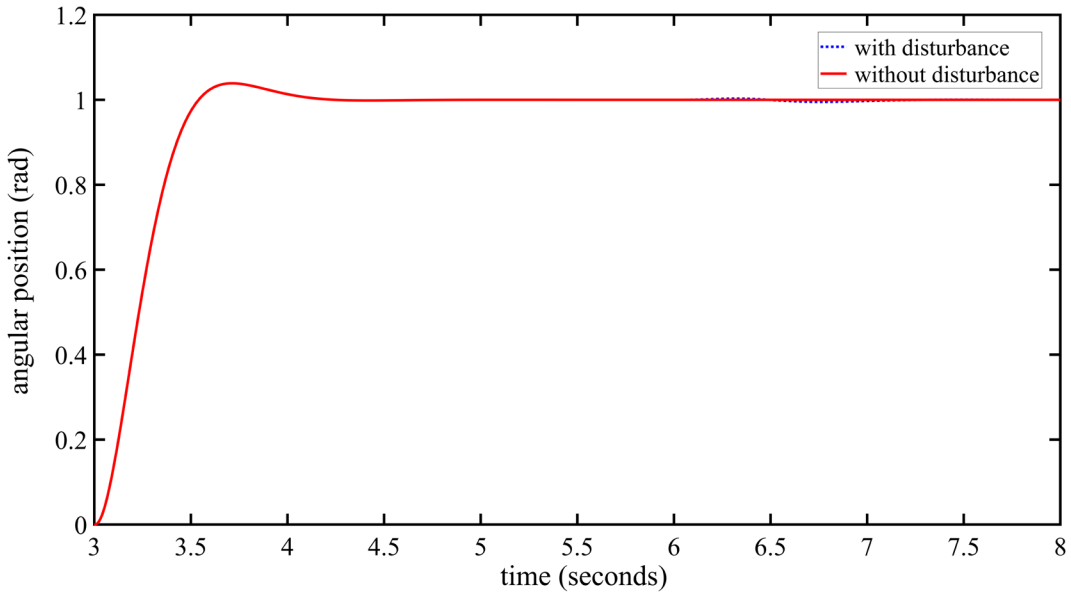

Figure 5.10 Middle sphere step response.

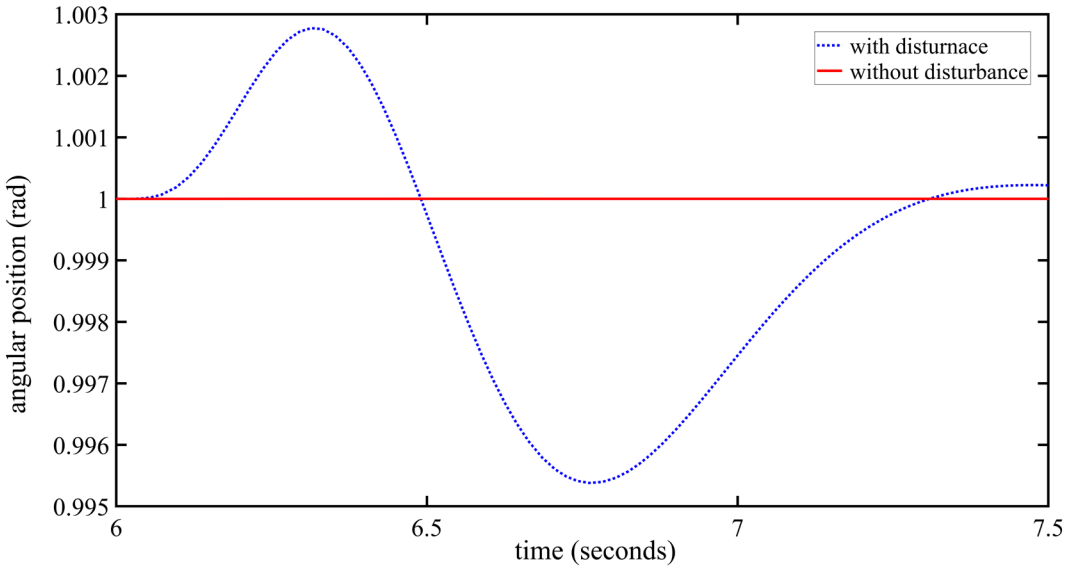

Figure 5.11 Middle Inner sphere step response detail.

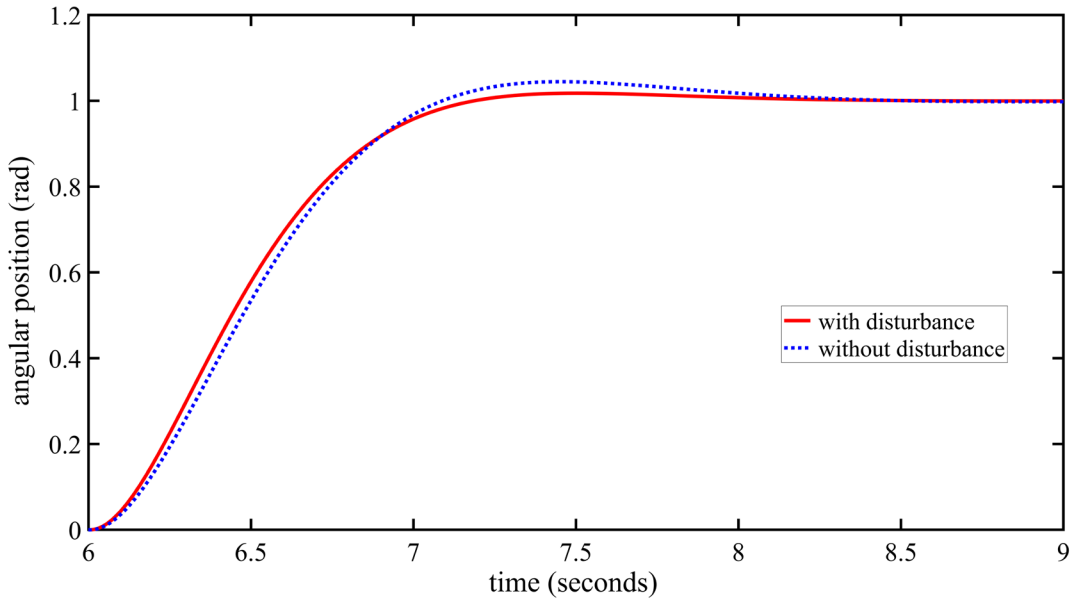

Figure 5.12 Outer sphere step response.

CHAPTER VI

RESULTS AND DISCUSSION

Although there are differences between the rise, peak and settling times of the designed controllers, it is observed that there is no significant difference when the maximum overshoot amounts are examined. The controller outputs designed for the inner sphere are as shown in Figure 24 during the simulation. While the maximum torque of the controller designed with pole placement method is 126.6 N.m, the maximum value is 62.2 N.m in the controller designed with LQR. The controller outputs designed for the middle sphere are as shown in Figure 25 during the simulation. While the maximum torque of the controller designed with pole placement method is 121.8 N.m, the maximum value is 62 N.m in the controller designed with LQR. The controller outputs designed for the outer sphere are as shown in Figure 26 during the simulation. While the maximum torque of the controller designed with the pole placement method was 147.7 N.m, the maximum value was 67.1 N.m in the controller designed with LQR. Considering the controller outputs, the maximum torque value required for successful control of the spherical flight simulator was 147.7 N.m. Since the maximum torque value that the direct current motor, whose technical specifications are given in Table 1, can produce is 203 N.m, it is physically possible to use it in the spherical flight simulator [42].

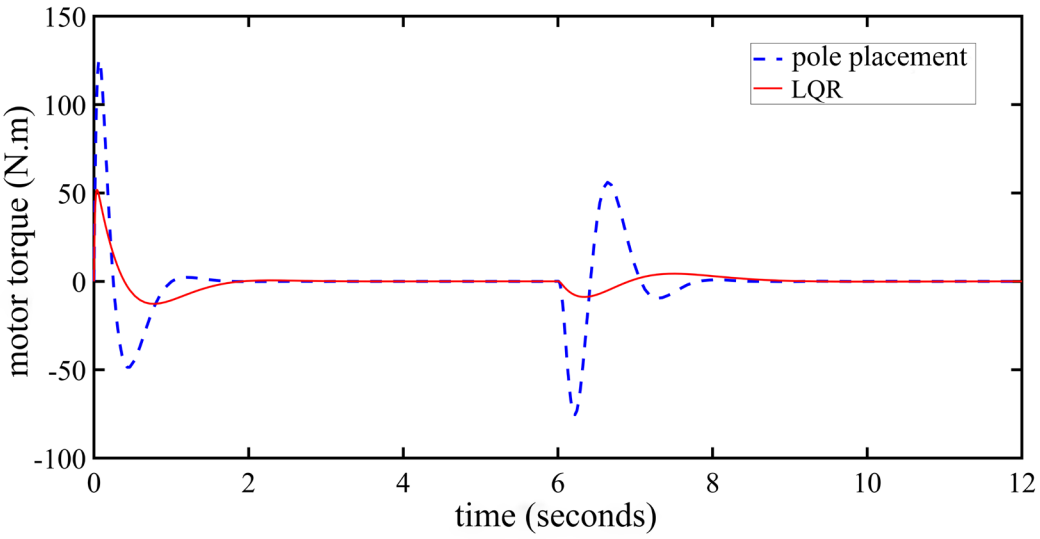

Figure 6.1 Inner Sphere motor torque values.

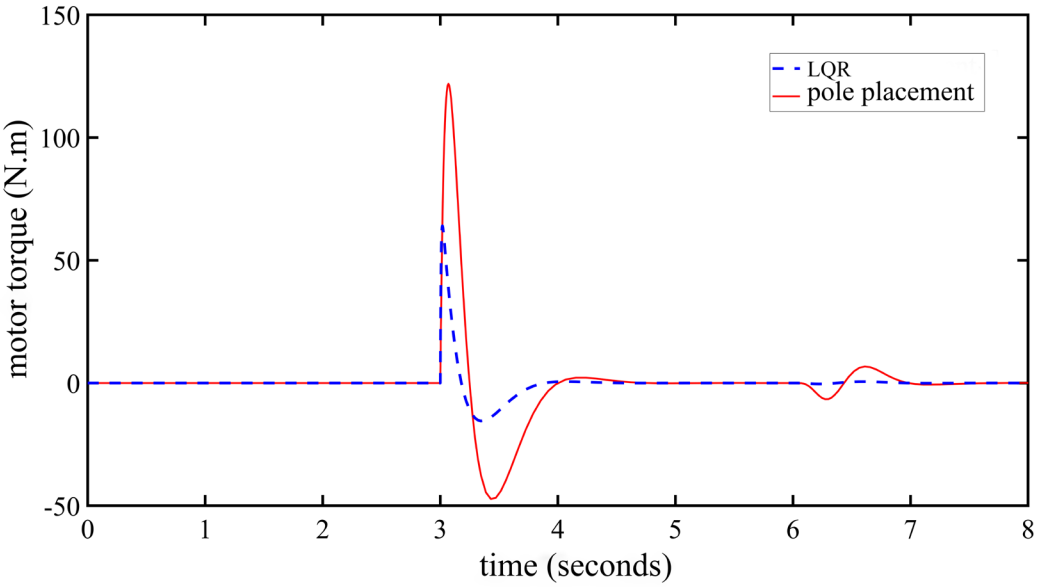

Figure 6.2 Middle Sphere motor torque values.

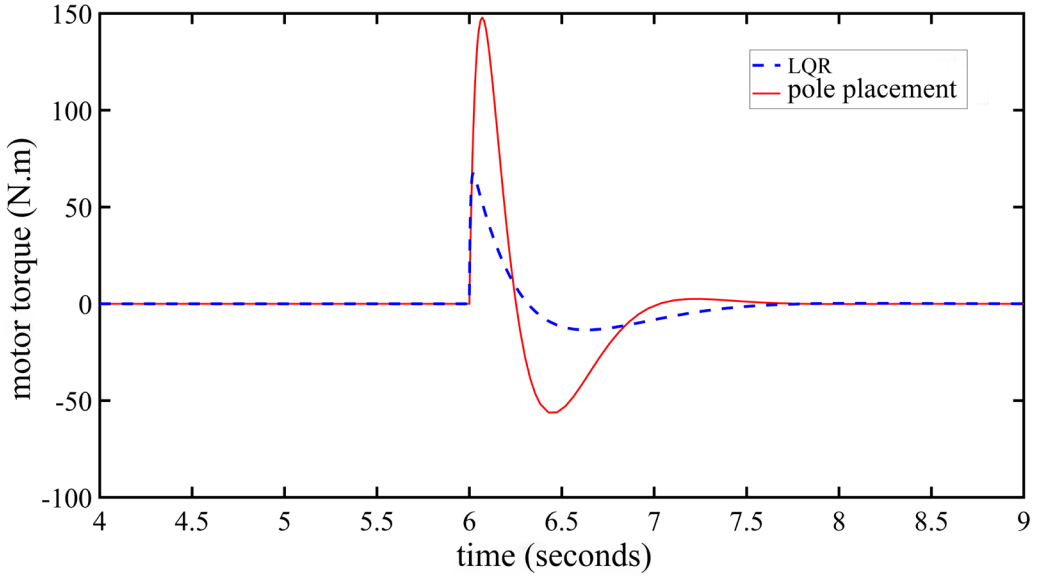

Figure 6.3 Outer Sphere motor torque values.

CHAPTER VII

CONCLUSION

In this study, a new spherical flight simulator is designed and its nonlinear mathematical model is obtained. Newton-Euler method is chosen to obtain this model. The nonlinear mathematical model is linearised and the nonlinear torques applied to each other by the nested rotating spheres are modelled as disturbance torques. For the obtained mathematical model, the controller design was carried out by using pole placement and linear quadratic regulator methods.

When the simulation results are analysed, it is seen that both control methods are successful in fulfilling the design requirements. Although both controllers were successful in eliminating the disturbance torques, the controller designed by pole placement method controlled the system faster. On the other hand, although the LQR controller was slower than the pole placement controller, it was more efficient in terms of controller effort. Although the disturbance torques acting on the spheres of the spherical flight simulator caused position errors, no steady state error was observed in both controller designs and the controllers ensured that the spheres reached the desired position

REFERENCES

1. Page R. L. 2000. Brief history of flight simulation, *SimTecT 2000 proceedings*. 11-17.

2. Szczepanski C. 2005. Anthropocentric Method of Flight Simulator Motion System Control Law Synthesis, *AIAA Modeling and Simulation Technologies Conference and Exhibit*. 6106.

3. Jeon C. 2015. The virtual flier: The link trainer, flight simulation, and pilot identity, *Technology and culture*. 28-53.

4. Jamson A. H. J., Motion cueing in driving simulators for research applications, University of Leeds, 2010.

5. Tomaske W. 1999. A Modular Automobile Road Simulator MARS for on and off-Road conditions, *DSC'99: Driving simulation conference (Paris, July 7-8 1999)*. 413-424.

6. Reymond G., Kemeny A. 2000. Motion cueing in the Renault driving simulator, *Vehicle System Dynamics*. **34(4)**, 249-259.

7. Bertollini G. P., et al. 1994. The general motors driving simulator, *SAE transactions*. 54-67.

8. Greenberg J. A., Park T. J., *The Ford driving simulator*. 1994, SAE Technical Paper.

9. Suetomi T., Horiguchi A., Okamoto Y., Hata S. 1991. The driving simulator with large amplitude motion system, *SAE transactions*. 94-101.

10. Freeman J., et al. 1996. The Iowa driving simulator: An implementation and application overview, *SAE transactions*. **104**, 113-122.

11. Suikat R. 2005. The new dynamic driving simulator at DLR, *Driving Simulator Conference*. 374-381.

12. Rolfe J. M., Staples K. J., Flight simulation, Cambridge University Press, 1988.

13. Allerton D., Principles of flight simulation, John Wiley & Sons, 2009.

14. Mohammadi A., Asadi H., Mohamed S., Nelson K., Nahavandi S. 2018. Multiobjective and interactive genetic algorithms for weight tuning of a model predictive control-based motion cueing algorithm, *IEEE transactions on cybernetics*. **49(9)**, 3471-3481.

15. Grottoli M., et al. 2019. Objective evaluation of prediction strategies for optimization-based motion cueing, *Simulation*. **95(8)**, 707-724.

16. Casas-Yrurzum S., Portalés-Ricart C., Morillo-Tena P., Cruz-Neira C. 2020. On the objective evaluation of motion cueing in vehicle simulations, *IEEE Transactions on Intelligent Transportation Systems*. **22(5)**, 3001-3013.

17. Casas S., Coma I., Portalés C., Fernández M. 2016. Towards a simulation-based tuning of motion cueing algorithms, *Simulation Modelling Practice and Theory*. **67**, 137-154.

18. Qazani M. R. C., et al. 2021. Adaptive motion cueing algorithm based on fuzzy logic using online dexterity and direction monitoring, *IEEE Systems Journal*.

19. Kitson A., Hashemian A. M., Stepanova E. R., Kruijff E., Riecke B. E. 2017. Comparing leaning-based motion cueing interfaces for virtual reality locomotion, *2017 IEEE Symposium on 3d user interfaces (3DUI)*. 73-82.

20. Asadi H., et al. 2018. A genetic algorithm–based nonlinear scaling method for optimal motion cueing algorithm in driving simulator, *Proceedings of the Institution of Mechanical Engineers, Part I: Journal of Systems and Control Engineering*. **232(8)**, 1025-1038.

21. Wu W., Cardullo F., Wu W., Cardullo F. 1997. Is there an optimum motion cueing algorithm?, *Modeling and Simulation Technologies Conference*. 3506.

22. Garrett N. J., Best M. C. 2013. Model predictive driving simulator motion cueing algorithm with actuator-based constraints, *Vehicle System Dynamics*. **51(8)**, 1151-1172.

23. Telban R. J., Wu W., Cardullo F. M., Houck J. A., *Motion cueing algorithm development: Initial investigation and redesign of the algorithms*. 2000.

24. Conrad B., Schmidt S., *The calculation of motion drive signals for piloted flight simulators*. 1969.

25. Nahon M. A., Reid L. D. 1990. Simulator motion-drive algorithms-A designer's perspective, *Journal of Guidance, Control, and Dynamics*. **13(2)**, 356-362.

26. Conrad B., Schmidt S., Douvillier J. 1973. Washout circuit design for multi-degrees-of-freedom moving base simulators, *Visual and Motion Simulation Conference*. 929.

27. You K. S., Lee M. C., Kang E., Yoo W. S. 2005. Development of a washout algorithm for a vehicle driving simulator using new tilt coordination and return mode, *Journal of mechanical science and technology*. **19(1)**, 272-282.

28. Fischer M., Sehammer H., Palmkvist G. 2010. Motion cueing for 3-, 6-and 8-degrees-of-freedom motion systems, *Actes INRETS*. 121-134.

29. Chang Y.-H., Liao C.-S., Chieng W.-H. 2009. Optimal motion cueing for 5-DOF motion simulations via a 3-DOF motion simulator, *Control Engineering Practice*. **17(1)**, 170-184.

30. Cleij D., Pool D. M., Mulder M., Bülthoff H. H. 2020. Optimizing an Optimization-Based MCA using Perceived Motion Incongruence Models, *Proceedings of the 19th Driving Simulation and Virtual Reality Conference, Antibes, France*. 9-11.

31. Garrett N. J., Best M. 2010. Driving simulator motion cueing algorithms–a survey of the state of the art.

32. Nehaoua L., Arioui H., Espie S., Mohellebi H. 2006. Motion cueing algorithms for small driving simulator, *Proceedings 2006 IEEE International Conference on Robotics and Automation, 2006. ICRA 2006.* 3189-3194.

33. Asadi H., Mohamed S., Rahim Zadeh D., Nahavandi S. 2015. Optimisation of nonlinear motion cueing algorithm based on genetic algorithm, *Vehicle System Dynamics*. **53(4)**, 526-545.

34. Asadi H., Mohamed S., Lim C. P., Nahavandi S. 2016. Robust optimal motion cueing algorithm based on the linear quadratic regulator method and a genetic algorithm, *IEEE Transactions on Systems, Man, and Cybernetics: Systems*. **47(2)**, 238-254.

35. Asadi H., et al. 2016. A Particle Swarm Optimization-based washout filter for improving simulator motion fidelity, *2016 IEEE International Conference on Systems, Man, and Cybernetics (SMC)*. 001963-001968.

36. Pais A. V., Wentink M., Van Paassen M. M., Mulder M. 2009. Comparison of three motion cueing algorithms for curve driving in an urban environment, *Presence*. **18(3)**, 200-221.

37. Feenstra P. J., Wentink M., Grácio B. J. C., Bles W. 2009. Effect of simulator motion space on realism in the Desdemona simulator,

38. Heesbeen B., Ruigrok R., Hoekstra J. 2006. GRACE-a Versatile Simulator Architecture Making Simulation of Multiple Complex Aircraft Simple, *AIAA modeling and simulation technologies conference and exhibit*. 6477.

39. Coiro D., De Marco A., Nicolosi F. 2007. A 6dof flight simulation environment for general aviation aircraft with control loading reproduction, *AIAA Modeling and Simulation Technologies Conference and Exhibit*. 6364.

40. Yang Y., Zheng S. T., Han J. W. 2011. Motion drive algorithm for flight simulator based on the stewart platform kinematics, *Key Engineering Materials*. 642-647.

41. Garrett N. J., Best M. C. 2012. Evaluation of a new body-sideslip-based driving simulator motion cueing algorithm, *Proceedings of the Institution of Mechanical Engineers, Part D: Journal of automobile engineering*. **226(11)**, 1433-1444.

42. Öztürk, E. Göv, K. 2023. Design and Control of A Novel 3 DOF Spherical Flight Simulator *Journal of the Faculty of Engineering and Architecture of Gazi University* **38(3)**.

43. Huang Y., Pool D. M., Stroosma O., Chu Q. P., Mulder M. 2016. A review of control schemes for hydraulic stewart platform flight simulator motion systems, *AIAA Modeling and Simulation Technologies Conference*. 1436.

44. Chin J.-H., Sun Y.-H., Cheng Y.-M. 2008. Force computation and continuous path tracking for hydraulic parallel manipulators, *Control Engineering Practice*. **16(6)**, 697-709.

45. Davliakos I., Papadopoulos E. 2009. Impedance model-based control for an electrohydraulic Stewart platform, *European Journal of Control*. **15(5)**, 560-577.

46. Kim H. S., Cho Y. M., Lee K.-I. 2005. Robust nonlinear task space control for 6 DOF parallel manipulator, *Automatica*. **41(9)**, 1591-1600.

47. Chen S.-H., Fu L.-C. 2011. Output feedback sliding mode control for a Stewart platform with a nonlinear observer-based forward kinematics solution, *IEEE Transactions on control systems technology*. **21(1)**, 176-185.

48. Honegger M., Corke P. 2001. Model-based control of hydraulically actuated manipulators, *Proceedings 2001 ICRA. IEEE International Conference on Robotics and Automation (Cat. No. 01CH37164)*. 2553-2559.

49. Öztürk, E. Göv, K., Kinematic Analysis of 3 DOF Flight Simulator, in *The International Conference of Materials and Engineering Technology* 2019: Gaziantep.

50. Usubamatov R. 2017. Mathematical models for principles of gyroscope theory, *AIP Conference Proceedings*. 020133.

51. Öztürk, E., Şahin, B., Göv, K., Modelling and Simulation of Spherical Flight Simulator Under Static Loading, in *The International Conference of Materials and Engineering Technology*. 2020: Gaziantep.

52. Göv K., İnsan Denge Çarkı Yapısında Bir Uçuş Simülatörü, T.P. Office, Editor. 2016: Turkey.

53. Göv K., Küresel Bir Uçuş Simülatörü, T.P. Office, Editor. 2019: Turkey.

54. Göv K., Yeni Bir Simülatör Mekanizması, T.P. Office, Editor. 2019: Turkey.

55. Anicin B., Davidovic D., Babovic V. 1993. On the linear theory of the elastic pendulum, *European journal of physics*. **14(3)**, 132.

56. Öztürk, E., Şahin, B., Göv, *Modelling and Simulation of Elastic Pendulum*, in *The International Conference of Materials and Engineering Technology (TICMET)*. 2020: Gaziantep. p. 88-96.

57. Dorf R. C., Bishop R. H., Modern control systems, Pearson Prentice Hall, 2008.

58. Ogata K., Modern control engineering, Prentice hall Upper Saddle River, NJ, 2010.

59. Poyrazoğlu E., Detailed modeling and control of a 2-dof gimbal system. 2017, *Middle East Technical University.*

60. Baruh H., Analytical dynamics, WCB/McGraw-Hill Boston, 1999.

CURRICULUM VITAE (CV)

Name: Edip ÖZTÜRK

Education:

Mechanical Engineering (B.Sc.)	Gaziantep University (2009-2015)
Aircraft and Aerospace Engineering (M.Sc.)	Gaziantep University (2015-2018)
Aircraft and Aerospace Engineering (Ph.D.)	Gaziantep University (2019-2022)

Work Experience:

Research assistant	Gaziantep University Faculty of Aerospace and Aeronautics (February 2016 -)

PUBLICATIONS

Articles:

Öztürk, E., Göv, K, *Design and Control of a Novel 3 DOF Spherical Flight Simulator* Journal of the Faculty of Engineering and Architecture of Gazi University. 10.17341/gazimmfd.1103916 (SCI-E)

Conference Papers:

R. Demir, M. H. Doğru & E. Öztürk, Analysis of Concept Unmanned Aerial Vehicle in Terms Of Wing Angle, Sözlü Sunum, The International Conference of Materials and Engineering Technology, 05 November 2020, 07 November 2020.

M. Deniz, E. Yeter, M. H. Doğru & E. Öztürk, Behaviour of Aluminum Alloys Under The Normal and oblique Ballistic Loads, Sözlü Sunum, The International Conference of Materials and Engineering Technology, 05 November 2020, 07 November 2020.

E. Öztürk, K. Göv & B. Şahin, Modelling and Simulation of Elastic Pendulum, Sözlü Sunum, The International Conference of Materials and Engineering Technology, 05 November 2020, 07 November 2020.

E. Öztürk, K. Göv & B. Şahin, Modelling and Simulation of Spherical Flight Simulator Under Static Loading, Sözlü Sunum, The International Conference of Materials and Engineering Technology, 05 November 2020, 07 November 2020.

E. ÖZTÜRK & K. GÖV, Kinematic Analysis of 3 DOF Flight Simulator, Sözlü Sunum, The International Conference of Materials and Engineering Technologies, 10 October 2019, 12 October 2019.

İ. H. Güzelbey, E. Öztürk & M. H. Doğru, Investigation of Barrel Clamp Effect on Vibrational characteristic In Gatling Gun Barrel, Sözlü Sunum, III. Uluslararasi Mesleki ve Teknik Bilimler Kongresi, 21 June 2018, 22 June 2018.

İ. H. Güzelbey, E. Öztürk & M. H. Doğru, Investigation of Fatigue Life of New Designed Gatling Gun Striker, Sözlü Sunum, Ejons International Congress on Mathematic, Engineering and Natural Sciences III, 21 April 2018, 22 April 2018

E. Öztürk, İ. H. Güzelbey & A. Şumnu, Simulation of Non-Linear Computed Torque Control on Simulink For Two Link Scara Type Manipulator, Sözlü Sunum, Conference on Advances In Mechanical Engineering Istanbul 2016 Icame2016, 11 May 2016, 13 May 2016.